



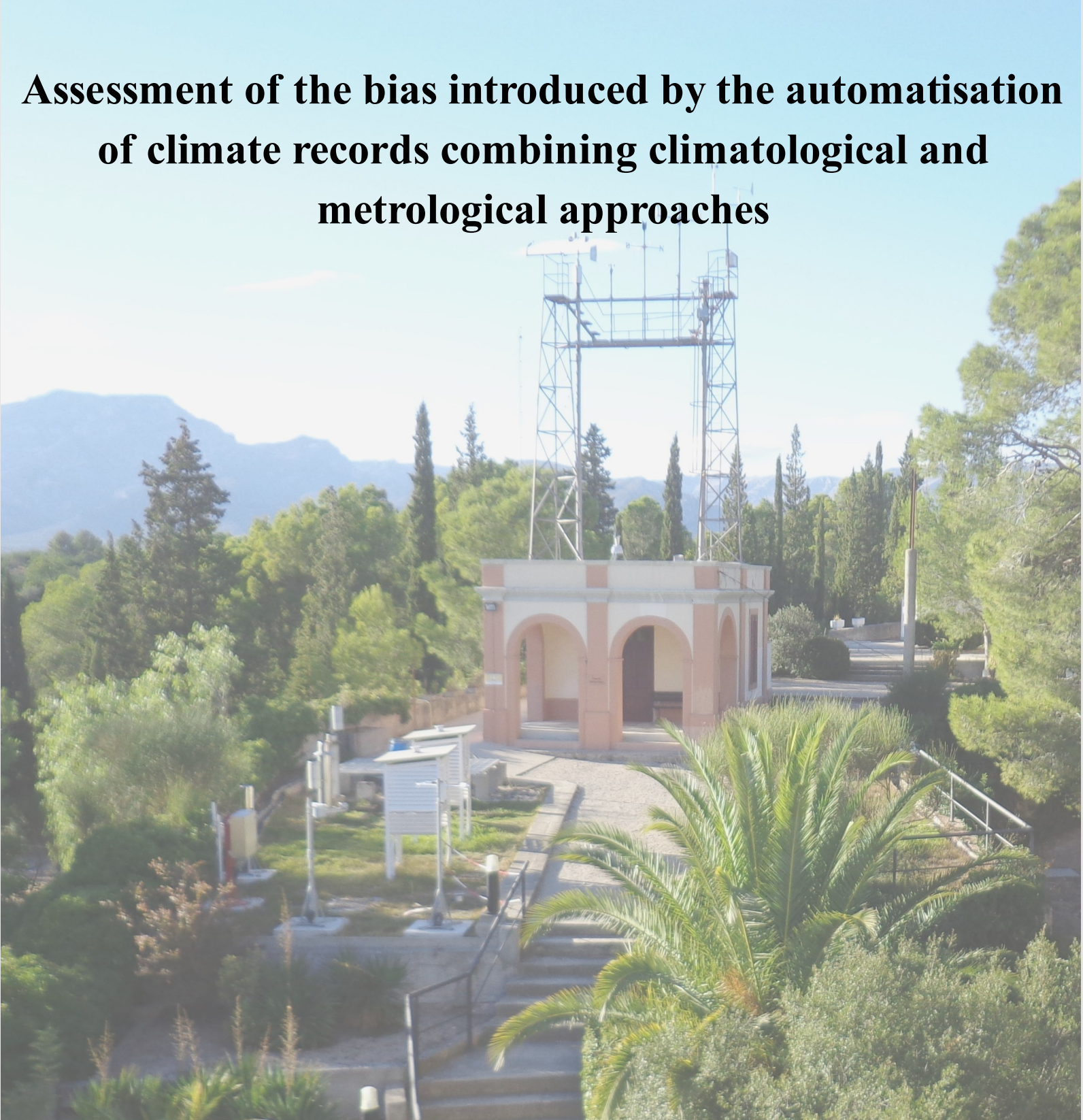
## ASSESSMENT OF THE BIAS INTRODUCED BY THE AUTOMATISATION OF CLIMATE RECORDS COMBINING CLIMATOLOGICAL AND METROLOGICAL APPROACHES

Alba Gilabert Gallart

**ADVERTIMENT.** L'accés als continguts d'aquesta tesi doctoral i la seva utilització ha de respectar els drets de la persona autora. Pot ser utilitzada per a consulta o estudi personal, així com en activitats o materials d'investigació i docència en els termes establerts a l'art. 32 del Text Refós de la Llei de Propietat Intel·lectual (RDL 1/1996). Per altres utilitzacions es requereix l'autorització prèvia i expressa de la persona autora. En qualsevol cas, en la utilització dels seus continguts caldrà indicar de forma clara el nom i cognoms de la persona autora i el títol de la tesi doctoral. No s'autoritza la seva reproducció o altres formes d'explotació efectuades amb finalitats de lucre ni la seva comunicació pública des d'un lloc aliè al servei TDX. Tampoc s'autoritza la presentació del seu contingut en una finestra o marc aliè a TDX (framing). Aquesta reserva de drets afecta tant als continguts de la tesi com als seus resums i índexs.

**ADVERTENCIA.** El acceso a los contenidos de esta tesis doctoral y su utilización debe respetar los derechos de la persona autora. Puede ser utilizada para consulta o estudio personal, así como en actividades o materiales de investigación y docencia en los términos establecidos en el art. 32 del Texto Refundido de la Ley de Propiedad Intelectual (RDL 1/1996). Para otros usos se requiere la autorización previa y expresa de la persona autora. En cualquier caso, en la utilización de sus contenidos se deberá indicar de forma clara el nombre y apellidos de la persona autora y el título de la tesis doctoral. No se autoriza su reproducción u otras formas de explotación efectuadas con fines lucrativos ni su comunicación pública desde un sitio ajeno al servicio TDR. Tampoco se autoriza la presentación de su contenido en una ventana o marco ajeno a TDR (framing). Esta reserva de derechos afecta tanto al contenido de la tesis como a sus resúmenes e índices.

**WARNING.** Access to the contents of this doctoral thesis and its use must respect the rights of the author. It can be used for reference or private study, as well as research and learning activities or materials in the terms established by the 32nd article of the Spanish Consolidated Copyright Act (RDL 1/1996). Express and previous authorization of the author is required for any other uses. In any case, when using its content, full name of the author and title of the thesis must be clearly indicated. Reproduction or other forms of for profit use or public communication from outside TDX service is not allowed. Presentation of its content in a window or frame external to TDX (framing) is not authorized either. These rights affect both the content of the thesis and its abstracts and indexes.



Assessment of the bias introduced by the automatisation of climate records combining climatological and metrological approaches | Ph.D. Thesis | Alba Gilabert Gallart

# Assessment of the bias introduced by the automatisation of climate records combining climatological and metrological approaches

Alba Gilabert Gallart

Ph.D Thesis

Universitat Rovira i Virgili



UNIVERSITAT ROVIRA I VIRGILI  
ASSESSMENT OF THE BIAS INTRODUCED BY THE  
AUTOMATISATION OF CLIMATE RECORDS COMBINING CLIMATOLOGICAL AND METROLOGICAL APPROACHES  
Alba Gilabert Gallart

Alba Gilabert Gallart

**ASSESSMENT OF THE BIAS INTRODUCED BY  
THE AUTOMATISATION OF CLIMATE RECORDS  
COMBINING CLIMATOLOGICAL AND  
METROLOGICAL APPROACHES**

PhD Thesis

Director: Dr. Enric Aguilar Anfrons

Geography Department

Centre for Climate Change



UNIVERSITAT  
ROVIRA I VIRGILI

Tortosa

2016

UNIVERSITAT ROVIRA I VIRGILI  
ASSESSMENT OF THE BIAS INTRODUCED BY THE  
AUTOMATISATION OF CLIMATE RECORDS COMBINING CLIMATOLOGICAL AND METROLOGICAL APPROACHES  
Alba Gilabert Gallart



FAIG CONSTAR que aquest treball, titulat: “Assessment of the bias introduced by the automatisisation of climate records combining climatological and metrological approaches”, que presenta Alba Gilabert Gallart per a l’obtenciól títol de Doctor, ha estat realitzat sota la meva direcció en el Departament de Geografia d’aquesta Universitat i que apleix els requeriments per poder optar a la Menció Europea

Tarragona, 28 de juny de 2016

El director de la tesi doctoral

Dr. Enric Aguilar Anfrons

UNIVERSITAT ROVIRA I VIRGILI  
ASSESSMENT OF THE BIAS INTRODUCED BY THE  
AUTOMATISATION OF CLIMATE RECORDS COMBINING CLIMATOLOGICAL AND METROLOGICAL APPROACHES  
Alba Gilabert Gallart

## Abstract

During the last third of the 20th century, Automatic Weather Stations (AWS) have gradually replaced manual observations systems in many places around the world. This transition has the potential to introduce a systematic bias (AWS bias) into climate time-series when combined with measurements taken from manual (MAN) observing systems and constitutes one of the most striking problems which the climate community faces, as the quality and homogeneity of most global records is compromised. The objective of this work is the statistical description bias and its minimisation from derived climate series.

This study can be divided into four parts. In the first parts the transition to AWS is examined with the exceptionally long parallel records of Ebro Observatory (Roquetes, Spain), Fabra Observatory (Barcelona, Spain) and Murcia Observatory (Murcia, Spain) at the daily scale. For this part is found that the main characteristic of the AWS bias is highly dependent on the AWS installed.

The second part demonstrates how the introduction of metrological calibration procedures can reduce or smooth the transition to AWS and give traceability and improve the quality and reliability of the temperature time-series. To achieve this, three field trials are installed. As result is concluded that the introduction of these procedures reduces the bias and improves the quality of the temperature time-series.

In the third part, the bias is analysed at the hourly scale. Here it is noted that the calibrated AWS (AWS<sub>c</sub>) reduces the bias at this scale, but other factors like the different response time of both sensors has a high effect on the differences AWS<sub>c</sub> – MAN.

In the fourth part, the traceability of the adjusted temperature series by estimating the combined homogenisation plus instrumental uncertainty is estimated. This study shows that the consideration of these uncertainties also has an effect on the long-term temperature trend.

As described in the previous paragraphs, this PhD thesis attempts to combine three disciplines -metrology, climatology and meteorology- to deal with the complex problem of automatic weather station transition, as a contribution to the global climate community.



## Resum

Des de l'últim terç del segle XX, les estacions meteorològiques automàtiques (AWS) han anat reemplaçant gradualment els sistemes d'observació manuals a nivell global. Aquesta transició té el potencial d'introduir biaixos sistemàtics (AWS biaix) a les series climàtiques quan aquestes estan combinades amb mesuraments fets amb sistemes de mesura manuals (MAN) i constitueix un dels problemes més importants als quals s'enfronta la comunitat climàtica, ja que la qualitat i homogeneïtat de la majoria de registres globals es veu compromesa. L'objectiu d'aquest treball és la descripció estadística del biaix i la seva minimització.

Aquest estudi es pot dividir en quatre parts. En la primera part s'examina gràcies a les inusualment llargues mesures paral·leles (AWS-MAN) de l'Observatori de l'Ebre (Roquetes, Espanya), de l'Observatori Fabra (Barcelona, Espanya) i de l'Observatori de Murcia (Murcia, Espanya) a l'escala diària. D'aquesta part, es conclou que la principal característica del AWS biaix és que aquest depèn de l'AWS instal·lada.

La segona part mostra com la introducció dels procediments metrollògics de calibració redueixen o almenys suavitzen la transició a les AWS i donen traçabilitat a les dades, millorant la qualitat i la fiabilitat de les series de temperatura. Per analitzar aquestes hipòtesis, es van instal·lar tres experiments de camp. Concloent que la introducció d'aquests procediments redueix el biaix i millora la qualitat de les series temporals de temperatura.

La tercera part, analitza el biaix a escala horària. S'observa que en aquest cas l'AWS calibrada (AWS<sub>c</sub>) a aquesta escala també redueix el biaix, però d'altres factors com el diferent temps de resposta dels sistemes té un efecte important en les diferències AWS<sub>c</sub>-MAN.

A la quarta part, s'aconsegueix donar traçabilitat a les series històriques de temperatura ajustades mitjançant l'estimació combinada de la incertesa instrumental més la de l'homogeneïtzació. Aquest estudi mostra com la consideració d'aquesta incertesa combinada també té un efecte sobre la tendència de les series de temperatura llargues.

Com s'ha descrit, aquesta tesi doctoral intenta combinar tres disciplines – la climatologia, la metrologia i la meteorologia – per fer front a un problema complex, la transició a les estacions meteorològiques automàtiques, és una contribució a la comunitat climàtica global.

## Acknowledgements

La tesi representa un punt d'inflexió. Però per arribar al moment en què comença aquesta etapa, hi ha hagut un llarg camí, moltes persones que amb el seu granet de sorra han fet que arribes el moment i d'altres que m'heu acompanyat en aquesta aventura.

Primer donar les gràcies a l'Enric, el director d'aquesta tesi, perquè en bona part va ser qui em va obrir les portes de la recerca. Perquè em vas introduir en el tema d'aquesta tesi i per la teva confiança en mi, per donar-me la llibertat per fer el meu camí.

També donar les gràcies a la Manola, directora del Centre for Climate Change per donar-me l'oportunitat de treballar amb els metròlegs i així donar-li un punt de vista diferent a la tesi i també per la teva confiança i suport. I com no gràcies, moltes gràcies a la resta de companys del C3 i especialment al Tortosa staff. Al JR per totes les xerrades, que no n'han segut poques i el teu suport, a l'Annamaria, la Linden, la Mercè, la Núria i el Xavi B. pel vostre temps, els vostres consells, perquè gràcies al "Journal Club" he pogut aprendre d'altres camps i sortir del meu món. I també gràcies a l'Elito i l'Olga, gràcies per facilitar-nos la feina, per les xerradetes i pel vostre suport. Perquè per molt difícil que sigui el camí en vosaltres tot és més fàcil!

Però aquest treball en bona part ha segut també gràcies a la gent de l'Observatori de l'Ebre, perquè va ser on va començar tot, on vaig descobrir que la climatologia era el què m'apassionava, per tots els estius que vaig passar fent pràctiques, perquè sou un gran equip, força!! I sobretot gràcies al Germán, quantes xerrades, quantes hores i sempre disposat a escoltar-me, a donar-me consells i acompanyar-me, segur que aquesta tesi no seria el què és sense els teus consells i la teva ajuda. Perquè l'èxit de l'experiment de camp de l'Obsebre també ha segut gràcies a vosaltres, per donar-me totes les facilitats i tota l'ajuda. I mil gràcies als observadors, perquè sempre m'heu facilitat la feina i m'heu ajudat. Realment dóna goig conèixer gent com vosaltres!

E grazie, grazie mille a Andrea, Giuseppina, Guido, Fabbio e Francesca, grazie per la vostra pazienza e per il vostro aiuto. Especially thanks to Andrea to give me the opportunity to participate in the MeteoMet project and to show me what is the metrology, a discipline that was unknown to me before 2013. Thanks for the four months in the INRiM, to teach me on metrology and to give me all the facilities to continue my work, to try to establish a real bridge between the metrology, the meteorology and the climatology. And thanks to bring

me the possibility to join you to the “Missione metrògica in piramide”, it was the best experience in my life.

Però per arribar fins aquí, hi ha hagut un llarg camí, moltes persones que han format part de la meva vida i que han fet possible que arribes aquest moment.

Perquè res d'això hagués segut possible sense els meus pares, els que sempre estan allí, sempre heu confiat amb mi i sempre m'heu recolzat, disposats a donar-me la mà en qualsevol moment. M'heu donat i ensenyat tot el necessari perquè avui sigui com sóc, saber que sempre esteu allí em donà la confiança per sempre tirar endavant, m'heu ensenyat que en esforç tot es possible. Gràcies a David sempre has segut un referent, el meu germà gran, perquè a la teva manera tu també sempre has estat al meu costat i gràcies a Begoña també per la teva ajuda i per fer-lo feliç. A Jordi, amb qui he començat a formar la meva família, tots els començaments són difícils però això serà una carrera de fons i gràcies pel teu suport durant aquesta tesi. I com no als iaïos, els que sempre esteu patint per nosaltres i encara que no us ho sembli, també m'heu ensenyat molt. I a la resta de família, als padrins (força padrí sempre hi ha un demà), tios/es, cosins/es, els nebots que poc a poc van arribant i especialment a la Paula i la Nerea. Amb aquesta família tot és més fàcil!

Gràcies també a tots aquells que heu format part de la meva vida pre-tesi, a tots aquells que va contribuir a la meva formació, perquè he pogut començar aquest treball en una motxilla ben carregada. Especialment gràcies a Manel R. perquè vas contribuir a que comences un nou camí, sempre et tindré present.

I com no als companys de geografia, especialment a la Mireia per ser com ets, no canviïs mai, de gent com tu n'hi ha poca i felicitats per l'Arlet! No canviaria els cinc anys de la llicenciatura per res, va ser uns grans companys i uns millors amics i espero que mai ens deixem de veure. I a la resta que heu format part en algú moment de la meva vida, pels moments compartits i les experiències viscudes.

I perdó a tots vosaltres perquè se que en molts moments he ficat aquest treball per davant de tots vosaltres. Gràcies per la vostra paciència i espero que estigui a l'altura!

---

*Aquesta tesi ha segut finançada gràcies al programa de beques pre-doctorals FI (Beca de formació i contractació de personal investigador novell) de la Generalitat de Catalunya. A més, en part aquesta recerca ha segut finançada pel projecte MeteoMet/REG 5. I voldria agrair a l'EMET, al Meteocat, a l'Observatori de l'Ebre i a la SMI les dades que han segut la base d'aquesta tesi.*

## Contents

<b>ABSTRACT</b> .....	<b>VI</b>
<b>ACKNOWLEDGEMENTS</b> .....	<b>VIII</b>
<b>CONTENTS</b> .....	<b>X</b>
<b>LIST OF ABBREVIATIONS</b> .....	<b>XIII</b>
<b>LIST OF TABLES</b> .....	<b>XVII</b>
<b>LIST OF FIGURES</b> .....	<b>XXII</b>
<b>ASSOCIATED PUBLICATIONS</b> .....	<b>XXVIII</b>
<b>CHAPTER 1 INTRODUCTION</b> .....	<b>32</b>
1.1 – CONTEXT.....	34
1.2 – RESEARCH AIMS AND OBJECTIVES.....	37
1.3 – THESIS STRUCTURE.....	39
<b>CHAPTER 2 – THE AIR TEMPERATURE TIME-SERIES</b> .....	<b>42</b>
2.1 – METROLOGY.....	44
2.1.1 – <i>What is a measurement?</i> .....	45
2.1.2 – <i>Instrument device</i> .....	47
2.1.2 – <i>Calibration and traceability</i> .....	48
2.1.3 – <i>The Uncertainty</i> .....	51
2.2 – METROLOGY OF TEMPERATURE MEASUREMENTS.....	53
2.2.1 – <i>The International Temperature Scale of 1990 (ITS-90)</i> .....	53
2.2.2 – <i>From the liquid-in-glass thermometers to the PT100</i> .....	55
2.2.3 – <i>What is an Automatic Weather Station</i> .....	58
2.2.4 – <i>Temperature instruments and measurement systems calibration, giving traceability to air temperature time-series</i> .....	60
2.3 – THE IMPACT OF THE TRANSITION TO AUTOMATIC WEATHER OBSERVING SYSTEMS IN TEMPERATURE SERIES.....	62

2.3.1 – <i>Assessing the non-climatic inhomogeneities through the study of parallel measurements</i> .....	62
2.3.2 – <i>Biases related to the introduction of automatic observing systems</i> .....	63
2.4 – RESEARCH GAPS IDENTIFIED .....	68
<b>CHAPTER 3 – FIELD TRIALS, DATA AND METHODOLOGY.....</b>	<b>70</b>
3.1 – FIELD TRIALS .....	72
3.1.1 – <i>Ebro Observatory</i> .....	73
3.1.2 – <i>Moncalieri</i> .....	78
3.1.3 – <i>Castello Borello</i> .....	81
3.2 – DATA USED FOR THE DIFFERENT ANALYSIS .....	83
3.2.1 – <i>Daily data used to assessing the differences AWSu – MAN (data used for the Chapter 4)</i> .....	83
3.2.2 – <i>Data used to assess the influence of the introduction of the calibration procedures (data used for the Chapter 5)</i> .....	90
3.2.3 – <i>Assessing the differences AWS – MAN at hourly scale (data used for the Chapter 6)</i> .....	91
3.2.4 – <i>The centennial air temperature time-series of Moncalieri (data used for the Chapter 7)</i> .....	92
3.3 – METHODOLOGY.....	93
3.3.1 – <i>Methodology used to assessing the differences AWSu – MAN (Chapter 4)</i> .....	93
3.3.2 – <i>Methodology used to assess the influence of the introduction of the calibration procedures (methodology used for the Chapter 5)</i> .....	94
3.3.3 – <i>Methodology used to assess the differences AWS – MAN at hourly scale (methodology applied on the Chapter 6)</i> .....	95
3.3.4 – <i>Methodology used for the homogenisation of Moncalieri centennial air temperature time-series and the estimation of the adjustment uncertainty budget (methodology applied on Chapter 7)</i> .....	96
<b>CHAPTER 4 – ASSESSING THE STATISTICAL CHARACTERISTICS OF THE AWSU – MAN DIFFERENCES.....</b>	<b>102</b>
4.1 – EBRO OBSERVATORY AWSU - MAN .....	104
4.2 – FABRA OBSERVATORY AWSU – MAN.....	114
4.3 – MURCIA OBSERVATORY AWSU – MAN .....	123

CHAPTER 4 SUMMARY .....	132
<b>CHAPTER 5 – CAN THE METROLOGICAL APPROACH IMPROVE THE QUALITY OF THE TEMPERATURE TIME-SERIES? – DAILY DATA.....</b>	<b>134</b>
5.1 – THE IMPACT OF THE ADOPTION OF THE CALIBRATION CURVE – MONCALIERI FIELD TRIAL.....	136
5.2 – THE DIFFERENCES BETWEEN AND AWSC AND AWSU – CASTELLO BORELLO FIELD TRIAL.....	141
5.3 – THE EBRO OBSERVATORY FIELD TRIAL, A TRIPLE ANALYSIS BETWEEN AWSC, AWSU AND MAN.....	147
CHAPTER 5 SUMMARY .....	153
<b>CHAPTER 6 - ASSESSING THE DIFFERENCES AWSC – MAN AT HOURLY SCALE .....</b>	<b>154</b>
6.1 – ADAPTING THE AWSC HOURLY TEMPERATURE TO THE MAN OBSERVING TIMES.....	156
6.2 – ADAPTING THE AWSC HOURLY TEMPERATURE TO THE MAN OBSERVING TIMES.....	160
CHAPTER 6 SUMMARY .....	162
<b>CHAPTER 7 – GIVING TRACEABILITY TO THE HISTORICAL TEMPERATURE SERIES.....</b>	<b>164</b>
7.1 - HOMOGENISATION RESULTS OF THE MONCALIERI MONTHLY MAXIMUM AND MINIMUM TEMPERATURE SERIES .....	166
7.2 – RESULTS FROM THE JOINT ESTIMATION OF INSTRUMENTAL PLUS HOMOGENISATION UNCERTAINTIES FOR MONCALIERI.....	170
CHAPTER 7 SUMMARY .....	174
<b>CHAPTER 8 : CONCLUSIONS, DISCUSSION AND FURTHER WORK.....</b>	<b>176</b>
8.1. CONCLUSIONS AND DISCUSSION .....	178
8.2 - FURTHER WORK .....	182
<b>REFERENCES.....</b>	<b>184</b>
<b>ANNEXES.....</b>	<b>193</b>
A.1 – EBRO OBSERVATORY TEMPERATURE MEASUREMENT SYSTEMS INSTALLED .....	194
A.2 – OTHER RESULTS.....	199
A.3 – LIST OF EQUATIONS .....	206



## List of abbreviations

AEMET	Agencia Estatal de Meteorologia
AWS	Automatic Weather Station
AWS <sub>c</sub>	AWS calibrated
AWS <sub>sch</sub>	AWS <sub>c</sub> with the observing time adjusted to the MAN
AWS <sub>schn</sub>	AWS <sub>c</sub> with the observing time not adjusted to the MAN
AWS <sub>u</sub>	AWS uncalibrated
BIPM	Bureau International des Poids et Mesures
BP	Breakpoint
CIMO	Commission for Instruments and Methods of Observation
DTR	Daily Temperature Range
EDIE	Earth Dynamics Investigation Experiment
EMPR	European Metrological Research Programme
ESOS	Surface semiautomatic observing station (spanish sigles)
ETCCDI	Expert Team on Climate Change Detection and Indices
FD	Frost days (ETCCDEI indice)
GCOS	Global Climate Observing System
GRUAN	Reference Upper Air Network
HSP	Homogeneous sub-period
INRiM	Istituto Nazionale di Ricerca Metrologica
IPCC	Intergovernmental Panel on Climate Change



ITS-90	International Temperature Scale
JCGM	Joint Committee for Guides in Metrology
LIG	Liquid-in-glass thermometers
MCV	Manufacture name
MeteoMet	Metrology for Meteorology project
MMTS	Maximum-Minimum Temperature System
NMHs	National Meteorological and Hydrological services
NMIs	National Metrological Institutes
PRT	Platinum Resistance Thermometer
RH	Relative humidity
SEAC	Manufacture name
SI	International System of Units
SMI	Società Meteorologica Italiana
SOSS	Surface semiautomatic observing system (spanish sigles)
SPRT25Ω	Standard Platinum Resistance Thermometer 25Ω
SU	Summer days (ETCCDEI indice)
<i>T</i> <sub>max</sub>	Daily maximum Temperature
<i>T</i> <sub>min</sub>	Daily minimum Temperature
TR	Tropical nights (ETCCDEI indice)
u	Standard uncertainty
U	Expanded uncertainty

WMO	World Meteorological Organisation
WS	Daily mean wind-speed
$\Delta T_{\max}$	Daily maximum Temperature differences
$\Delta T_{\min}$	Daily minimum Temperature differences



## List of tables

<i>Table 2.1: Difference between measurement accuracy and measurement precision shown by the distribution of golf balls depending on a high and low accuracy and a high and a low precision</i>	46
<i>Table 2.2: Difference between repeatability and reproducibility condition of measurement</i>	46
<i>Table 2.3: A shematic illustrating the difference between measurement error and measurement uncertainty. Is shown that the distribution of the observations depending on the low and high error and low and high uncertainty. The dashed blue line indicates the true value.</i>	52
<i>Table 3.1: Results of the AWSc Ebro Observatory calibration. The values of the constants A, B and C, the values of the SPRT25<math>\Omega</math> and the AWSc under calibration for every measuring point.</i>	76
<i>Table 3.2: Estimation of the Ebro Observatory MAN uncertainty. For every uncertainty source the contribution to standard uncertainty. The total standard uncertainty and the expanded uncertainty (U)</i>	78
<i>Table 3.3: Results of the AWSc Moncalieri calibration. The values of the constants A, B and C and the values of the SPRT25<math>\Omega</math> (<math>T_s</math>) and the <math>T_c</math> for every measuring point.</i>	80
<i>Table 3.4: Results of the AWSc Castello Borello calibration. The values of the constants A, B and C and the values of the SPRT25<math>\Omega</math> and the <math>T_c</math> for every measuring point.</i>	82
<i>Table 3.5: Characteristics of AEMET AWSu systems and thermometric sensors installed at the Ebro Observatory from 01/07/1991 onwards.</i>	85
<i>Table 3.6: Metadata of the AWSu installed in Fabra Observatory, information courtesy of Catalonia Meteorological Service (SMC)</i>	87
<i>Table 3.7: Daily mean windspeed and sunshine hours thresholds for Ebro Observatory, Fabra Observatory and Murcia Observatory.</i>	94
<i>Table 4.1: Basic statistics estimated for each homogeneous sub-period (HSP) providing the number of parallel AWSu – MAN observations of Ebro Observatory, mean differences and root-mean square deviation (RMSD) for maximum temperature differences (<math>\Delta T_{max}</math>) and minimum temperature differences (<math>\Delta T_{min}</math>).</i>	105
<i>Table 4.2: Spearman's correlation coefficients (<math>\rho</math>) estimated among the maximum (<math>\Delta T_{max}</math>) and minimum (<math>\Delta T_{min}</math>) temperature differences AWSu-MAN of Ebro Observatory and <math>T_{max}</math> – <math>T_{min}</math> MAN (<math>T_{max}</math> MAN, <math>T_{min}</math> MAN) observations, daily temperature range (DTR), daily mean wind</i>	

*speed (WS) and sunshine hours (sunshine) for the SEAC2, SOSS2 and ESOS3 sub-periods. In bold are the coefficients that are statistically significant at the 95 % confidence level. \_\_\_\_\_ 110*

*Table 4.3: Basic statistics estimated for each homogeneous sub-period (HSP) providing the number of parallel AWSu – MAN observations of Fabra Observatory, mean differences and root-mean square deviation (RMSD) for maximum temperature differences ( $\Delta T_{max}$ ) and minimum temperature differences ( $\Delta T_{min}$ ). \_\_\_\_\_ 115*

*Table 4.4: Spearman’s correlation coefficients ( $\rho$ ) estimated among the maximum ( $\Delta T_{max}$ ) and minimum ( $\Delta T_{min}$ ) temperature differences and  $T_{max} - T_{min}$  MAN ( $T_{max}$  MAN,  $T_{min}$  MAN) observations, daily temperature range (DTR), wind speed (WS) and sunshine hours (sunshine) for the MCV1.2, MCV2.2 and Vaisala sub-periods, Fabra Observatory. In bold are the coefficients that are statistically significant at the 95 % confidence level. \_\_\_\_\_ 120*

*Table 4.5: Basic statistics estimated for each homogeneous sub-period (HSP) providing the number of parallel AWSu – MAN observations of Murcia Observatory, mean differences and root-mean square deviation (RMSD) for maximum temperature differences ( $\Delta T_{max}$ ) and minimum temperature differences ( $\Delta T_{min}$ ). \_\_\_\_\_ 123*

*Table 4.6: Spearman’s correlation coefficients ( $\rho$ ) estimated among the maximum ( $\Delta T_{max}$ ) and minimum ( $\Delta T_{min}$ ) temperature differences and  $T_{max} - T_{min}$  MAN ( $T_{max}$  MAN,  $T_{min}$  MAN) observations, daily temperature range (DTR), wind speed (WS) and sunshine hours (sunshine) for the SEAC4, SEAC3, SEAC2 and SEAC1 sub-periods, Murcia Observatory. In bold are the coefficients that are statistically significant at the 95 % confidence level. \_\_\_\_\_ 128*

*Table 5.1: Annual and seasonal (winter and summer) mean differences ( $^{\circ}\text{C}$ ) applying (AWS<sub>c</sub>) or not (AWS<sub>u</sub>) the calibration curve for daily maximum ( $\Delta T_{max}$ ) and minimum ( $\Delta T_{min}$ ) temperatures, along with the Root Mean Square Deviation (RMSD), the percentage of differences falling into the calibration uncertainty ( $\%|0.32| \text{ }^{\circ}\text{C}$ ) and the number of parallel observations ( $n$ ) for the period 21/09/2012 – 20/09/2013. \_\_\_\_\_ 138*

*Table 5.2: Annual averaged results for daily maximum ( $T_{max}$ ) and minimum ( $T_{min}$ ) temperatures and the number of Frost days (FD), Summer days (SU) and tropical nights (TR) calculated applying (AWS<sub>c</sub>) or not (AWS<sub>u</sub>) the calibration curve of the observations taken at Moncalieri Observatory. \_\_\_\_\_ 140*

*Table 5.3: Annual and season (winter and summer) mean differences ( $^{\circ}\text{C}$ ) applying (AWS<sub>c</sub>) or not (AWS<sub>u</sub>) the calibration curve for daily maximum ( $\Delta T_{max}$ ) and minimum ( $\Delta T_{min}$ ) temperatures, along with the Root Mean Square Deviation (RMSD) and the percentage of differences falling into the calibration uncertainty ( $\%|0.16| \text{ }^{\circ}\text{C}$ ) for the period 21/09/2013 – 20/09/2014. \_\_\_\_\_ 143*

Table 5.4: Spearman's correlation coefficients ( $\rho$ ) estimated among the maximum ( $\Delta T_{max}$ ) and minimum ( $\Delta T_{min}$ ) temperature differences  $AWS_c - AWS_u$  and  $T_{max} - T_{min}$  of  $AWS_c$  observations, daily temperature range (DTR), wind speed (WS), radiation (RA) and relative humidity (RH) for the Castello Borello field trial observations. In bold are the coefficients that are statistically significant at the 95 % confidence level. \_\_\_\_\_ 146

Table 5.5: Statistical results (mean, RMSD and percentage of observations falling inside the combined calibration uncertainty  $\pm|U|$ ) for the daily maximum ( $\Delta T_{max}$ ) and minimum ( $\Delta T_{min}$ ) differences series estimated from the calibrated AWS ( $AWS_c$ ) minus manual (MAN),  $AWS_c$  minus uncalibrated AWS ( $AWS_u$ ) and  $AWS_u$  minus MAN. The combined calibration uncertainty is  $\pm 0.38$  °C for  $AWS_c$ -MAN and  $AWS_u$ -MAN and  $\pm 0.16$  °C for  $AWS_c - AWS_u$  148

Table 6.1: Statistical results (mean, RMSD and percentage of observations falling inside the combined calibration uncertainty  $\pm|U|$ , 0.38 °C-) for the hourly temperature differences at 6h, 7h, 9h, 13h, 15h and 18h U.T.C  $AWS_c - MAN$ , correcting the  $AWS_c$  observing times to the MAN observations ( $\Delta T_h$ ) or without applying this correction ( $\Delta T_{nh}$ ) \_\_\_\_\_ 157

Table 6.2: Mean for the hourly temperature differences at 6h, 7h, 9h, 13h, 15h and 18h U.T.C  $AWS_c - MAN$  for the  $AWS_{ch}$ ,  $AWS_{cnh}$ ,  $AWS_c$  taking the 5' mean centered,  $AWS_c$  taking the mean of the 5' before and  $AWS_c$  taking the mean of the 5' after. \_\_\_\_\_ 160

Table 7.1: Uncertainty budget estimated from the adjusted monthly maximum temperature ( $T_{max}$ ) for every Homogeneous Sub-Period (HSP) identified by the homogenisation assessment applied to Moncalieri monthly data 1866-2012, along with the causes documented by the metadata.  $u_h$  is the uncertainty related to the homogenisation procedure,  $U_r$  is the calibration uncertainty of the reference stations,  $U_c$  is the instrumental uncertainty of the candidate stations,  $U_H$  is the total homogenisation uncertainty plus instrumental. \_\_\_\_\_ 168

Table 7.2: As Table 7.1, but for monthly minimum temperature series of Moncalieri Observatory. \_\_\_\_\_ 169

Table 7.3: Trend for the annual Maximum and Minimum Temperature of the periods 1866-2012, 1950-2012 and 1980-2012 using Ordinary Least Squares (OLS) and Weighted Least Squares (WLS). Significance trend at 95% in bold. \_\_\_\_\_ 173

Table A2.1: The percentage of the daily maximum and minimum temperature differences  $AWS_u - MAN$  of Ebro Observatory ( $\Delta T_{max}$  and  $\Delta T_{min}$ ) for the 8 HSPs detected for the differences lower than -1.5 °C, between -1.5 and -1 °C, between -1 and -0.5 °C, between -0.5 and 0.0 °C, between 0 and 0.5 °C, between 0.5 and 1 °C, between 1 and 1.5 °C and greater than 1.5 °C. 199

*Table A2.2: Basic statistics estimated for each homogeneous sub-period (HSP) mean differences and root-mean square deviation (RMSD) for maximum temperature differences ( $\Delta T_{max}$ ) and minimum temperature differences ( $\Delta T_{min}$ ) for the difference seasons of Ebro Observatory. \_\_\_\_\_ 200*

*Table A2.3: The mean for maximum and minimum temperature difference series AWSu-MAN of Ebro Observatory of SEAC2, SOSS2 and ESOS2 according the stratification of the days depending the wind speed and the sunshine hours. W-O windy and overcast days, W-C (windy and clear days), C-O (calm and overcast days) and C-C (calm and clear days). On methodology (Page 89) to see the wind speed and sunshine hours thresholds. \_\_\_\_\_ 201*

*Table A2.4: The percentage of the daily maximum and minimum temperature differences AWSu – MAN of Fabra Observatory ( $\Delta T_{max}$  and  $\Delta T_{min}$ ) for the 6 HSPs detected for the differences lower than  $-1.5$  °C, between  $-1.5$  and  $-1$  °C, between  $-1$  and  $-0.5$  °C, between  $-0.5$  and  $0.0$  °C, between  $0$  and  $0.5$  °C, between  $0.5$  and  $1$  °C, between  $1$  and  $1.5$  °C and greater than  $1.5$  °C. 202*

*Table A2.5: The mean for maximum and minimum temperature difference series AWSu-MAN of Fabra Observatory of MCV1.2, MCV2.2 and Vaisala according the stratification of the days depending the wind speed and the sunshine hours. W-O windy and overcast days, W-C (windy and clear days), C-O (calm and overcast days) and C-C (calm and clear days). On methodology (Page 89) to see the wind speed and sunshine hours thresholds. \_\_\_\_\_ 203*

*Table A2.6: The percentage of the daily maximum and minimum temperature differences AWSu – MAN of Murcia Observatory ( $\Delta T_{max}$  and  $\Delta T_{min}$ ) for the 4 HSPs detected for the differences lower than  $-1.5$  °C, between  $-1.5$  and  $-1$  °C, between  $-1$  and  $-0.5$  °C, between  $-0.5$  and  $0.0$  °C, between  $0$  and  $0.5$  °C, between  $0.5$  and  $1$  °C, between  $1$  and  $1.5$  °C and greater than  $1.5$  °C. 204*

*Table A2.7: The mean for maximum and minimum temperature difference series AWSu-MAN of Murcia Observatory of SEAC4, SEAC3, SEAC2 and SEAC1 according the stratification of the days depending the wind speed and the sunshine hours. W-O windy and overcast days, W-C (windy and clear days), C-O (calm and overcast days) and C-C (calm and clear days). On methodology (Page 89) to see the wind speed and sunshine hours thresholds. \_\_\_\_\_ 205*

## List of figures

<i>Figure 1.1: Thesis schematic. In the second level the different results chapters and in the third level the data used to assess the questions of every chapter</i>	40
<i>Figure 2.1: Traceability diagram for the Measuring System (in this case, a Platinum Resistance Temperature (PRT) sensor) showing the unbroken chain of comparisons from the Unit Definition of International System of Units (SI) (the International Temperature Scale of 1990 (ITS-90)). See section 2.1.2 for more details.</i>	49
<i>Figure 2.2: Picture of a water triple point cell and diagram of this cell. Image source: www.campbellsci.com (last visit: June 2016)</i>	50
<i>Figure 2.3: Picture of a Standard Platinum Resistance Thermometer (SPRT 25Ω). Image source: INRiM</i>	50
<i>Figure 2.4: Platinum Resistance Thermometer (Pt100). Pt100 installed in Ebro Observatory field trial. Source image: A. Gilabert</i>	51
<i>Figure 2.5: Diagram of the most important fixed points that defines the International Temperature Scale of 1990 (ITS-90). The most important is the Water's triple point. Image source: www.electro-optical.com (last visit: June 2016)</i>	54
<i>Figure 2.6: Image of a Fuess Liquid-in-glass thermometer. This image shows the following different parts of this type of thermometer: the bulb, the stem, the scale, the liquid column, the capillary tube and the expansion chamber. Image source: Fuess</i>	55
<i>Figure 2.7: Fuess maximum and minimum liquid-in-glass thermometers, installed in Ebro Observatory. Source image: A.Gilabert</i>	56
<i>Figure 2.8: A thermohygrograph. We can see the arm and the pen, the band and the drum that rotates driven by a clockwork system. Source image: Ebro Observatory</i>	57
<i>Figure 3.1: Localisation map of the different field trials start up and the base of part of this thesis.</i>	73
<i>Figure 3.2: Picture of the meteorological garden (picture courtesy of Ebro Observatory).</i>	73
<i>Figure 3.3: On the left the image of the Stevenson Screen in which are placed the different temperature instruments. On the right, a view of the interior of the Stevenson Screen: the LIG Thermometers, the AWSu, the AWSc and the thermograph. Image source: A. Gilabert</i>	74
<i>Figure 3.4: Pictures of the new sensor inside a Young – aspirated Screen. Image source: A. Gilabert</i>	75
<i>Figure 3.5: The climatic chamber EDIE-1. Image source: MeteoMet project</i>	76



Figure 3.6: The view of the Moncalieri Stevenson Screen in which there is the AWS. Image source: SMI ..... 78

Figure 3.7: Picture of EDIE-0 and the interior of the Stevenson Screen. Image source: MeteoMet ..... 79

Figure 3.8: Calibration results, the blue dots the difference between the temperature of the SPRT25 $\Omega$  and the AWSc of Moncalieri in  $^{\circ}\text{C}$  for every measuring point. The black line is the calibration curve. .... 80

Figure 3.9: Picture of the Stevenson Screen in which there are the two AWS (a) and a view of the new AWSc installed and the older AWSu from the SMI. Image source: MeteoMet ..... 81

Figure 3.10: Calibration results, the blue dots the difference between the temperature of the SPRT25 $\Omega$  and the AWSc of Castello Borello in  $^{\circ}\text{C}$  for every measuring point. The black line is the calibration curve. .... 82

Figure 3.11: Localisation map of the three stations considered: Ebro Observatory, Fabra Observatory and Murcia Observatory. .... 83

Figure 3.12: Daily maximum temperature difference series ( $\Delta T_{\text{max}}$ ) (upper plot) and daily minimum temperature difference series ( $\Delta T_{\text{min}}$ ) (lower plot) between the uncalibrated automatic station (AWSu) and manual (MAN) observations of the Ebro Observatory. The vertical grey lines indicate breakpoints (BP) positions (in black the documented BPs). The horizontal black lines indicate the AWSu-MAN mean for each HSP. .... 86

Figure 3.13: Daily maximum temperature difference series ( $\Delta T_{\text{max}}$ ) (upper plot) and daily minimum temperature difference series ( $\Delta T_{\text{min}}$ ) (lower plot) between the uncalibrated automatic station (AWSu) and manual (MAN) observations of the Fabra Observatory. The vertical black lines indicate breakpoints (BP) positions. .... 88

Figure 3.14: Daily maximum temperature difference series ( $\Delta T_{\text{max}}$ ) (upper plot) and daily minimum temperature difference series ( $\Delta T_{\text{min}}$ ) (lower plot) between the uncalibrated automatic station (AWSu) and manual (MAN) observations of the Murcia Observatory. The vertical black lines indicate breakpoints (BP) positions. .... 90

Figure 3.15: Localisation map of the seven reference stations for the homogenisation. The dot colour indicates the Pearson correlation ( $r$ ) between each reference station and the candidate station (Moncalieri). The empty black dot indicates the localisation of the candidate station. 97

Figure 3.16: Diagram of the combined uncertainty budget methodology followed in this study ..... 100

Figure 4.1: Histogram of the daily maximum and minimum temperature differences AWSu – MAN of Ebro Observatory ( $\Delta T_{\text{max}}$  and  $\Delta T_{\text{min}}$ ) for the 8 HSPs detected. .... 106

Figure 4.2: Seasonal boxplots (DJF winter, MAM spring, JJA summer and SON autumn) for maximum (upper plots) and minimum (lower plots) temperature difference series AWSu-MAN of

*Ebro Observatory for one HSP for every period (the largest and most continuous HSP) the ESOS3 (for the ESOS period), SOSS2 (for the SOSS period) and SEAC2 (for the SEAC period) sub-periods.* ..... 107

*Figure 4.3: Boxplots for maximum (upper plots) and minimum (lower plots) temperature difference series AWSu-MAN of Ebro Observatory of SEAC2, SOSS2 and ESOS3 for those days in which daily maximum temperatures ( $T_{max}$ ) is lower than 15 °C, 15-30 °C and upper than 30 °C and days in which daily minimum temperatures ( $T_{min}$ ) is lower than 10 °C, 10-20 °C and upper than 20 °C, it is also shown the mean of the  $\Delta T_{max}$  and  $\Delta T_{min}$  for the whole period.* 109

*Figure 4.4: Boxplots for maximum (left plots) and minimum (right plots) temperature difference series AWSu-MAN of Ebro Observatory of SEAC2, SOSS2 and ESOS2 according the stratification of the days depending the wind speed and the sunshine hours. W-O windy and overcast days, W-C (windy and clear days), C-O (calm and overcast days) and C-C (calm and clear days). On methodology (Page 89) to see the wind speed and sunshine hours thresholds.* 113

*Figure 4.5: Histogram of the daily maximum and minimum temperature differences AWSu-MAN of Fabra Observatory ( $\Delta T_{max}$  and  $\Delta T_{min}$ ) for the 6 HSPs detected.* ..... 117

*Figure 4.6: Seasonal boxplots of the  $\Delta T_{max}$  (upper plots) and  $\Delta T_{min}$  (lower plots) for the MCV1.2, MCV2.2 and Vaisala sub-periods, Fabra Observatory.* ..... 118

*Figure 4.7: Boxplots for maximum (upper plots) and minimum (lower plots) temperature difference series AWSu-MAN of Fabra Observatory of MCV1.2, MCV2.2 and Vaisala for those days in which daily maximum temperatures ( $T_{max}$ ) is lower than 15 °C, 15-30 °C and upper than 30 °C and days in which daily minimum temperatures ( $T_{min}$ ) is lower than 10 °C, 10-20 °C and upper than 20 °C.* ..... 119

*Figure 4.8: For the MCV1.2, MCV2.2 and Vaisala sub-periods (Fabra Observatory) the boxplots of  $\Delta T_{max}$  (left plots) and  $\Delta T_{min}$  (right plots) according the stratification of the day depending on the wind speed and the sunshine hours. W-O (windy and overcast days), W-C (windy and clear days), C-O (calm and overcast days), C-C (calm and clear days). See Table A2.5 (page 187) for the values.* ..... 122

*Figure 4.9: Histogram of the daily maximum and minimum temperature differences AWSu-MAN of Murcia Observatory ( $\Delta T_{max}$  and  $\Delta T_{min}$ ) for the 4 HSPs detected, SEAC4, SEAC3, SEAC2 and SEAC1, Table A2.6, page 188 to see the values.* ..... 125

*Figure 4.10: Seasonal boxplots of the  $\Delta T_{max}$  (upper plots) and  $\Delta T_{min}$  (lower plots) for the four HSPs detected in Murcia Observatory. DJF winter, MAM spring, JJA summer and SON autumn.* ..... 126

*Figure 4.11: Boxplots for maximum (upper plots) and minimum (lower plots) temperature difference series AWSu-MAN of Murcia Observatory of the four HSPs detected for those days in which daily maximum temperatures ( $T_{max}$ ) is lower than 15 °C, 15-30 °C and upper than 30 °C*

and days in which daily minimum temperatures ( $T_{min}$ ) is lower than 10 °C, 10-20 °C and upper than 20 °C. \_\_\_\_\_ 127

Figure 4.12: Boxplots of  $\Delta T_{max}$  (left plots) and  $\Delta T_{min}$  (right plots) for the four sub-periods determinate according the stratification of the day depending the wind speed and the sunshine hours. W-O windy and overcast days, W-C windy and clear days, C-O calm and overcast days and C-C calm and clear days. Page 89 to see the thresholds. \_\_\_\_\_ 131

Figure 5.1: Daily maximum (upper plot) and minimum (bottom) temperature differences applying (AWS<sub>c</sub>) or not (AWS<sub>u</sub>) the results of the calibration curve in Moncalieri Observatory. Dotted grey lines surround the calibration uncertainty range ( $\pm 0.32$  °C). Red and blue (dark red and dark blue) circles identify differences inside (outside) the calibration uncertainty. \_ 137

Figure 5.2: Histogram of the daily maximum and minimum temperature differences applying (AWS<sub>c</sub>) or not (AWS<sub>u</sub>) the calibration curve of Moncalieri Observatory observations ( $\Delta T_{max}$  and  $\Delta T_{min}$ ). In dark red and dark blue (for  $\Delta T_{max}$  and  $\Delta T_{min}$ ) the  $\Delta T_{max}$  and  $\Delta T_{min}$  outside the calibration uncertainty (0.32 °C) \_\_\_\_\_ 139

Figure 5.3: Boxplot of monthly maximum ( $\Delta T_{max}$ ) and minimum ( $\Delta T_{min}$ ) temperature differences applying (AWS<sub>c</sub>) or not (AWS<sub>u</sub>) the results of the calibration curve from the period 01/09/2012 to 31/08/2013 at the Moncalieri Observatory. Dotted line indicates the calibration uncertainty  $\pm 0.32$  °C. \_\_\_\_\_ 139

Figure 5.4: Daily maximum (upper plot) and minimum (bottom) temperature differences between the AWS calibrated and the AWS<sub>u</sub> uncalibrated (AWS<sub>c</sub> – AWS<sub>u</sub>) of Castello Borello field trial. Dotted grey lines surround the calibration uncertainty range ( $\pm 0.16$  °C). Red and blue (dark red and dark blue) circles identify differences inside (outside) the calibration uncertainty. \_\_\_\_\_ 142

Figure 5.5: Histogram of the daily maximum and minimum temperature differences between the AWS calibrated (AWS<sub>c</sub>) and the not calibrated (AWS<sub>u</sub>) of Castello Borello field trial observations ( $\Delta T_{max}$  and  $\Delta T_{min}$ ). In dark red and dark blue (for  $\Delta T_{max}$  and  $\Delta T_{min}$ ) the  $\Delta T_{max}$  and  $\Delta T_{min}$  outside the calibration uncertainty (0.16 °C) \_\_\_\_\_ 143

Figure 5.6: Boxplot of monthly maximum ( $\Delta T_{max}$ ) and minimum ( $\Delta T_{min}$ ) temperature differences between the AWS calibrated (AWS<sub>c</sub>) and the AWS uncalibrated (AWS<sub>u</sub>) from the period 21/09/2013 – 20/09/2014 at the Castello Borello Observatory. Dotted line indicates the AWS<sub>c</sub> calibration uncertainty  $\pm 0.16$  °C. \_\_\_\_\_ 144

Figure 5.7: Boxplot for maximum (left plot) and minimum (right plot) temperature difference series AWS<sub>c</sub> – AWS<sub>u</sub> of Castello Borello field trial for those days in which daily maximum temperatures ( $T_{max}$ ) is lower than 10 °C, 10-20 °C and upper than 20 °C and days in which daily minimum temperature ( $T_{min}$ ) is lower than 5 °C, 5-10 °C and upper than 10 °C. \_\_\_\_\_ 145

Figure 5.8: Paired daily maximum (left plots) and minimum (right plots) temperature differences AWSc - MAN (upper plots), AWSc - AWSu (middle plots) and AWSu - MAN (bottom plots) at the Ebro Observatory during the period 01/06/2013 to 31/05/2015. Horizontal grey lines represent the combined calibration uncertainty and vertical grey lines correspond to changes on AWSu. \_\_\_\_\_ 149

Figure 5.9: Histogram of the daily maximum (left plots) and minimum (right plots) temperature differences between AWSc - MAN (upper plots), AWSc - AWSu (middle plots) and AWSu - MAN (bottom plots) at the Ebro Observatory during the period 01/06/2013 to 31/05/2015. In dark red and dark blue (for  $\Delta T_{max}$  and  $\Delta T_{min}$ ) the  $\Delta T_{max}$  and  $\Delta T_{min}$  outside the calibration uncertainty ( $0.38\text{ }^{\circ}\text{C}$  for AWSc - MAN and  $0.16\text{ }^{\circ}\text{C}$  for AWSc-AWSu) \_\_\_\_\_ 150

Figure 5.10: Boxplot of monthly maximum ( $\Delta T_{max}$ , left plots) and minimum ( $\Delta T_{min}$ , right plots) temperature differences between AWSc - MAN (upper plots), AWSc - AWSu (middle plots) and AWSu - MAN (bottom plots) at the Ebro Observatory during the period 01/06/2013 to 31/05/2015. In dark red and dark blue (for  $\Delta T_{max}$  and  $\Delta T_{min}$ ) the  $\Delta T_{max}$  and  $\Delta T_{min}$  outside the calibration uncertainty ( $0.38\text{ }^{\circ}\text{C}$  for AWSc - MAN and  $0.16\text{ }^{\circ}\text{C}$  for AWSc-AWSu). \_\_\_\_\_ 151

Figure 6. 1: Boxplots for the hourly differences at 6h, 7h, 9h, 12h, 13h, 15h and 18h UTC for the differences AWSc - MAN correcting the AWSc observing times to the MAN observations  $\Delta T_h$  (upper left), without applying this correction  $\Delta T_{nh}$  (upper right) and AWSch and AWSu. \_\_\_\_\_ 158

Figure 6.2: Winter (upper plots) and summer (bottom plots) boxplots for the hourly differences at 6h, 7h, 9h, 12h, 13h, 15h and 18h UTC for the differences AWSc - MAN correcting the AWSc observing times to the MAN observations  $\Delta T_h$  (left) and without applying this correction  $\Delta T_{nh}$  (right) \_\_\_\_\_ 159

Figure 6.3: : Boxplots for the hourly temperature differences at 6h, 7h, 9h, 13h, 15h and 18h U.T.C AWSc - MAN for the AWSch (upper-right plot), AWSc taking the 5' mean centered (upper-left plot), AWSc taking the mean of the 5' before (bottom-left plot) and AWSc taking the mean of the 5' after (bottom-right). \_\_\_\_\_ 161

Figure 7.1: Seasonal breakpoint detection results of pairwise detection of HOMER for Moncalieri maximum ( $T_{max}$ ) temperature series. Triangles are the potential breakpoints (BPs). \_\_\_\_\_ 167

Figure 7.2: Annual evolution of the Moncalieri adjusted annual maximum (upper plots) and minimum (bottom plots) temperature series (grey thick line) for the 1866-2012 period, along with the homogenisation uncertainty bars for each year and the OLS (dotted line) and WLS (striped line) trends. \_\_\_\_\_ 171

<i>Figure A1.1: Image of the 4 wires Pt100 connected to the harness. Image source: A. Gilibert</i>	194
<i>Figure A1.2: Image of the computation unit installed in Ebro Observatory field trial. Image source: A. Gilibert</i>	196
<i>Figure A1.3: Image of the measuring and transmitting module installed in Ebro Observatory field trial. Image source: A. Gilibert</i>	196
<i>Figure A1.4: Image of the two antennas, (a) connected to the measuring and transmitting module and (b) connected to the receiving module. Image source: A. Gilibert</i>	197
<i>Figure A1.5: Image of the receiving module installed in Ebro Observatory field trial. Image source: A. Gilibert</i>	197
<i>Figure A1.6: The computer that stores the data and in which is installed the program which manages the temperature measurement system and transforms the data. Image source: A. Gilibert</i>	198
<i>Figure A1.7: Image inside the Stevenson Screen (in which there is installed the AWSc 1) and image of the Stevenson Screen and at rear the Young Screen (in which there is installed the AWSc 2). Image source: A. Gilibert</i>	198

## Associated Publications

### 1. Peer reviewed papers:

Bertiglia F., Lopardo G., Merlone A., Roggero G., Cat Berro D., Mercalli L., **Gilabert A.**, Brunet M., 2015. [Traceability of Ground-Based Air-Temperature Measurements: A Case Study on the Meteorological Observatory of Moncalieri \(Italy\)](#). *Int. J. Thermophys.* 36: 589-601 DOI 10.1007/s10765-014-1806-y

### 2. Papers not yet published:

**Gilabert A.**; Aguilar E; Brunet M; Lopardo, G; Merlone A.; Solé G.; Ashcroft L.; Bertiglia F. The transition to the Automatic Weather Stations (AWS) at the Ebro Observatory (North-eastern Spain), Part 1: understanding the characteristics of the AWS bias from daily air temperatures paired observations and exploring a metrological approach to minimise it. *In final preparation (Chapter 4 and 5)*

**Gilabert A.**; Brunet M; Lopardo, G; Merlone A.; Aguilar, E. Jones P.; Roggero G.; Bertiglia F.; Cat Berro D.; Mercalli L. Statistical analysis of combined metrological and homogenisation procedures to ensure enhanced temperature series traceability to international standards. *In final preparation (Chapter 5 and 7)*

**Gilabert A.**; Aguilar E; Brunet M; Lopardo, G; Merlone A.; Solé G.; Ashcroft L.; Bertiglia F. The transition to the Automatic Weather Stations at the Ebro Observatory (North-eastern Spain), Part 2: understanding the characteristics of hourly temperature AWS bias from paired observations. *In preparation (Chapter 6)*

### 3. Conference contributions:

#### 2015:

**Gilabert, A.**; Brunet, M.; Lopardo, G.; Merlone, A.; Aguilar, E.; Roggero, G.; Bertiglia, F.; Jones, P. A Joint-Metrological and Climatological approach to improve quality of climate time-series. International Symposium CLIMATE-ES 2015, 11-13 March 2015, Tortosa, Spain. (Oral Presentation)

**Gilabert, A.**; Brunet, M.; Lopardo, G.; Merlone, A.; Jones, P.; Beriglia, F.; Aguilar, E. Incorporating metrological calibration procedures to improve temperature data series quality and ensure their traceability. EGU General Assembly. 12 -17 April 2015, Vienna, Austria (Poster)

**Gilabert, A.**; Brunet, M.; Lopardo, G.; Merlone, A.; Aguilar, E.; Solé, G.; Roggero, G.; Berithlia, F.; Jones, P. An exploratory analysis of the impact of the changeover to automatic weather stations considering the primary national standards calibration procedures: Observatori de l'Ebre case study. International Symposium CLIMATE-ES 2015, 11-13 March 2015, Tortosa, Spain. (Poster)

**2014:**

**Gilabert, A.** Brunet, M., Lopardo, G., Merlone, A., Aguilar, E., Roggero, G., Beriglia, F., Jones, P. Exploratory analysis of the bias induced in temperature series related to the changeover to automatic observin systems: combining metrological and homogenisation techniques to estimate the uncertainty budget. International workshop on Metrology for Meteorology and Climate, 15-18 September 2014, Brdo, Slovenia. (Oral presentation)

**2013:**

**Gilabert, A.** Importance of the generation of quality measurements from the Himalaya data series for climate evolution analysis. A synergic cooperation in the frame of the MeteoMet project. Workshop and training at the Nepal Academy of Science and Technology, 10 September, 2013, Kathmandu, Nepal. (Oral presentation)

**Gilabert, A.**, Lopardo G., Brunet M., Merlone A., Aguilar E., Roggero G., Beriglia F. Incorporating metrology techniques to analyse and minimise the bias introduced in temperature series related to the automation of weather stations. 13th EMS Annual Meeting & 11th European Conference on Applications of Meteorology (ECAM), 9-13 September, 2013, Reading, United Kingdom. (Oral presentation)

**Gilabert, A.** Brunet M. Centre for Climate Change (C3) activities within the MeteoMet project - ENV07/REG5 MetoMet Workshop. Agencia Estatal de Meteorologia, 12 June, 2013, Madrid, Spain. (Oral presentation)

#### 4. Other work during the PhD thesis period:

##### Papers:

Merlone A.; Lopardo G.; Sanna F.; Bell S.; Benyon R.; Bergerud R. A.; Bertiglia F.; Bojkovski; J. Böse; N.; Brunet M.; Cappella A.; Coppa G.; del Campo D.; Dobre M.; Drnovsek J.; Ebert; V. Emardson; R. Fernicola; V. Flakiewicz; K. Gardiner; T.; Garcia-Izquierdo; C.; Georgin; E.; **Gilabert; A.**; GrykaBowska; A.; Grudniewicz; E.; Heinonen; M.; Holmsten; M.; Hudoklin; D.; Johansson; J.; Kajastie; H.; Kayk1s1z1l1; H.; Klason; P.; KHazovická; L.; Lakka; A.; Kowal; A.; Müller; H.; Musacchio; C.; Nwaboh; J.; Pavlasek; P.; Piccato; A.; Pitre; L.; de Podesta; M.; Rasmussen; M. K.; Sairanen; H.; Smorgon; D.; Sparasci; F.; Strnad; R.; Szmyrka- Grzebyk; A. and Underwood; R. 2015. [The MeteoMet project - metrology for meteorology: challenges and results](#) *Meteorological applications*. 22: 820-829 DOI 10.1002/met.1528

Brunet M. **Gilabert A.**, Jones PD. 2014. [A historical surface climate dataset from station observations in Mediterranean North Africa and Middle East areas](#). *Geosciences Data Journal*. DOI: 10.1002/gdj3.12

##### Datasets:

Centre for Climate Change / URV. (2015). C3-EURO4M-MEDARE Mediterranean historical climate data - v.2. Zenodo. [10.5281/zenodo.16702](#)

##### Capacity buildings and workshops:

International Workshop on the Recovery of Climate Heritage, Maputo, Mozambique, 21-24/4/2014

Taller Regional para la elaboración de Índices de Cambio Climático en Mesoamérica, Ciudad de Guatemala, Guatemala. 5-9/10/2015

Capacity building workshop on Quality Control and Data Homogenisation to Support Climate Assessments and Services in the Indian Ocean Rim Countries and Islands, Arusha, Tanzania, 9-14/11/2015

Medare Workshop and Training to develop high quality data sets in support of climate watch systems, 14-18/12/2015



**Participation in other projects during the PhD program:**

O-REG for the Parent JRP MeteoMet (ENV07/REG5).

European Reanalysis and Observations for Monitoring (EURO4M).

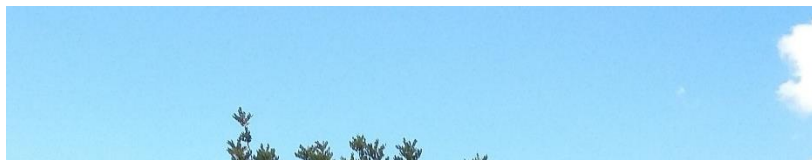
The World Meteorological Organization MEDiterranean climate DATA REscue (MEDARE) Initiative.

Parallel Observations Science Team (POST)

Determinación y ajuste del sesgo introducido por la automatización de las estaciones meteorológicas en las series climáticas (DAAMEC: CGL2012-32193)

Evaluación del impacto de las series de temperatura de las transiciones entre sistemas de observación (IMPACTRON: CGL2015-70192-REDT).

## Chapter 1 INTRODUCTION





## Chapter 1: Introduction

This chapter is divided into three parts. In the first section, the context of this thesis is presented; in the second section the aims and objectives are described; the third section describes the structure of this manuscript.

### 1.1 – Context

Climate is certainly a limiting factor for the environment and also for the development of most human activities. It is very important to study the climate to understand its current and future changes in order to develop adaptation measures and to try to minimise the negative effects of climate variability and human induced climate change. Despite these factors, we should first know how the climate has evolved in the past and how the different components were affected as well as the feedbacks between the different components.

Fortunately, interest in the climate and climate changes studies has increased in the last decades. In part for the implications that climate changes have on the environment but also on the different economic activities. The IPCC with the publication of the different Assessment Reports, the scientific contributions and the interest from the media in recent years, give more visibility to the problem and obviously, the constant consequences of a world in change have increased the interest of the general public on this topic. For all of these reasons, climate change is one of the hot topics in high level agendas, which means a constant and continuous demand for improved climate data and improved climate analysis. When discussing climate change issues, temperature is indeed the most studied variable.

The first thermometer was invented by Galileo Galilei (1564-1642) in 1597 improved later by Ferdinand II De'Medici, the Grand Duke of Tuscany, in close collaboration (1610-1670), who was the founder of the first meteorological network in the second half of the XVII century (Camuffo, 2002, 2010). The main characteristic of this first network was the accuracy to try to maintain the same measurement conditions across all stations. In this way, they do not only designed a network, they also gave some instructions on how to do the observations: the same type of thermometer, with the same (or the most similar)

thermometer exposure conditions, and also with the same observation practice (e.g., observation hours, regularity of the daily observations).

Since this first meteorological network, especially in Europe we can find others pre industrial climate time-series that in some cases maintain continuous observations to the present day. There are several stations in the Greater Alpine Region (GAR) (Auer *et al.*, 2007, Böhm *et al.*, 2001 and 2009), in Central England (Manley G. 1974, Parker *et al.*, 1992), in Italy (Brunetti *et al.*, 2006, Buffoni *et al.*, 1996 or Maugeri *et al.*, 2002), in Sweden (Bergström *et al.*, 2002 or Moberg *et al.*, 2002) and also some series out of Europe, for example, in Australia (Ashcroft *et al.*, 2012) or India that those stations started before the industrialisation in the 19<sup>th</sup> century. These datasets are very important to study the effect of industrialisation. After industrialisation, the number of stations increased, and we have a large number of climate data series that started in the second half of the 19<sup>th</sup> century, as is the case for the Spanish dataset, SDATS (Brunet *et al.*, 2006) or the Australian dataset (Ashcroft *et al.*, 2014). In America and Africa most part of the observations starts in the 20<sup>th</sup> century, although we can find several observations that starts at the end of 19<sup>th</sup> century. These historical networks are a reliable treasure for the study of climate. The real increase in the number of meteorological stations was with the introduction of the automatic weather stations (AWS).

These historical climatological time-series are regularly affected by random and/or systematic biases or inhomogeneities. A homogeneous climate time-series is that in which the time variations shown are mainly forced by weather and climate factors. Climate time-series homogeneity has been a hot topic since Conrad and Pollak (1950) showed the impact of diverse artificial biases in the observed records and the importance of ensuring their homogeneity through statistical homogenisation. Since the 1950s, the scientific community developed many homogenisation methods (Peterson *et al.*, 1998). Common causes having the potential to induce breakpoints (BP) in time-series homogeneity have been associated with relocations, changes in instrumentation and their exposure, changes in surroundings or in the observing procedures and schedules (Peterson *et al.*, 1998; Aguilar *et al.*, 2003). Among these causes, the worldwide changeover to automatic observing systems, especially AWS, has gathered much attention since its initial deployment (Anyuan *et al.*, 2006; Milewska *et al.* 2002; Quayle *et al.*, 1991; Wendland *et al.*, 1993). Weather station automation has enabled a remarkable increase in the spatial and temporal resolution of meteorological observations and in real-time data availability (Fiebrich *et al.*, 2009), but this

change has also incorporated systematic biases in temperature series that compromise their homogeneity and, therefore, it has reduced their robustness and reliability.

Recently, the EU-Cost Action HOME "Advances in homogenisation methods of climate series: an integrated approach" tested most of the currently available methods in a blind experiment against a realistically simulated benchmark (Venema *et al.*, 2012).

The most efficient approaches are the relative methods that involve comparisons between the candidate time-series and a set of reference series from nearby and well-correlated stations or with an estimated reference time-series using also nearby and well-related records for its generation (Venema *et al.*, 2012). This procedure considers the candidate and references series as having the same climate characteristics and the biases they contain are not simultaneous in their occurrence. For this, it is difficult to homogenise the different transitions in the observation conditions, as from the manual (MAN) to automatic weather stations (AWS) measurements, because in general, this transition (the same for other types of transitions, like changes on screen, relocations to airports) occurs at the same time in a network. To deal with this type of transitions, the common procedure is the study of the specific biases through parallel measurement series.

Many National Meteorological and Hydrological services (NMHS) do not apply standard metrological procedures to periodically calibrate their temperature measurement systems regarding the standard metrological procedures. Besides, it is not usual that studies based on temperature time-series consider the uncertainty estimation of the temperature measurement systems. For those reasons, the quality of these time-series can be compromised by the quality and the homogeneity and also by not adopting metrological procedures to ensure measurements traceability.

In addition, most of the currently available homogenisation methods have not integrated and analysed uncertainties associated with each estimated adjustments. Only a few studies have tried to determine the uncertainty of data homogenisation and analyse the goodness of adjustments, as is the case of Brohan *et al.* (2006), Willet *et al.* (2013, 2014) or Zhang *et al.* (2012). This PhD thesis intends to contribute to solve these problems.

## 1.2 – Research aims and objectives

The thesis hypothesis states that transition to the AWS introduces a bias to the temperature time-series. Different authors have analysed parallel records and found some differences between the older manual (MAN) and the new AWS observations. Thus, our principal objective is to analyse these differences and extract the characteristics of the AWS bias introduced in air-temperature time-series. The novelty of this thesis respect to the other studies that deal with this AWS bias is to study this transition not only from the climatological (statistical approach) point of view, but also by introducing metrological procedures (experimental approach) and the metrological knowledge in order to understand better what a measurement is and how to improve these measurements to minimise or smooth the AWS transition. The second objective is to give a complete traceability to the historical time-series to improve their reliability to the climate and climate change studies.

To achieve these goals, the scientific and technical specific objectives can be divided in three blocks:

1. Statistical analysis of the AWS-MAN transition using historical air-temperature time-series without the introduction of the metrological standard procedures:
  - Detection of homogeneous subperiods in the parallel measurements.
  - Characterise the AWS-MAN transition with the homogeneous sub-periods (HSP) determined by the previous sub-objective, at a daily scale. This analysis will involve not only the mean differences, but also the differences associated with extreme temperatures and different weather conditions.
2. Analysis of the introduction of the metrological procedures to minimise first the AWS-MAN transition and secondly, to give traceability to the historical temperature time-series.
  - Installation and exploitation of an AWS in a historical site (more than 100 years of air-temperature measurements).
  - Management of the field trial and maintain the AWS in standard conditions, collecting, organising and conducting quality control of the different parallel measurements.

- Evaluation the advantages of the introduction of the metrological standard procedures to the AWS measurements, at the daily scale.
  - Characterisation of the AWS-MAN transition with the double comparison AWS calibrated (AWSc) – MAN, AWS uncalibrated (AWSu) – MAN at daily scale. As in the previous block, the daily mean differences if not also the differences will be analysed as well as the differences associated with the extreme temperatures and different weather conditions.
  - Characterisation of the AWSc – MAN differences at hourly scale, due to the different temperature measurement systems and observation conditions.
3. The integration of the metrological and climatological methodologies in order to ensure a complete traceability and uncertainty budget of air-temperature time-series.
- Homogenisation of the montly maximum and minimum air-temeperature series of Moncalieri (1866-2012)
  - Development of a preliminary approach to determine the homogenisation plus measurement uncertainty.



### 1.3 – Thesis structure

This thesis is divided into eight chapters plus appendices. This **first chapter** contains the research context and the research aims and objectives.

**Chapter 2** – The air temperature time-series – is also divided into four parts. Metrological concepts are introduced, together with the standard metrological procedures that can help to improve the reliability of the air-temperature time-series. Related with this, the second sub-section of chapter 2 is the metrology of temperature measurements, including information about the device for the air-temperature measurements and how to give traceability to these measurements with the application of the standard metrological procedures. The third sub-section is the background of other studies that use parallel measurements to assess another type of transition, and that deals with this AWS-MAN bias. In the last sub-section identified research gaps are discussed.

In **Chapter 3** – Field trials, data and methodology - there is information about the field trials designed for this thesis and for the MeteoMet/REG5 project, as well as data and methodology applied in this thesis. The data and methodology sub-sections are organised following the order of the results chapters (Figure 1.1).

The results are then organised in the next four chapters:

- **Chapter 4** – Assessing the statistical characteristics of the AWSu – MAN differences, presents three Spanish parallel measurements (Ebro observatory, Fabra observatory and Murcia observatory) to give the main characteristics of these differences.
- **Chapter 5** – Can the metrological approach improve the quality of the temperature time-series? – Daily data. In this chapter the data of the three field trials are used, in order to provide replies to the following two questions: can metrology improve the quality and reliability of the temperature time-series? Finally, can the introduction of the standard metrological procedures minimise or even smooth the AWS bias?
- **Chapter 6** - Assessing the differences AWSc – MAN at hourly scale. This chapter discusses the characteristics of the AWSc - MAN bias at the hourly scale
- **Chapter 7** – Giving traceability to the historical temperature series, gives a first approximation of the complex problem of providing traceability to the individual

historical temperature measurements combining the homogenisation plus instrumental uncertainties

In the last **chapter 8**, there are the conclusion, the discussion and some ideas further work.

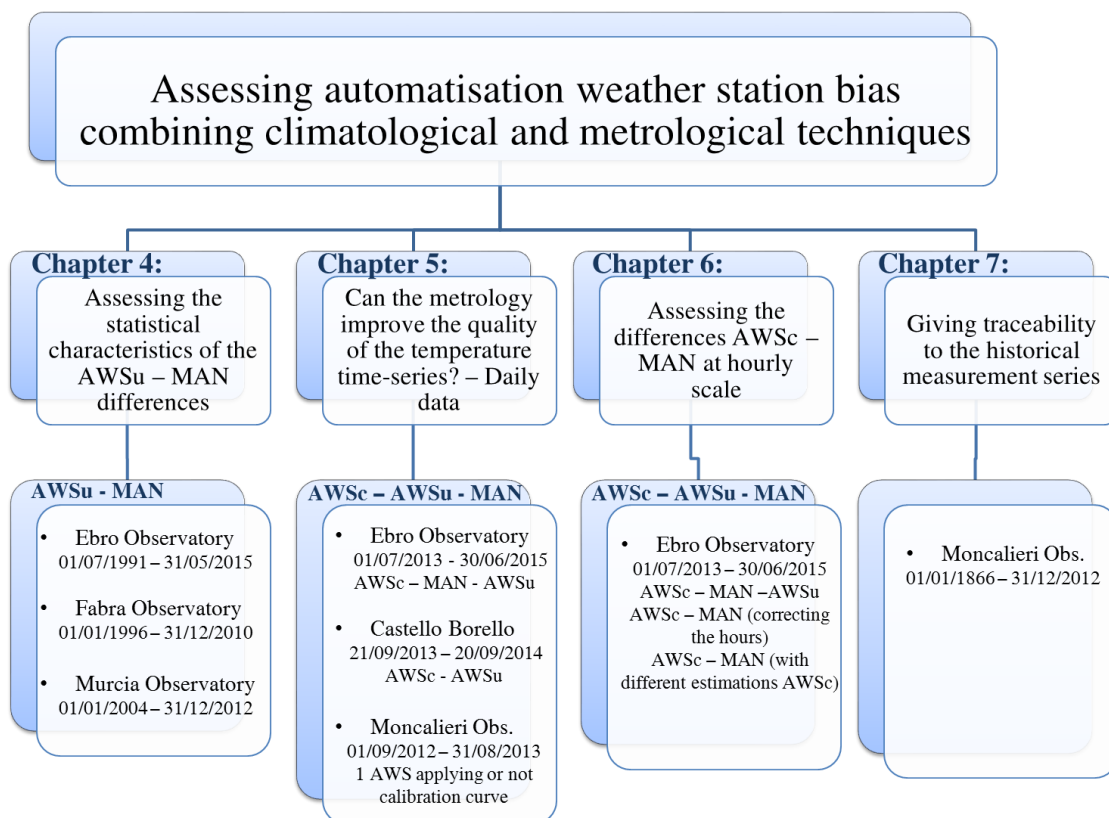


Figure 1.1: Thesis schematic. In the second level the different results chapters and in the third level the data used to assess the questions of every chapter



## Chapter 2 – The air temperature time-series





## Chapter 2: The air temperature time-series

This chapter is divided into three parts. First, some basic concepts and procedures of metrology are explained. Second, it is described how to apply these concepts and procedures so as to improve the reliability of air temperature time-series. Third, it is explained the impact of the AWS and other types of transitions on air temperature time-series. And lastly, from the previous parts some research gaps are identified.

### 2.1 – Metrology

Metrology is the science of measurements and its application (JCGM, 2012). The metrological community is in charge of defining and maintaining the international units system and their standards. Therefore, the introduction of metrological procedures can improve the measurement of temperature or any other climatic variable ensuring the measurement traceability. Only adopting these procedures can allow the comparability of different measurements and the regional and global climate time-series comparability.

Metrology became a discipline in 1875 when the *Convention du Metre* was signed and the *Bureau International des Poids et Mesures* (BIPM) was funded. The BIPM together with the National Metrological Instituts (NMIs) are responsible for maintaining the International System of Units (SI) in a way to ensure that the units will be stable over time and, most importantly, uniform worldwide to permit the comparability of the measurements among nations.

The World Meteorological Organisations (WMO) and the BIPM started a joint cooperation study in 2010 to encourage the adoption of metrological procedures in both conventional and automatic observing systems. In this way, the *Guide to Meteorological Instruments and Methods of Observations* (WMO, 2010) elaborated by the WMO Commission for Instruments and Methods of Observations (CI-MO) includes some of the definitions from the *International Vocabulary of Basic and General Terms in Metrology* (JCGM, 2012) developed by the Joint Committee for Guides in Metrology (JCGM).

### 2.1.1 – What is a measurement?

The JCGM 2012 guide defines measurement as the *process of experimentally obtaining one or more quantity values that can reasonably be attributed to a quantity*. Then, the objective of a measurement is to determine the value of some quantity and the result of this measurement should be such as: number + uncertainty + measurement unit (e.g.:  $21.6 \pm 0.1$  °C). We understand quantity as *the property of a phenomenon, body or substance, where the property has a magnitude that can be expressed as a number and a reference* (JCGM, 2012). And a measurand is *quantity intended to be measured*.





In every measurement we have to ensure the measurement reliability, so the measurement result should be independent of the instrument, of the measurement method, of the measurement procedure and of the conditions under which the measurement is carried out. The confidence in the correctness of the measurement is based on international agreements, continuous checks and quality control.

The metadata of measurements also have to give information about the measurement procedure, the measurement principle (as for example the thermoelectric effect applied to the measurement of temperature), the measurement method (direct or indirect) and any calculation applied to obtain a measurement result.

The measurement can therefore be characterised by different factors:



- The **measurement accuracy** and **measurement precision** (Table 2.1): the first term refers to the closeness between a measured quantity value and the true quantity value of a measurand, and it is a qualitative term. It cannot be expressed as a quantity. On the other side, the measurement precision refers to the agreement between measured values obtained by repeated measurements under the same or similar conditions.

Table 2.1: Difference between measurement accuracy and measurement precision shown by the distribution of golf balls depending on a high and low accuracy and a high and a low precision

		Accuracy	
		Accurate	Not accurate
Precision	Precise		
	Not Precise		

- The **repeatability** and **reproducibility** of measurement (Table 2.2). Repeatability refers to the closeness of agreement between the results of successive measurements of the same measurand carried out under the same measurement conditions and with the same procedure. Reproducibility is the closeness of agreement between the results of different measurements of the same measurand but carried out under different measurement conditions with -different measurement methods, observers, measurement instrument, measurement time, etc.

Table 2.2: Difference between repeatability and reproducibility condition of measurement

High repeatability Low reproducibility	Low repeatability Low reproducibility
	



### 2.1.2 – Instrument device

A measurement instrument is a device used for making measurements (JCGM, 2012). Sometimes the measurement instrument can be used alone, such as the liquid-in-glass thermometers, or in other cases, the measurement is taken by different devices and, can be composed by using a measuring instrument plus another components, where all parts form the measuring system, as the AWS.

Different factors characterises the measuring instruments and measuring systems (JCGM, 2012):

- The **measuring interval** is the set of values of quantities of the same measurand that can be measured by a measuring instrument or measuring system under specified conditions.
- The **limiting operating conditions** are the extreme operating conditions in which a measuring instrument or measuring system can work without any damage or degradation.
- The **step response time** is the duration between the instant in which a quantity value of a measuring system changes and the instant when the indication varies and maintains within specific limits around its final steady value.
- The **resolution** is the smallest quantity variation being measured that can be perceived by the measuring instrument or measuring system (it is the last digit in a digital instruments and it is generally the half scale interval in an analogic instrument).
- The **sensitivity** is the relationship between the change in sensor response and the corresponding variation in a value of a quantity being measured.
- **Stability** of a measuring system and the **instrumental drift**. The stability is ability of the measuring instrument or measuring system to maintain its constant metrological characteristics in time (the more stability a measuring instrument has, the more spaced the periodic calibration can be). The instrumental drift is the continuous or incremental change over time in measurements due to changes in metrological properties of the measuring instrument or measuring system.

- The **hysteresis** is the dependence of the measuring instrument or measuring system on thermal cycles, or on the previous temperature. For example, the hysteresis of a maximum and minimum liquid-in-glass thermometer is generally larger than the hysteresis of a Pt100 resistance.
- The **linearity** is the accuracy of response over a measurement range.

### 2.1.2 – Calibration and traceability

The WMO (2010) indicates that the calibration is *an operation that, under specified conditions, tries to establish a relation between the observations taken by the sensor under scrutiny and the reference sensor*. Using this information, one can establish a relationship between both to correct the observations taken by the sensor under scrutiny (Bertiglia *et al.*, 2015).

This standard procedure is not the same as with in-situ comparison, the most common procedure in most national weather services (Lopardo *et al.*, 2012). These on site comparison are only a verification that the sensor is working appropriately. In the case of a sensor malfunction or larger differences between the two, the sensor is generally replaced by a new one or a correction is applied, losing the data traceability and introducing possible BPs in the data-series. The calibration, in the case of the temperature sensors should be done in a climatic chamber, in order to try to correct the observations and to maintain the instrument in a proper working state. In addition, the calibration should cover the temperature range that the instrument has to cover. Conversely, comparisons are usually done only for a limited range of values and the instrument cannot be corrected. Therefore, calibration of the temperature sensors is required to guarantee the traceability of the measurements and to improve their quality.

The CIMO Guide defines traceability as *a property of the result of a measurement or the value of a standard whereby it can be related to stated references, usually national or international standards, thorough an unbroken chain of comparisons all having stated uncertainties* (WMO, 2010). In other words, metrological traceability is a straightforward connection between a measurement made in the field and a measurement made in a calibration chamber following the national pattern. Traceability ensures that different instrumentation in use in different countries at different times produces reliable, repeatable, compatible and comparable measurement results. Moreover, these

measurements are metrologically traceable and linked to the internationally accepted measurement reference. Therefore, calibration of the temperature sensors is required to guarantee the traceability of the measurements and enables full confidence in the measurements results and in its time-series. Figure 2.1 provides a traceability diagram, which illustrates the unbroken chain of comparisons from the Unit Definition of International System of Units (SI) to the Measuring System and as an illustration the traceability diagram of a Platinum Resistance Temperature (PRT) sensor.

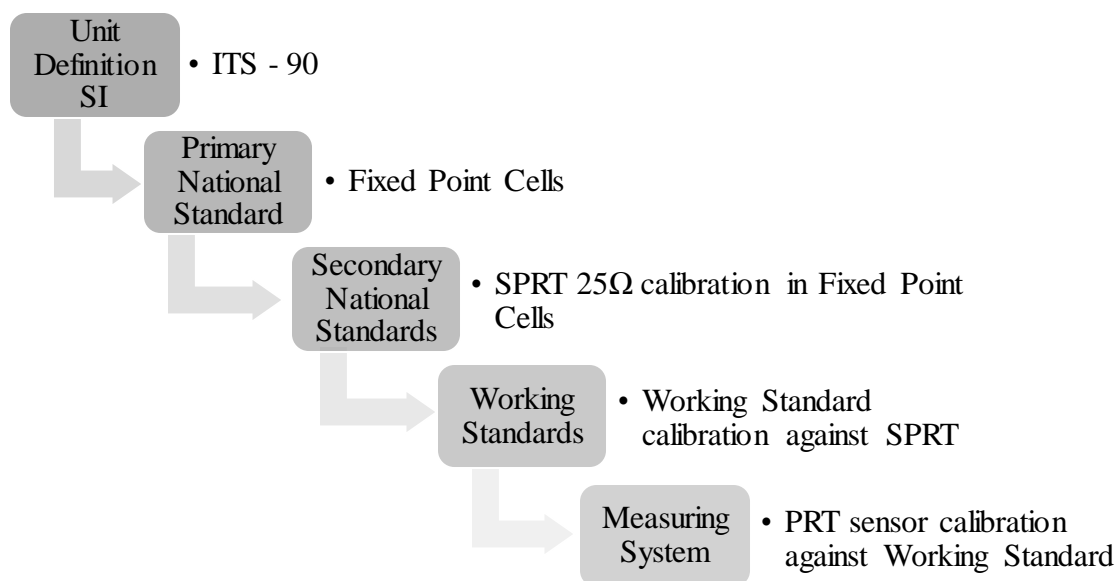


Figure 2.1: Traceability diagram for the Measuring System (in this case, a Platinum Resistance Temperature (PRT) sensor) showing the unbroken chain of comparisons from the Unit Definition of International System of Units (SI) (the International Temperature Scale of 1990 (ITS-90)). See section 2.1.2 for more details.

There are different types of metrological laboratories, classified hierarchically according to the measuring standard quality. The primary or national laboratories are the ones that have the primary national standard and the national measurement standards. The secondary or intermediate laboratories are typically the university or research centres laboratories. Finally, industrial laboratories are those in the factories for quality control checks and prototype tests.

There are also different measurement standards, which are classified hierarchically as well. The **Primary measurement standard** is established by using a primary reference measurement procedure or created as an artefact depending on the quantity. In the case of temperature, the Primary National Standard are the Fixed Point Cells. These fixed point

cells are stabilised to the different fixed temperature points defined by the International Temperature Scale 1990 (ITS-90). Figure 2.2 shows a picture and a diagram of a water triple point cell. These cells are cylindrical quartz glass containers that reproduce the triple point temperature (0.01 °C) in which water can exist with its solid, liquid and gas phases in equilibrium.

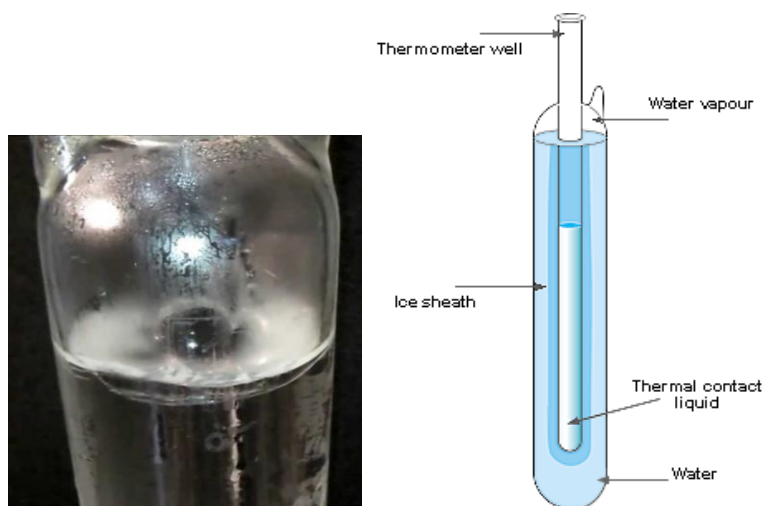


Figure 2.2: Picture of a water triple point cell and diagram of this cell. Image source: [www.campbellsci.com](http://www.campbellsci.com) (last visit: June 2016)

The **Secondary Measurement Standard** is established through calibration with respect to a Primary Measurement Standard. In the case of temperature calibration, the secondary measurement standard is a Standard Platinum Resistance Thermometer 25 $\Omega$  (SPRT 25 $\Omega$ ), which must be free of mechanical tensions and made of pure platinum (Figure 2.3).



Figure 2.3: Picture of a Standard Platinum Resistance Thermometer (SPRT 25 $\Omega$ ). Image source: INRiM

The **Working Measurement Standard** is calibrated with respect to a Secondary Measurement Standard and is routinely used to calibrate or verify measuring systems. The

**measuring system** or **measuring instrument** is calibrated with the working measurement standard; Figure 2.4 shows a conventional Platinum Resistance Thermometer 100  $\Omega$  (PT100).



Figure 2.4: Platinum Resistance Thermometer (Pt100). Pt100 installed in Ebro Observatory field trial. Source image: A. Gilibert

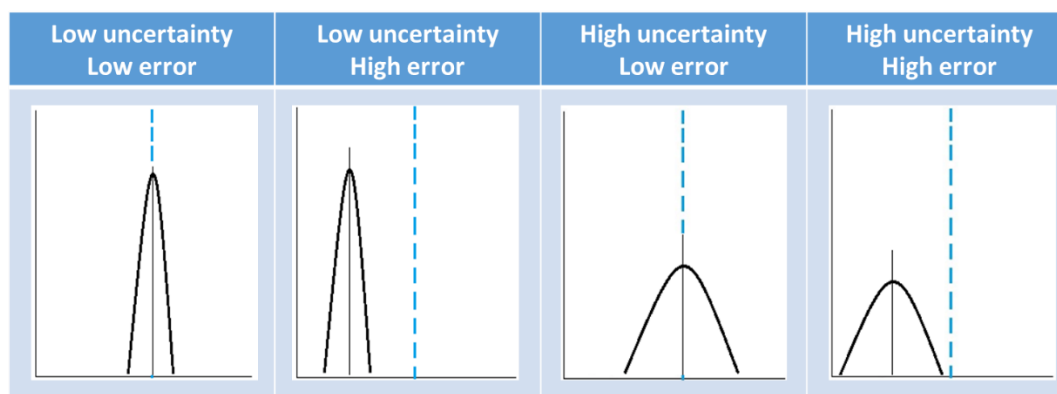
Through this unbroken chain of comparisons, the calibration procedure is generated an uncertainty that have to be considered to give a complete traceability to a measurement.

### 2.1.3 – The Uncertainty

The JCGM, 2012 defines measurement uncertainty as a *non-negative parameter characterising the dispersion of the quantity values being attributed to a measurand based on the information used*. In other words, the uncertainty given to the result of a measurement is a quantitative indication of the quality of the results, without which, we cannot compare the results with other reference values or with other measurements. In all the cases, a measurement result has to be expressed by a single measured quantity value and its measurement uncertainty.

We cannot confuse measurement uncertainty with measurement error (Table 2.3), because a measurement error is the difference between the measured value and the true value whereas the uncertainty is a quantification of the doubt about the measurement results. Thus, errors can be corrected, for example with the application of the calibration results and the uncertainty only can be estimate. And the uncertainty gives as information about the accuracy of the measurement system or measurement instrument.

Table 2.3: A shematic illustrating the difference between measurement error and measurement uncertainty. Is shown that the distribution of the observations depending on the low and high error and low and high uncertainty. The dashed blue line indicates the true value.



Generally the evaluation of the uncertainty budget is based on the probability distribution and composed by different components that can be classified as two types according to the way that they are estimated.

- The **Type A uncertainty** is based on the results of any valid statistical method for treating data and is estimated by using a measure of the spread of the observations to quantify the random effects of the measurement. Type A uncertainty is, therefore, the result of the analysis of repeated observations.
- On the contrary, the **Type B uncertainty** is the method used to assess uncertainty by means other than the statistical analysis of series of observations evaluated by a Type A uncertainty. We can distinguish two ways for the analysis of the Type B uncertainties: the estimation of the uncertainty based on the external information, such as from past experience, manufacturer specifications; or calibrations certificates, or what can be gained from an assumed distribution.

However, the metrological community is debating on a future different classification of uncertainties that overcomes the currently limited Type A and Type B definitions.

## 2.2 – Metrology of temperature measurements

According to WMO (1992) air temperature is defined as *the temperature indicated by a thermometer exposed to the air in a place sheltered from direct solar radiation*". This implies there are mainly two factors influencing air-temperature measurements: the thermometric measurement system and its radiation shield, which both have to ensure a correct coupling with the atmosphere (Hubbard *et al.*, 2005). So largely, the reliability of air temperature measurements is determined by the quality of the thermometric measurement systems. This denotes the need for standardising these measurements and ensuring their traceability to the international standards. In this way, the WMO Guide 2010, explains the general requirements for meteorological instruments is that these should be able to maintain known uncertainty over a long period. This is much better than having a high level of initial confidence (meaning a low uncertainty value) that cannot be retained for long under operational conditions.

### 2.2.1 – The International Temperature Scale of 1990 (ITS-90)

ITS-90 defines the unit of temperature and the way to realise the temperature scale in different sub-ranges (Preston-Thomas, 1990). ITS-90 has been constructed in such a way that for any given temperature, the numerical value given from this scale (an empirical value) is a close approximation to the numerical value of the thermodynamic temperature (based on invariant physical laws) according to best estimates at the time the scale was adopted. For this reason, the scale is periodically updated. The previous versions date back to 1927, 1948 and 1968.

ITS-90 covers the temperature range from 0.65 K to the highest temperature the Planck radiation law states can be measurable. The ITS-90 is composed of different ranges and sub-ranges throughout each  $T_{90}$  (Kelvin temperature) are defined. Some of these ranges or sub-ranges overlap, so in these cases, we dispose of different definitions of  $T_{90}$ . Generally, it is maintained from the triple point of mercury (-38.8344 °C) to the freezing point of silver (961.78 °C). Figure 2.5 shows the diagram of the different fixed points that define the ITS-90. The fixed points are based on various thermodynamic equilibrium states of different pure chemical elements, most of them based on stable temperature during phase transition, as these fixed points are reproducible and repeatable. The triple point of water (0.01 °C) is the most important fixed point.

The unbroken chain of comparisons shows that the SPRT25Ω thermometers are calibrated from different fixed point cells and using interpolation function of the different fixed points. The meteorological range is between the triple point of mercury (-38.8344 °C) and freezing point of indium (156.5985 °C). The temperature is determined in terms of the ration of resistance  $R(T_{90})$  at temperature  $T_{90}$  and the resistance  $R(273.16K)$  at the triple point of water:  $W(T_{90}) = \frac{R(T_{90})}{R(273.16K)}$  (Eq. 2.1) and the interpolation function are defined according to the range of temperatures.

- From -200 to 0°C:  $R_t = R_0 [1 + A t + B t^2 + C (t-100) t^3]$  (Eq. 2.2)

- From 0 to 850 °C:  $R_t = R_0 (1 + A t + B t^2)$  (Eq. 2.3)

where:  $A = 3.90802 \cdot 10^{-3} \text{ } ^\circ\text{C}^{-1}$ ;  $B = -5.802 \cdot 10^{-7} \text{ } ^\circ\text{C}^{-2}$ ;  $C = -4.27350 \cdot 10^{-12} \text{ } ^\circ\text{C}^{-4}$

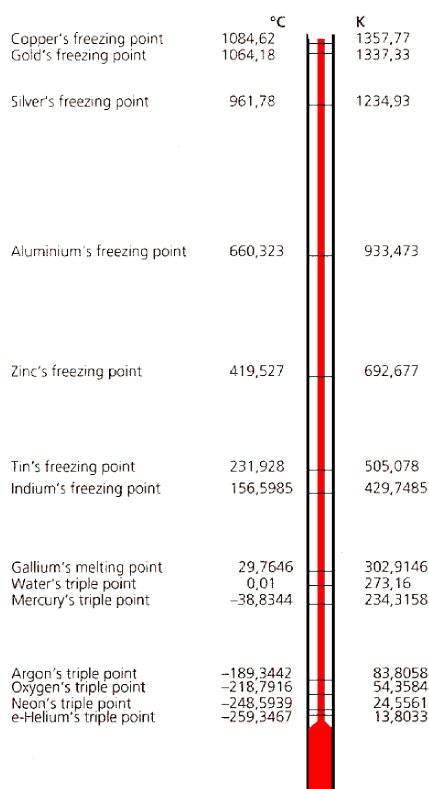


Figure 2.5: Diagram of the most important fixed points that defines the International Temperature Scale of 1990 (ITS-90). The most important is the Water's triple point. Image source: [www.electro-optical.com](http://www.electro-optical.com) (last visit: June 2016)



## 2.2.2 – From the liquid-in-glass thermometers to the PT100

From the first thermoscope of Galileo Galilei to current temperature sensors there has been a continuous evolution of the temperature instruments. All of these thermometers are contact thermometers that are based on the principle of change of some of their characteristics as a result of a change of temperature. We can classify temperature measurement instruments depending on the sensitive element:

### a. Liquid-in-glass Thermometers

These thermometers are the first uses and rely on the expansion of a liquid; the liquid volume depends on the temperature changes. Depending on the temperature range in which the thermometer operate, the liquid used is different, generally mercury or alcohol. The main parts of a liquid-in-glass thermometer (Figure 2.6) are the bulb, the liquid column, the scale, the stem, the meniscus, the capillary tube and the expansion chamber.

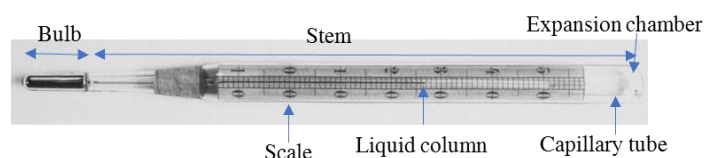


*Figure 2.6: Image of a Fuess Liquid-in-glass thermometer. This image shows the following different parts of this type of thermometer: the bulb, the stem, the scale, the liquid column, the capillary tube and the expansion chamber. Image source: Fuess*

For meteorological observations, we can distinguish four thermometers: the ordinary thermometers, the maximum and minimum liquid-in-glass thermometers and the soil thermometers. The ordinary liquid-in-glass thermometer registers the instantaneous temperature.

Conversely, the maximum thermometer has a constriction in the tube near the bulb. When the temperature increases, the mercury expands and passes this constriction but when the temperature decreases it cannot return to the bulb, so it marks the maximum temperature. The minimum thermometers contain an enamel index in the liquid. This index is forced to move with the bulb when the temperature decreases,

but then, when the temperature increases this index cannot move, marking the minimum temperature (Figure 2.7).



*Figure 2.7: Fuess maximum and minimum liquid-in-glass thermometers, installed in Ebro Observatory. Source image: A.Gilabert*

Some advantages of these thermometers are their easy of use, the most economical price, the high repeatability and the fact that a power supply is not required. On the contrary, some significant disadvantages are the need to conduct manual readings, the maximum and minimum liquid-in-glass thermometer is required to be reset every day. The observations also cannot be automated, which introduces subjectivity on the readings and finally, the limited observational frequency.

#### **b. Mechanical thermographs**

The thermograph is usually composed of a pen, a revolving cylinder and a bi-metal strip. The sensitive element due to the temperature changes is the bi-metal strip that bends depending on the temperature, expands with increasing temperatures and contracts with decreasing temperature.

An amplification system then transmits these tiny movements to the tip of the arm. In this tip of the arm there is a pen that draws the variations over the band. The last part of the system is this band that rolls on a drum which rotates driven by a clockwork system, allowing the user to know the temperature in every moment. Figure 2.8 shows a thermograph in which we can see the different parts that make up the temperature measurement system.



*Figure 2.8: A thermohygrograph. We can see the arm and the pen, the band and the drum that rotates driven by a clockwork system. Source image: Ebro Observatory*

This system also has some strengths and weakness. The main strength with respect to the thermometers are that this system records the temperature continuously and automatically. The main weakness is the maintenance of this system which is more complicated than for the thermometers, because weekly, it is necessary to change the band manually, and experimental staff member has to put the pen in the correct location and the time control, there are not any external signal.

### **c. Electrical thermometers**

The electrical thermometers, as a result of their ability to provide an output signal that can be stored, transmitted or/and sent remotely. They also give the possibility to increase the number of temperature stations and especially measure the temperatures in remote places.

Basically there are two types of electrical thermometers (WMO, 2010): the thermocouples and the electrical resistance thermometers.

- The thermocouples are the first electrical thermometers, which were discovered in 1821 by Seebeck. The thermocouples consist of two wires of different metals. The extremes of these wires are welded together, creating a junction. This junction is used to measure the temperature. When the temperature changes, also the junction has a change and a voltage is generated. This voltage can be transformed to a temperature with a thermocouple reference tables. There are different types of thermocouples according to the metals used.

- The electrical resistance thermometers are the more commonly used nowadays. The type of sensitive element in this kind of thermometer is a resistance that varies in a known manner with the temperature variations. Generally, the most frequent resistance material is platinum, because it is very stable, precise, linear, easy to obtain in a pure state, ductile and resistant to corrosion. Other metals used are copper and nickel. Copper is stable and inexpensive but has a lower sensitivity, whereas nickel has lower resolution than the platinum. The platinum resistance name is PtX, as Pt is the chemical symbol of platinum and X the resistance value in ohms at 0°C, Pt 100, Pt 25, Pt 1000. This resistance has to accomplish some requirements, such as:
  - Its physical and chemical properties should remain unalterable through the temperature measurement range.
  - Its resistance has to react without any discontinuity to the temperature increase – decrease through the temperature measurement range.
  - Its resistance cannot be altered by external influences such as humidity or corrosion.
  - Its metrological characteristics will be stable over a large period, around one to two years. After this period, they should be recalibrated.

### 2.2.3 – What is an Automatic Weather Station

We see that the electrical thermometers allow us to record the output signal, store the data and give us the possibility to transfer the observation remotely. Nevertheless, these electrical thermometers are only the sensitive element, other parts make up the temperature (and/or other climatic variables) measurement systems.

The WMO, 1992 defines AWS as a *meteorological station at which observations are made and transmitted automatically*.

The apparition of the AWS has really marked a turning point in the meteorological observations. They give us the possibility to increase not only the spatial resolution but also the temporal resolution. No doubt that societies benefit from the density and time resolution of AWSs, but when they replace long-term manual records, the time series used by climatologist degradate and become inhomogeneous.

The main strengths of these AWS are the real-time continuous observations (0-24 h 365 days), automatic data archiving, higher resolution, free from subjectivity, access to archived data remotely or data collection from remote sites and harsh environments.

Their main weaknesses are the impossibility to observe some of the parameters, such as the clouds type and average, the need of more frequent maintenance and calibration, compared to manual systems, and the need of well trained technicians for the start-up and maintenance and the high cost of instrumentation and operation.

The AWS are composed by different parts. To see as a graphical form the various components, in the annexes (A.1 – Ebro Observatory temperature measurement systems installed, page 194):

a. The **sensor**.

Usually, for the temperature observations, the AWS are equipped by a pure metal resistance thermometer, generally this metal is platinum, a Pt100 for their good long-term stability.

b. The **Central Processing Unit (CPU)**.

The other most important part is the CPU. The main functions of this unit are: data acquisition, data processing and data transmission. These functions can be done only by one microprocessor-based system or by different units. Generally, this unit is located in the meteorological garden as closest to the sensors as possible.

- The data acquisition hardware is also composed by two parts. The signal conditioning and the data acquisition function. The signal conditioning is one of the critical parts, it's composed by the sensor cables, is very important to avoid the unwanted noise. The data acquisition function consist in translate the sensor output to a signal readable by a computer, which is generally done by an Analog to Digital Converter (A/D converter)
- The data processing is carried out by the CPU or by the sensor interface of by the combination of both. The main function of this part is control the input/output of data. Some of the operations are the initialisation, the sampling and filtering, raw data conversion, quality control, data storage, data display.

- The data transmission, there are different ways to connect the CPU's and the way chosen have to take into account especially the distance between the elements. Can be only real time communication (cabled communication) or also wireless communication (radio modem).

c. **Other basic components**

The most important, and in some cases the limiting factor is the power supply, sometimes it can be generated by solar panels if the station is in remote sites, but it's very important to maintain a continuous power supply and protect the AWS for damages. Other basic components can be the RS485 to RS232 converters or another type of converters.

#### **2.2.4 – Temperature instruments and measurement systems calibration, giving traceability to air temperature time-series**

As is explained in the previous section, the calibration procedure is crucial to ensure that the measurement system or instrument system is free of errors but also to give traceability to the data, a very important fact, especially to ensure the comparability of our results between different measurement systems.

Mainly, the calibration can be done: in a liquid bath or in a climatic chamber. For the latest, we also can find the portable climatic chamber. This liquid bath and climatic chambers keep measured quantities (in our case temperature) stable during the calibration procedure in each measuring point and uniform into the chambers.

The goal of the climatic chambers is that the instrument is calibrated under more similar operation conditions than if it's calibrated into a bath. On the other side, in the last years, there are developed different portable climatic chambers that allow us *in situ* calibration campaigns (Lopardo *et al.*, 2015).

As seen with the traceability diagram (Figure 2.1), the calibration of the Pt100 can be done by comparison with a working standard or another standard like the SPRT25 $\Omega$  to reduce the calibration uncertainty; this will be the reference instrument. For the calibration, we also need a data acquisition unit (for the reference instrument), generally a multimeters.

One of the most important factors during the calibration is the controlled temperature medium; this means that not into a bath, not into a climatic chamber, the temperature is

completely stable in time and homogeneous all over its volume. So one of the limiting factors is the time stability and spatial homogeneity, which is the gradient observed into a climatic chamber.

For the calibration we have to define the number and the distribution of the measuring points. For example, for a temperature measurement range from -10 °C to 40 °C, we can define 6 measuring points every 10 °C (-10 °C, 0 °C, 10 °C, 20 °C, 30 °C and 40 °C). Another important point to define is the number of repeatability and frequency of measurement in each measuring points (for example 10 measurements and the frequency every minute). For all of this, it's obtained a correction linked to the calibration standard.

The main sources of calibration uncertainty are due to the resolution of calibrated instrument, repeatability, time stability and spatial homogeneity of calibration bath or climatic chamber and uncertainty contribution of data acquisition unit.

However, to assess a complete air-temperature measurement uncertainty (the measurement uncertainty) is necessary to consider others sources of uncertainty. For example the uncertainty related with the screen, the uncertainty related with the siting, observation practice... Consequently, the investigation on this topic has to continue and also the joint work between the three communities: metrological, climatological and meteorological.

### **2.3 – The impact of the transition to automatic weather observing systems in temperature series**

Being aware of the potential impact over the homogeneity of long-term records that the transition from MAN to AWS observing systems can have on the combined series using both sources of data, the WMO - CIMO recommend to conduct parallel observations to ensure a smooth transition to the new observing system (WMO, 2010). Therefore, long records with historical temperature observations provide a valuable opportunity to assess the impact of the AWS.

#### **2.3.1 – Assessing the non-climatic inhomogeneities through the study of parallel measurements.**

With the relative homogenisation methods it is difficult to adjust inhomogeneities occurring almost simultaneously across a network, such as instrument replacement, times of observations or sitting changes. But these types of inhomogeneities also have an important impact on the studies of daily extremes because some of them have a larger effect on the tails of the distribution than on the mean. One of the ways to avoid this impact is the study of this type of non-climatic inhomogeneities through parallel measurements. With simultaneous observations we can determine the magnitude and size of the differences between the old and the new measurement conditions and attempt to correct or minimise these inhomogeneities.

To this end, a Parallel Observations Science Team (POST) ([http://www.surface temperatures.org/databank/parallel\\_measurements](http://www.surface temperatures.org/databank/parallel_measurements)) is currently being established as part of the International Surface Temperature Initiative (ISTI) (<http://www.surface temperatures.org/>) to compile a global database with parallel measurements to try to study these types of inhomogeneities. This initiative plus the recommendations of the WMO to use parallel measurements to assess the differences in the automation or another changes on the observation conditions, shows the usefulness of the studies based on parallel measurements.

Several studies of non-climatic changes using parallel measurements at local or regional scale have been published in recent years. Early, the parallel measurements are the base to the study of the measurement differences according different shelters. Its good know that before the internationalisation of the Stevenson Screens different shelters were used, so



there have been different studies that try to minimise the impact the transition between the different older thermometer screens and the standard Stevenson Screen.

In this way, Brunet *et al.* (2011) try to minimise the screen bias between Montsouris and Stevenson Screen by doing an exploratory statistical analysis to determine the principal characteristics of the bias and then develop a regression model to minimise this bias. Slonosky 2014 explores the differences between the north wall exposures and the sheltered readings in Canada. Nordli *et al.* (1997) studied differences between different screens used in the North Atlantic region. Auchmann and Bröimann (2012) studied the impact of the change from the Wild to the Stevenson Screens on the homogeneity of the temperature time-series. Or Buisan *et al.* (2015) studied the differences on the daily temperature measurements due to the different size of the Stevenson Screen, compare the observations taken into a medium-sized and large-sized Stevenson Screens in Spain.

While Van der Meulen and Brandsma, (2008) and Brandsma and Van der Meulen, (2008) analyse the differences between different thermometer screens through the parallel measurements. These studies show the importance of using parallel measurements to study and correct or minimise some specific biases introduced by the changeover of measurement conditions. Furthermore, Lopardo *et al.* (2013) found a clear increase in the heating of the AWS depending on its age. They conclude that after three years of operation, this effect becomes larger due to the radiative contribution.

Other studies analyse the influence of the relocations as the case of Linden *et al.* 2015 they installed different temperature sensors in two historical locations that conforms the temperature time-series of Geisenheim (Germany) and Haparanda (Sweden).

### **2.3.2 – Biases related to the introduction of automatic observing systems**

In recent years, many scientists have analysed the differences between MAN and AWS systems or among different AWS types to understand the influence of these instrumentation changes on climate data series. Many of the differences in shape and size found between MAN and AWS and different AWS systems are dependent on the network assessed (Hubbard *et al.*, 2005 or Trewin 2010). It could be associated with technological differences among automatic sensors, their manufacturers and brand choices in national network deployments. Since every manufacturer has its own strategy to design the sensor, as well as, the datalogger, this cause different characteristic in its response time, hysteresis

or self-heating among AWS brands. All this contributes to the instrumental uncertainty budget.

Various scientists have used parallel measurements to characterise the differences between different instruments. Some of these studies are based on the analysis of the differences between Liquid-in-glass Thermometers (LIG) and thermistor-based maximum–minimum temperature systems (MMTS) in the USA. For example Wendland and Armstrong (1993) analyse the differences between parallel observations taken at one site during three years and found that there was a negative bias, especially for the daily maximum temperatures for which the annual mean differences between the two systems is  $-0.4\text{ }^{\circ}\text{C}$ . This is similar to the difference of  $-0.34\text{ }^{\circ}\text{C}$  found by Holder *et al.* 2006 using the parallel measurements of 13 stations. For the daily minimum temperature differences, the magnitude is lower and different sign according to the two studies. The bias between the LIG and other measurement systems is also analysed by other scientists in other networks, for example Milewska and Hogg (2002) use the parallel daily maximum and minimum temperature measurements taken by five stations for a year in Canada. The average of the daily mean temperature differences is  $0.2^{\circ}\text{C}$  and the bias is positive for both the daily maximum and minimum temperature, although smaller in the latter case.

Other studies try to identify the difference between temperature measurements taken by different AWS or between different semi-automatic measurement systems (such as the HO-83 hygrothermometer). Guttman *et al.* 1996 compare the measurements taken by a HO-83 hygrothermometer and a 1088 hygrothermometer using 10 stations for one year in the USA and concluded that during overcast and calm nights the difference is better identified as these conditions are responsible for  $\pm 0.17$  and  $\pm 0.22\text{ }^{\circ}\text{C}$  of the daily minimum differences, respectively. Fiebrich and Crawford (2009) compare three years of the observations taken by MMTS and AWS in USA and conclude that 65.8% of the daily mean temperature differences are inside  $\pm 1^{\circ}\text{C}$ . Hubbard *et al.* (2004) compare the observations taken for at least one year between different AWSs and determine that biases are station-dependent and the mean of the daily temperature differences can be larger than  $\pm 1\text{ }^{\circ}\text{C}$ .

In the previous paragraphs we have mentioned a number of studies looking at the differences between automatic and semi-automatic or manual systems. Most of them recognise that the studied parallel measurements include several non-climatic effects (station relocations or the introduction of a new screen or even changes in observing

practices) in addition to automatization, thus affecting the comparability of the measurements. In Guttman *et al.* (1996), the authors found large differences when the examined pair of stations (AWS-MAN) was more than 500m apart. These differences are derived not only from the distance itself, but accounted for altitudinal differences and distinct land-use/land-cover between both observing sites.

Besides, Lin *et al.* (2004) also include the influence of the data logger in the AWS measurements, in addition to the bias associated with the sensor (platinum resistance). Another issue is related to the different measurements time, since MAN observations are instantaneous values with a large hysteresis of the measurement element, while for AWS measurements the WMO do not define an exact procedure to determine the observed value, since it only indicates that the instantaneous measures have to be estimated using the 1-10 minutes average of the 10-20 seconds observations. In addition, Lin *et al.* (2008) found the 7 minutes average of the 20 seconds observations has the best coupling with conventional measures.

There is also an impact related to the thermometer shelter, since it has been verified a changeover from wooden screens to fibre glass and plastic screens (Quayle *et al.*, 1991 and Wu *et al.* 2005). In addition, MAN screens have a different heat capacity and opening times that cause a different interaction under diverse atmospheric conditions, which make that MAN and AWS systems react differently to various weather conditions. The shelter of the sensors has also an impact. Anyuan *et al.* (2006) analysed AWS and MAN differences at Chinese stations, finding very marked differences associated with screen changes.

This different response-time related to different atmospheric conditions has been widely studied by Wendland (1993), Hubbard *et al.* (2001, 2004, 2005), Milewska (2002), Lin *et al.* (2004) or Sun (2005). These studies are focused on determining the behaviour of both radiation and wind speed on the AWS performance when compared with MAN instruments. The Hubbard's studies found AWS being more sensitive to sunny days, since the difference between AWS and MAN is more sensitive to daily maximum radiation when differences will be larger. In addition, these two observing systems also react differently to terrestrial radiation, especially under snow cover conditions. Also wind and calm conditions affect the readings between both observing systems, since windy conditions increase the differences. Lin *et al.* 2004 found, for wind speeds larger than 2

m/s, that the differences between both systems increase, being AWS sensors more influenced than MAN instruments.

Furthermore, Anyuan *et al.* (2006) analysed AWS and MAN differences at Chinese stations, finding very marked differences associated with screen changes. The authors also concluded that daily maximum temperature ( $T_{max}$ ) observations recorded by AWS sensors have a larger variation, which is on average 0.79 °C larger than under MAN thermometers and highlighted the impact of the diurnal cycle. They also noted that automatic sensors are more sensitive to changes in atmospheric conditions, since under situations of maximum radiation, the AWS records are about 0.6 °C higher than MAN thermometers.

Therefore, weather station automation has enabled a remarkable increase in the spatial and temporal resolution of the observations and in the real-time data availability (Fiebrich *et al.*, 2009), but this change has also incorporated systematic biases in temperature series that compromise their homogeneity and, therefore, it has reduced their robustness and reliability in their posterior use.

Otherwise, none of the previous studies considered the uncertainty estimation of the measurements and whether or not the temperature sensors were calibrated against metrological national standards.

Although several papers analyse the efficiency of homogenisation approaches either using blind tests (Venema *et al.*, 2012) or comparisons between methods (Freitas *et al.*, 2013), most of them do not analyse the uncertainties associated with the adjustment process. However, when dealing with the generation of large climate datasets, the calibration uncertainty has been considered (Brohan *et al.*, 2006; Parker *et al.*, 2005; Jones *et al.*, 1997 in their studies evaluating global and regional temperature change or Willett *et al.* 2013, 2014 to develop a global dataset for humidity).

However, in these studies only Type A uncertainty is estimated or the estimation of the Type B uncertainty is general and computed for the whole dataset without taking into account the characteristics of the individual stations that comprise the dataset. For example in the case of Brohan *et al.* 2006, they consider that the calibration uncertainty is 0.2 °C for the whole dataset, but they do not estimate uncertainties associated with every station due to the impossibility of doing so.

Under the WMO Global Climate Observing System (GCOS) Reference Upper-Air Network (GRUAN) effort, the estimation of Type B uncertainties are also added to the upper-air measurements. In addition, the GCOS GRUAN Guide (2013) states the estimation of the uncertainty of every measurement will significantly improve the robustness and utility of the data.

## 2.4 – Research gaps identified

The bias introduced by the transition to the AWS is studied previously by different authors, but if we take the results of these studies, in many cases the sign and magnitude of the bias depends on the network studied. Otherwise, is detected that in most part of them, the study of this concrete bias is also influenced by other transitions.

In many cases, we see that the sensors used for the comparison are not placed into the same screen, it is obvious that the introduction of the AWS means not only a change on the sensible element and on the temperature measurement system, but also in many cases means also the change of the screen. The Stevenson screens in many cases are replaced by multiplate screens. But if we take for the assessment of the AWS bias parallel measurements taken in different screens, at the end is impossible to know what is due to the different temperature measurement system and what is due to the different screen. Otherwise, in many cases, the transition to the AWS are accompanied to a relocation of the weather stations, this also has a influence on the differences AWS-MAN and also affects the correct assessment of the AWS-MAN bias.

On the other side, is not so usual that the temperature measurement systems have been calibrated again the metrological standards periodically, also the AWS used for the comparisons. This means that the results of the measurements and of the comparison can be also biased for this fact. In many cases, the AWS are only submitted to comparisons procedures that not ensure the correct operation of the AWS for the whole range of temperatures that it has to works.

And finally, form 1950s there will be an intensive improvement of the homogenisation procedures and methods, but not with the computation of the homogenisation uncertainties. Is obvious that the application of these methods improves the reliability of the climate time-seires but it is also necessary to give the uncertainty and traceability to all the historical temperature series to improve them comparability.



### **Chapter 3 – Field trials, data and methodology**







## Chapter 3: Field trials, data and methodology

This chapter is divided into three parts. The first part provides information about the different field trials; the second part, information about the data that is going to be the base for the thesis; the third one describes our methodology. The field trials represent one of the novel aspects in this thesis. Different authors are analysing this transition but for the most part of them, the differences AWS – MAN are affected by other factors, such as different shelters, different emplacements. For this, especially the field trial of Ebro Observatory was designed to avoid these factors, and to achieve the characteristics of this bias. Moreover, the other novelty aspect is the introduction of the metrological procedures, this thesis can be a real joint work with the metrological, climatological and also with the meteorological communities.

It is good to note the work that has been behind these field trials, especially behind the field trial in Ebro Observatory, the start-up and mainly the maintenance of this is done under this thesis project, maintenance is done periodically to avoid any eventual problem and to maintenance the field trial with the best reliable conditions.

### 3.1 – Field trials

This thesis has involved in cooperation with the *European Metrological Research Programme (EMPR) Research Grant (REG5/URV) to support the Parent Joint Research Project ENV07 MeteoMet (<http://www.meteomet.org/>)*. Thanks to this project, different field trials have been started at different locations in Spain and Italy with the goal of isolating and analysing the bias introduced by the automation of the weather stations, considering also the influence of the calibration. Figure 3.1 shows the localisation of the three field trials. In Spain the field trial was installed in Ebro Observatory and in Italy in Moncalieri Observatory and in Castello Borello.

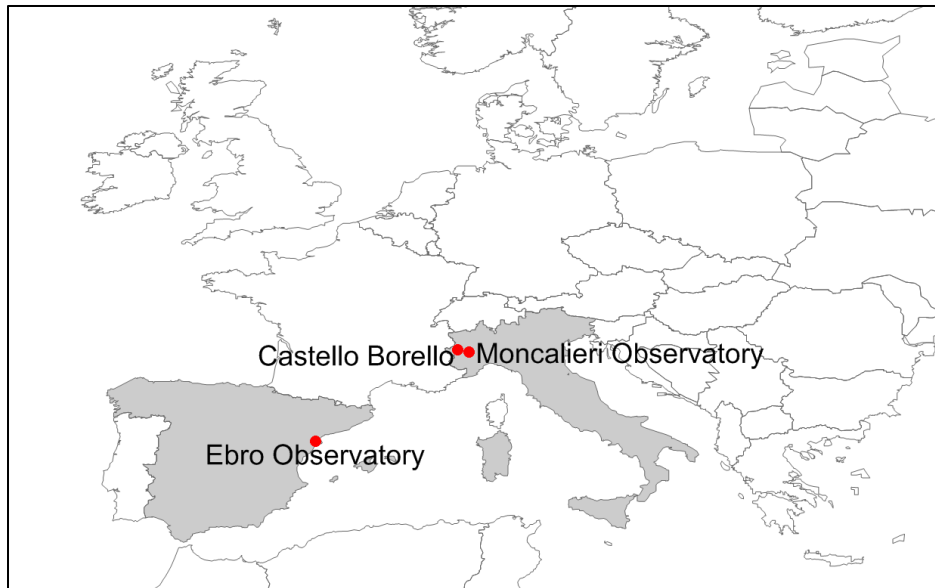


*Figure 3.1: Localisation map of the different field trials start up and the base of part of this thesis.*

### **3.1.1 – Ebro Observatory**

The Ebro Observatory is located in Roquetes, north-eastern Spain ( $40^{\circ} 49' 14''$  N,  $0^{\circ} 29' 23''$  E, 50 m a.s.l.). It is on a hill slope near a small town (about 8000 inhabitants) with little or negligible urban influence and surrounded by natural vegetation mainly composed of Mediterranean pine grove and shrubs. Figure 3.2 provides a photograph of the meteorological garden in which is installed the field trial.



*Figure 3.2: Picture of the meteorological garden (picture courtesy of Ebro Observatory).*

This station, included in the main observational network of the Spanish National Agency of Meteorology (AEMET), is part of the WMO network (9981A) and hosts a continuous climate record since 1880 (from 1905 onwards at the same site) including a remarkably long record of paired temperature (observations taken in parallel in the same Stevenson Screen). The series included liquid in glass thermometers (MAN) and AWS sensors uncalibrated (AWSu).

### 3.1.1.1 – Temperature measurement systems installed

A new temperature measurement system (AWSc) manufactured by Lombard & Marozzini and calibrated following metrological standard procedures, was specifically installed for conducting the MeteoMet/REG5 experiments associated with this thesis was installed on 01/06/2013 and is still in operation. The joint analysis of MAN, AWSu and AWSc observations runs between 01/06/2013 - 31/05/2015. The three thermometric measurement systems (MAN, AWSu and AWSc) are placed into the same Stevenson Screen (Figure 3.3) to ensure all the instruments register air temperature in identical conditions, since our first aim is evaluating instrumental biases, instead of the impact of other factors on the measurements, such as installing them in different screens and avoiding other microclimatic influences. In annexes (pag. 193) the main characteristics and the different components of this new temperature measurement system (AWSc).



*Figure 3.3: On the left the image of the Stevenson Screen in which are placed the different temperature instruments. On the right, a view of the interior of the Stevenson Screen: the LIG Thermometers, the AWSu, the AWSc and the thermograph. Image source: A. Gilabert*

In 01/05/2016 the field trial has been adding a new AWSc with the same characteristics than the first one, but in this occasion the new temperature sensor is installed into an aspirated screen, a Young Screen model 43502. Figure 3.4 shows the new sensor inside the Young – aspirated screen, the both screens are into the same meteorological garden

and the distance between the both is 2 m. From this thesis it will be not possible to have the enough data to analyse it.



Figure 3.4: Pictures of the new sensor inside a Young – aspirated Screen. Image source: A. Gilibert

### 3.1.1.2 – Calibration of the AWSc and estimation of the MAN uncertainty

Under the project *MeteoMet*, a climatic chamber Earth Dynamics Investigation Experiment (EDIE-1) manufactured at the Istituto Nazionale di Ricerca Metrologica, Torino, Italy (INRiM) was used for the calibration (Lopardo *et al.* 2015). The goal of the EDIE-1 is that the calibration is done in air, not in a bath. This means that the operational conditions of the sensor under calibration are better simulated. In this case, the sensor response characteristics to temperature changes are more carefully simulated. Besides, the dimensions of the calibration chamber permit to transport it and do the calibrations *in-situ* (Lopardo *et al.* 2015), Figure 3.5.



Figure 3.5: The climatic chamber EDIE-1. Image source: MeteoMet project

In the calibration process, the temperature sensor under calibration has to be placed into the climatic chamber at the same height of the reference thermometer (SPRT25 $\Omega$ ) to reduce the uncertainty due to the temperature gradient. For this case, the calibration curve was estimated on 5-point temperatures: 40 °C, 25 °C, 10 °C, 0 °C, -10 °C to cover the whole range of temperatures in the study area. The calibration starts at the lowest temperature to be covered, in our case -10 °C. When the temperature into the chamber is stabilised at the different points, we can take the readings of the SPRT25 $\Omega$  and Pt100, generally 10 readings at least 1 minute apart. For every calibration point is computed  $\Delta T = T_r - T_c$  where  $T_r$  is the temperature recorded by the SPRT25 $\Omega$  and  $T_c$  is the temperature recorded by the PT100 under calibration. The calibration function is evaluated by a function  $T = f(T_c) = T_c + \Delta T$ , so is obtained the  $\Delta T$  of the 5 points and for fitting the function is applied a second order polynomial curve, so the calibration function is  $T = T_c + AT_c^2 + BT_c + C$  (Eq. 3. 1).

Table 3.1: Results of the AWSc Ebro Observatory calibration. The values of the constants A, B and C, the values of the SPRT25 $\Omega$  and the AWSc under calibration for every measuring point.

	<b>A</b> <b>0.000002 °C<sup>-1</sup></b>	<b>B</b> <b>0.389741</b>	<b>C</b> <b>99.87349 °C</b>
<b>Measuring point [°C]</b>	<b>T SPRT25<math>\Omega</math> (°C)</b>	<b>R (ohm)</b>	<b>Uncertainty (°C)</b>
40 °C	40.150	115.5446	0.13
25 °C	25.607	109.9819	0.13
10 °C	10.573	104.0247	0.13
0 °C	0.486	100.0262	0.13
-10 °C	-10.213	95.79915	0.13

In the calibration process we account for different sources of uncertainty that determine the total calibration uncertainty of the AWSc. Main uncertainties are:

- The **thermal inhomogeneity** in the chamber: the temperature into the chamber is not uniform
- The **resolution of the sensor** in calibration: it is the smallest change of temperature that the sensor can detect when measuring.
- The **uncertainty of the primary thermometer**: the uncertainty of the reference sensor used in the calibration.
- The **interpolation uncertainty**: the calibration is obtained from the interpolation of the comparison of the temperature taken by the sensor under calibration and the reference sensor on some temperature points. This process generates the interpolation uncertainty, which is the standard deviation (SD) of the residuals of the fit.

The total calibration uncertainty ( $u$ ) is the squared root of the squared sum of all source of uncertainty and the expanded uncertainty ( $U$ ) is the  $u$  multiplied by the coverage factor  $K=2$  to estimate with a confidence level of the 95% (JCGM, 2008b). The calibration uncertainty for the AWSc is:  $u = 0.065$  °C (confidence level of 68%) and  $U = 0.13$  °C (confidence level of 95%).

For the estimation of the MAN uncertainty, as we cannot calibrate the LIG thermometers into a climatic chamber we use the results of Knazovicka & Strnad (2013) to estimate it. We consider the theoretical calibration of the thermometer, the drift of the thermometer, the resolution of the thermometer, the human error and the application error (Table 3.2). The standard uncertainty ( $u$ ) is the square root of the quadratic sum of the different components.

Table 3.2: Estimation of the Ebro Observatory MAN uncertainty. For every uncertainty source the contribution to standard uncertainty. The total standard uncertainty ( $u$ ) and the expanded uncertainty ( $U$ )

Uncertainty source	Contribution to standard uncertainty [°C]
Calibration	0.05
Drift	0.1
Resolution	0.12
Human error	0.06
Application error	0.1
Standard uncertainty: $u$	0.18
Coverage factor	2
Expanded uncertainty: $U$	0.36

### 3.1.2 – Moncalieri

The Moncalieri Observatory is located in Moncalieri (Torino), Italy (44° 59' 52'' N - 07° 41' 43'' E, with an elevation of 260 m). It was set up in 1859 and temperature measurements began in 1865 extending to the present. This observatory is managed by Società Meteorologica Italiana (SMI). The relevance of this observatory lies in the record length (more than 150 years of continuous observations). Figure 3.6 provides a general view of the Moncalieri tower where the experimental setting is installed.



Figure 3.6: The view of the Moncalieri Stevenson Screen in which there is the AWS. Image source: SMI



### 3.1.2.1 – Temperature measurement system installed

In this field trial there is only one AWS, is a temperature – humidity sensor (SIAP-SM3840, installed in 2001), protected by a Stevenson Screen, placed on the tower balcony with a NNW exposure and it was calibrated regarding the standard calibration procedure. The main characteristic of this field trial is that is designed especially to evaluate if the introduction of the standard calibration procedure can improve the quality of the climate data series.

For this, in this experimental setting, only one AWS is measuring temperatures and is applied or not the calibration curve derived from our calibration strategy to the measurements. By doing so, we get from this AWS two time-series: one where the calibration curve has been applied to the readings (AWSc) and another that has not (AWSu). With this, is ensured that any other factor different to the application or not of the calibration curve can influence the observations and the differences will be only due to this fact.

### 3.1.2.2 – Calibration of the AWS

In June 2012, INRiM calibrated the sensor against primary national standards (Bertiglia *et al.* 2015). In this case for the calibration is used the EDIE-0, a prototype also manufactured by the INRiM under the MeteoMet project, Figure 3.7.



Figure 3.7: Picture of EDIE-0 and the interior of the Stevenson Screen. Image source: MeteoMet

Table 3.3 shows the results of the calibration and the Figure 3.8 the graph with the results of the calibration and the calibration curve. The calibration procedure is the same that for the AWS of Ebro Observatory.

Table 3.3: Results of the AWSc Moncalieri calibration. The values of the constants A, B and C and the values of the SPRT25Ω ( $T_s$ ) and the  $T_c$  for every measuring point.

	<b>A</b> <b>-0.000255 °C<sup>-1</sup></b>	<b>B</b> <b>0.023347</b>	<b>C</b> <b>0.685355 °C</b>
<b>Measuring point [°C]</b>	<b><math>T_s</math> [°C]</b>	<b><math>T_c</math> [°C]</b>	<b><math>\Delta T = T_s - T_c</math></b>
-20	-19.14	-18	-1.14
-10	-10.45	-9.4	-1.05
0	-0.39	0.2	-0.59
15	14.92	15.3	-0.38
30	30.24	30.5	-0.26
40	39.96	40.1	-0.14

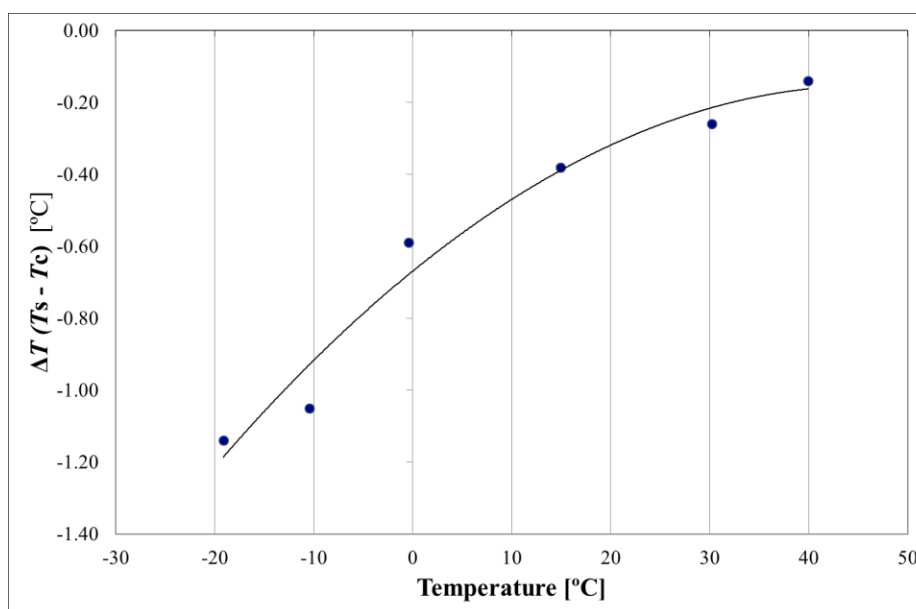


Figure 3.8: Calibration results, the blue dots the difference between the temperature of the SPRT25Ω and the AWSc of Moncalieri in °C for every measuring point. The black line is the calibration curve.

The uncertainty source for this case is similar than for the calibration of the AWS of Ebro Observatory, the main difference here is the higher uncertainty due to the higher inhomogeneity of the EDIE-0. In this case the uncertainty derived by the climatic chamber is 0.11 °C, the uncertainty derived by the SPRT25Ω is 0.001 °C and the uncertainty derived to the AWSc and the calibration interpolation uncertainty is 0.09 °C. For this case, the total calibration uncertainty ( $u$ ) of the AWSc is 0.154 °C so the expanded uncertainty ( $U$ ) is 0.32 °C with a confidence level of the 95% (JCGM, 2008b).

### 3.1.3 – Castello Borello

The Castello Borello Observatory is located in Bussoleno, Italy (45° 7' 18.5" N and 7° 9' 44.14" E at an elevation of 630m), Figure 3.9. In a typical rural location surrounded by an agroforestry landscape (arable lands and forest) at a distance of 40 m from the nearest building. Meteorological observations began in 2005. This rural site is reasonably free of any artificial influence, such as buildings, barns or nearby developments that could systematically affect the measurements. But with completely different climatic conditions than for the other two field trials.

#### 3.1.3.1 – Temperature measurement system installed

In this case, it equip a Stevenson Screen (Figure 3.9) containing the automatic temperature sensor, which was only calibrated by the manufacturer before installation, AWSu. In addition, and since the 21st of September 2013, a new sensor (Rotronic) calibrated at the INRiM according to procedures traceable to primary national standards AWSc is in operation in the same shelter to avoid different influences to those affecting the uncalibrated sensor.

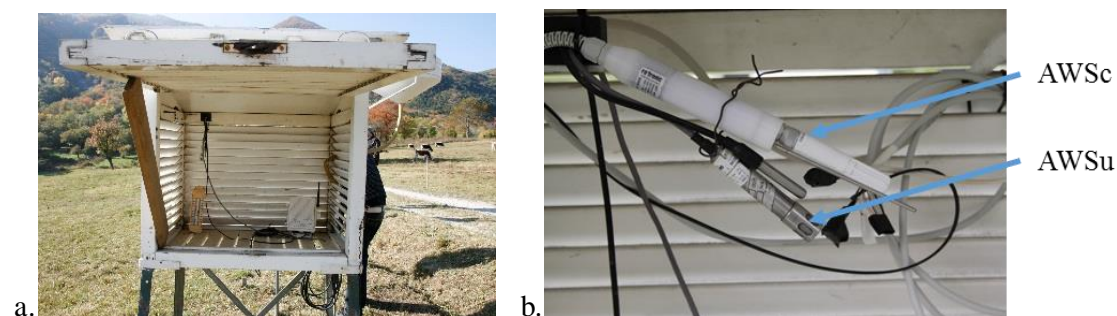


Figure 3.9: Picture of the Stevenson Screen in which there are the two AWS (a) and a view of the new AWSc installed and the older AWSu from the SMI. Image source: *MeteoMet*

#### 3.1.3.2 – Calibration of the AWS

The new Rotronic sensor (AWSc) was also calibrated with the climatic chamber EDIE-1 as in the case of the AWSc installed in Ebro Observatory. Table 3.4 shows the results of the calibration and the Figure 3.10 the graph with the results of the calibration and the calibration curve.

Table 3.4: Results of the AWSc Castello Borello calibration. The values of the constants A, B and C and the values of the SPRT25Ω and the Tc for every measuring point.

	<b>A</b> <b>-0.00002 °C<sup>-1</sup></b>	<b>B</b> <b>-0.0032</b>	<b>C</b> <b>-0.0473 °C</b>
<b>Measuring point [°C]</b>	<b>T<sub>s</sub> [°C]</b>	<b>T<sub>c</sub> [°C]</b>	<b>ΔT = T<sub>s</sub> - T<sub>c</sub></b>
-20	-22.876	-22.89	0.014
-10	-10.761	-10.755	-0.006
0	0.889	0.936	-0.047
15	14.696	14.802	-0.106
25	25.523	25.668	-0.145
30	30.945	31.100	-0.155

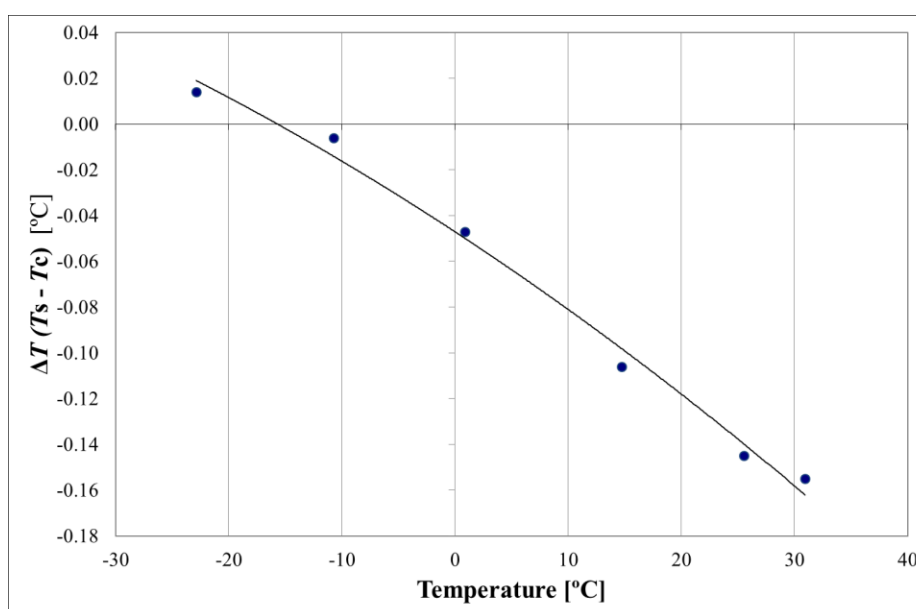


Figure 3.10: Calibration results, the blue dots the difference between the temperature of the SPRT25Ω and the AWSc of Castello Borello in °C for every measuring point. The black line is the calibration curve.

As in the other case, is also computed the uncertainty associated to the calibration procedure. The uncertainty sources are the same, and the thermal inhomogeneity in the chamber is the main uncertainty source. In this case the uncertainty derived by the climatic chamber is 0.08 °C, the uncertainty derived by the SPRT25Ω is 0.001 °C and the uncertainty derived to the AWSc and the calibration interpolation uncertainty is 0.006 °C. So For this case, the total calibration uncertainty ( $u$ ) of the AWSc is 0.08 °C so the expanded uncertainty ( $U$ ) is 0.16 °C with a confidence level of the 95% (JCGM, 2008b).

### 3.2 – Data used for the different analysis

This thesis deals with the study of a complex problem, because as we see there are many other factors that can influence the study of the AWS transition. The AWS transition means a complete change of temperature measurement systems, from the sensitive element to the way to compute the instantaneous measurements. In addition, the novelty of this thesis is the introduction of the metrological procedures, thus, it's required, to analyse and compare different data-series. The data used is divided in four parts as the thesis results; every part refers to one results chapter.

#### 3.2.1 – Daily data used to assessing the differences AWSu – MAN (data used for the Chapter 4)

This section uses the data of three different observatories, all of them in Spain. These observatories are chosen because they are centennial observatories and because nowadays remains the parallel measurements AWS – MAN. The three observatories are: Ebro Observatory, Fabra Observatory (Barcelona) and Murcia Observatory (Figure 3.11).

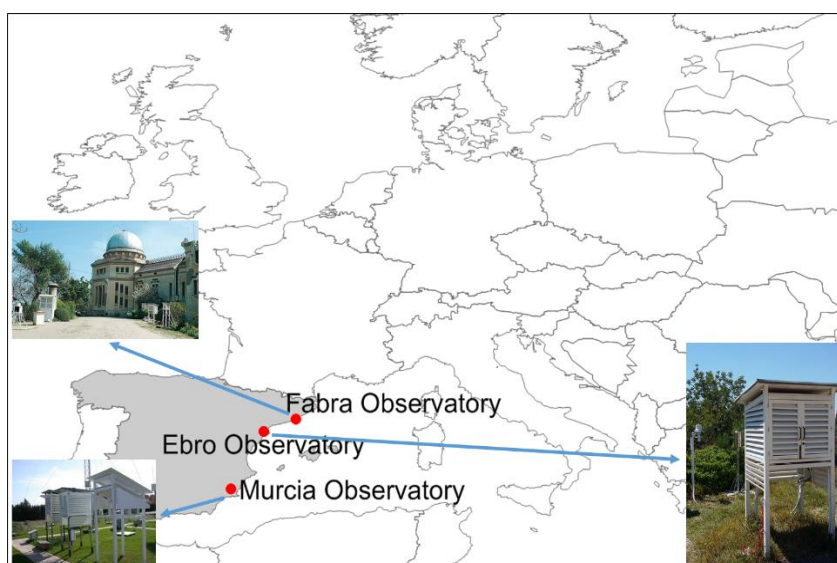


*Figure 3.11: Localisation map of the three stations considered: Ebro Observatory, Fabra Observatory and Murcia Observatory.*

The daily maximum temperature ( $T_{max}$ ) and daily minimum temperature ( $T_{min}$ ) difference series AWSu – MAN ( $\Delta T_{max}$  and  $\Delta T_{min}$ ) for the three observatories have been subjected to quality control and homogeneity testing. The quality control is done in two parts. In the first part, is only considered the AWSu  $T_{max}$  and  $T_{min}$  time-series, and

is checked that to compute the daily values at least 75% of the 10 minute averages were available. In the second part, the  $\Delta T_{\max}$  and  $\Delta T_{\min}$  time-series are quality controlled with the software RClindex\_extraqc (Aguilar and Prohom, 2011).

The next step consist in identifying the possible break points (BP) in the  $\Delta T_{\max}$  and  $\Delta T_{\min}$  time-series. The detection of the possible BPs is done by statistical BP detection and visual inspection of the  $\Delta T_{\max}$  and  $\Delta T_{\min}$  and in some cases supported by the metadata information (for Ebro Observatory and Fabra Obseratory). The statistical testing was performed with the residuals of the differences AWSu – MAN series, using the Standard Normal Homogeneity Test (Alexandersson and Moberg, 1997).

### 3.2.1.1 – Daily parallel measurements AWSu - MAN from Ebro Observatory

The overlap period with AWSu and MAN measurements started in 01/07/1991 and is on-going, although for this analysis includes data until 31/05/2015.

The MAN measurements are taken from a LIG thermometer, with the following characteristics:

- The maximum thermometer is a **Fuess 5961/69** model, which was in operation from 1991 until 27/10/2013 when it was replaced by another **Fuess 10554** model (in use from 28/10/2013 onwards). Both are mercury thermometers with cut-off threads and their scale divisions are every 0.2 °C.
- The minimum thermometer is a **Fuess 2235/82** model in use from the beginning of the parallel series (1991) up to 1999, when it was substituted by a **Fuess 2048** model (from 2000 onwards). Both minimum thermometers are filled with alcohol and the divisions are also every 0.2 °C.

During this observing parallel period, AEMET installed three different AWS and temperature measurement sensors (Table 3.5): SEAC, SOSS and ESOS AWSs. None of these automatic sensors have been periodically calibrated following a traceable procedure (into a calibration chamber), since only instantaneous on site comparisons of the sensors in use with a national pattern have been made irregularly (Lopardo *et al.* 2012). These on site comparisons are only a verification of the functioning of the sensor, if malfunctions or large differences between the both (the reference sensor and the sensor under scrutiny), the sensor is replaced by a new one or a correction is applied, losing the data traceability and introducing possible BPs on the data-series.

Table 3.5: Characteristics of AEMET AWSu systems and thermometric sensors installed at the Ebro Observatory from 01/07/1991 onwards.

	SEAC	SOSS	ESOS
Period	01/07/1991 – 14/7/2001	15/7/2001 – 28/3/2011	11/8/2011 – ongoing
Acronym	Manufacture name	Surface semiautomatic observing system	Surface semiautomatic observation station
Period	01/07/1991 – 14/7/2001	15/7/2001 – 28/3/2011	11/8/2011 - onwards
Sensor	THIES 1.1005	THIES 2:1235:00:000	THIES 2:1280:00:000
Measuring element	Pt100	Pt100	Pt100
Accuracy	1/3 class B	1/3 Class B	1/3 Class B
Elect. connection	4-lead circuit	4-lead circuit	4-lead circuit
Measuring range	-30 / +50 °C	-30 / +100 °C	-30 / +70 °C

$T_{max}$  and  $T_{min}$  time-series from the AWSu observing system were extracted by identifying the highest and lowest of 1-minute average observations. And for LIG the  $T_{max}$  and  $T_{min}$  were taken over 0-24 hours. Next, were estimated the difference (AWSu – MAN)  $T_{max}$  ( $\Delta T_{max}$ ) and  $T_{min}$  ( $\Delta T_{min}$ ) time-series.

From the two quality control checks the 5% of the  $\Delta T_{max}$  and  $\Delta T_{min}$  were removed. With the first check that extract the daily values when at least 75% of the 10 minute average were available, the 4.6% of the daily data not pass this test and the other 0.4% of the daily data not pass the RCLimdex\_extraQC quality control. Most part of these 5% of values removed are during the older parallel observations (SEAC period), when there are an important number of missing 10 minute values.

For the BP's detection, in the case of Ebro Observatory the availability of metadata helps us to guide and verify the statistical testing. Combining the metadata and the statistical and visual detection, are detected 9 BPs that could be partially explained by the known changes in the AWS instrumentation (Table 3.5). This fact points to the instability and frequent changes of instrumentation affecting the new automatic observing system when

compared with the manual observing system. From a theoretical point of view, this can be related, among other factors, to the lack of periodical calibrations. There are also other BPs detected inside the operational periods of each sensor (Figure 3.12), although two of them (SEAC1.1 and SEAC2.1) are very short and could possibly be caused by improper functioning of the sensors. For this reason, are only validated the clearest 8 HSPs, which can be divided by:

- The initial installation of a SEAC AWS (hereinafter the SEAC period) between 1991 and 2001. For this period there are two HSPs (SEAC1 and SEAC2)
- Followed by the change to SOSS automatic systems (SOSS period) between 2001 and 2011. For this period there are three HSPs (SOSS1, SOSS2 and SOSS3).
- Finally, the replacement of the AWS by an ESOS system (the ESOS period) from 2011 onwards. For these period there are also three HSPs (ESOS1, ESOS2 and ESOS3), in this case, the 2 BPs were also validated with the metadata, in this days there were a comparisons procedures.

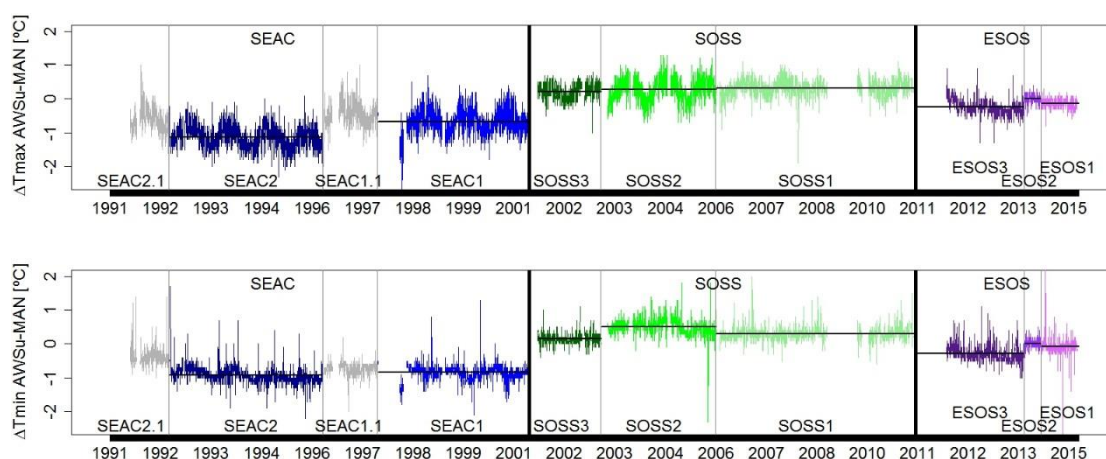


Figure 3.12: Daily maximum temperature difference series ( $\Delta T_{max}$ ) (upper plot) and daily minimum temperature difference series ( $\Delta T_{min}$ ) (lower plot) between the uncalibrated automatic station (AWSu) and manual (MAN) observations of the Ebro Observatory. The vertical grey lines indicate breakpoints (BP) positions (in black the documented BPs). The horizontal black lines indicate the AWSu-MAN mean for each HSP.



The AWSu-MAN series are contrasted against the daily number of sunshine hours and the daily mean wind-speed to describe the impact of those elements in the relation between manual and automatic sensors.

### 3.2.1.2 - Daily parallel measurements AWSu - MAN from Barcelona Fabra Observatory

The Fabra Observatory is located in Barcelona, north-eastern Spain (41° 25' 07'' N, 2° 07' 25'' W, 415 m a.s.l.). For this thesis the daily temperature parallel measurements AWSu – MAN extended between 01/01/1996 to 31/12/2010. As in the case of Ebro Observatory, some metadata is available (Table 3.6 is a compilation of all the documented changes of the Fabra Observatory AWSu). For the data recorded prior to 08/2007, the automatic sensor is sheltered into a multiplate screen, meanwhile after this date, its moved into the same Stevenson Screen which shelters the manual thermometers.

Table 3.6: Metadata of the AWSu installed in Fabra Observatory, information courtesy of Catalonia Meteorological Service (SMC)

Datalogger changes	
01/01/1996	MCV EM300
02/12/2003	MCV EM300 (replaced)
31/07/2007	Campbell CR1000
Changes in temperature measurement system	
01/01/1996	MCV STA-01
01/01/2003	MCV STA-02P
26/10/2004	MCV STA-02P (new)
31/07/2007	Vaisala HMP45AL
Screen	
01/01/1996	MCV multiplate screen ventilated
31/07/2007	Stevenson Screen

In this case, the hourly data of the AWSu was not available, so we only dispose of the daily  $T_{max}$  and  $T_{min}$  data. For this, the data are only subjected to the rclimdex\_extraQC. As result of this QC check only the 0.3% of the  $\Delta T_{max}$  and  $\Delta T_{min}$  data was rejected.

Figure 3.13 shows the  $\Delta T_{max}$  and  $\Delta T_{min}$  time-series and the position of the BPs. In this case, some metadata are available, thus, can help with the BPs detection, 7 BPs are

detected and can be partially explained by the known changes in the AWS instrumentation and shelter (Table 3.6). As in the case of the Ebro Observatory, this shows the inhomogeneities caused to the time-series for the changes of instrumentation. There are also other BPs not explained by the metadata, besides the BPs detected on 28/4/2006 and 14/2/2006 delimited a very short HSP and probably caused by a malfunction or probably to some artificial cause, so, this is not considered for the analysis, and another BP on 01/01/2000 delimiting the first AWSu measurements and is also not considered (there are missing data and some jumps). For these reasons, are only validated the clearest 6 HSPs:

- The initial MCV STA-01 (hereinafter the MCV1 period) between 2000 and 2002. For this period there are two HSPs (MCV1.1 and MCV1.2)
- Followed by the change to MCV STA-02 (MCV2 period) between 2003 and 2007. For this period there are three HSPs (MCV2.1, MCV2.2 and MCV2.3).
- Finally, the replacement of the AWSu by a Vaisala HMP45AL and the installation of the AWSu inside the Stevenson Screen with the LIG thermometers (the Vaisala period) from 2007. For this period there are not any HSP.

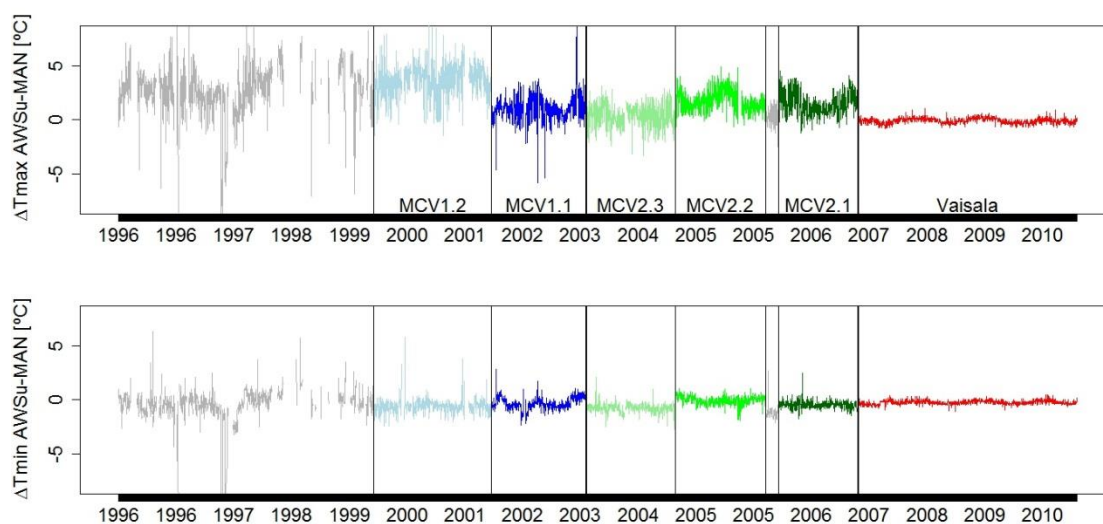


Figure 3.13: Daily maximum temperature difference series ( $\Delta T_{max}$ ) (upper plot) and daily minimum temperature difference series ( $\Delta T_{min}$ ) (lower plot) between the uncalibrated automatic station (AWSu) and manual (MAN) observations of the Fabra Observatory. The vertical black lines indicate breakpoints (BP) positions.

For the analysis of the differences AWSu-MAN is also used another data plus the parallel temperature time-series. In this case, is also used the daily number of sunshine hours and the wind-speed.

### 3.2.1.3 – Daily parallel measurements AWSu - MAN from Murcia

The Murcia Observatory is located in Murcia, south-eastern Spain (38° 00' 07'' N, 1° 10' 15'' W, 61 m a.s.l.). For this thesis the daily temperature parallel measurements AWSu – MAN came from 01/01/2004 to 31/12/2012. For this case, the information about the instruments is not so complete as the case of Ebro Observatory. In the case of the AWSu the sensor and datalogger was a SEAC, as for the first part of the Ebro Observatory AWSu observations.

As result of the both QC checks, the percentage of  $\Delta T_{max}$  and  $\Delta T_{min}$  removed is 4.9%, similar than in the case of Ebro Observatory. In this case, the 4% of the  $T_{max}$  and  $T_{min}$  of the AWSu were eliminated because more than 25% of the 10 min average was not available and only the 0.9% of the daily  $\Delta T_{max}$  and  $\Delta T_{min}$  not pass the RClindex\_extraQC quality control.

After the QCs, the  $\Delta T_{max}$  and  $\Delta T_{min}$  series have been subject to BPs detection, with the same procedure previously described for other stations. In this case, 4 BPs were detected, so 5 HSP are identified. One of them is very short and probably due to a malfunction of the sensor, so this is not considered for the analysis. Figure 3.14 shows the  $\Delta T_{max}$  and  $\Delta T_{min}$  time-series with the BPs detected, the HSP not considered is the HSP3.1.

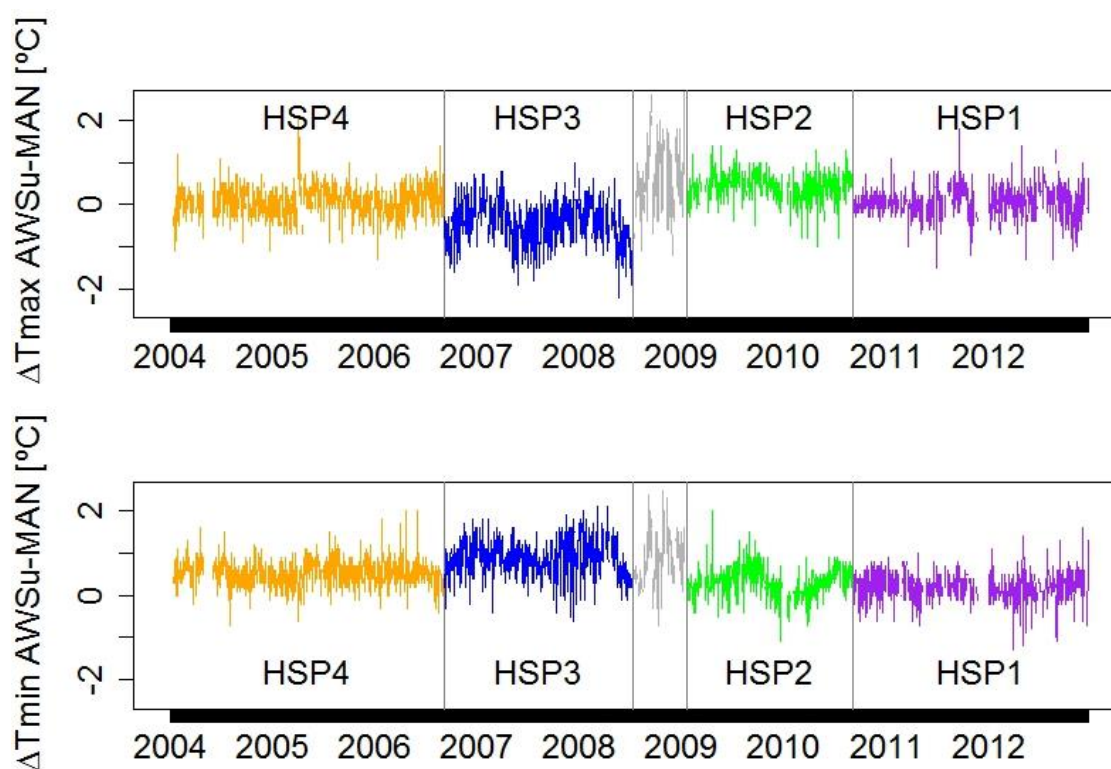


Figure 3.14: Daily maximum temperature difference series ( $\Delta T_{max}$ ) (upper plot) and daily minimum temperature difference series ( $\Delta T_{min}$ ) (lower plot) between the uncalibrated automatic station (AWSu) and manual (MAN) observations of the Murcia Observatory. The vertical black lines indicate breakpoints (BP) positions.

As for the other two cases, for the analysis of the differences AWSu-MAN is also used the daily number of sunshine hours and the daily mean wind-speed data.

### 3.2.2 – Data used to assess the influence of the introduction of the calibration procedures (data used for the Chapter 5)

The next part of this thesis is the evaluation of the introduction of the calibration procedures. As is previously explained (subsection 3.1 – Field trials, p. 72), for the MeteoMet/REG-5 project and subsequently for this thesis, different field trials have been started. In these field trials (Ebro Observatory, Moncalieri Observatory and Castello Borello) different AWSu, calibrated according to the standard metrological procedures are installed (sub-sections 3.1.1.2, 3.1.2.2 and 3.1.3.2, respectively). Figure 3.1 shows the localisation of the different field trials.

- Ebro Observatory: the AWSc was installed 01/06/2013 and the three temperature measurement systems are recording in parallel (AWSc, AWSu and MAN). For this thesis, the parallel measurements from 01/06/2013 to 31/05/2015 are taken, considering that two years of data can already provide a good estimation of the differences between both systems. The measurements of the three temperature measurement systems are periodically subjected to quality control to detect/correct possible errors. Before analysis the two parallel time-series AWSc – MAN and AWSc – AWSu are subjected to a quality checks with RCLimdex\_extraQC.
- Castello bordello: since 21/09/2013 to 20/09/2014, the AWSu and AWSc recorded parallel observation. It was considered that one year of paired temperature observations is still a long enough, as other studies indicate (e.g. Lin *et al.* 2008 or Sun *et al.* 2005), to reach meaningful results, since the main aim of this intercomparisons exercise is to explore the influence of adopt the metrological calibration on temperature data series.
- Moncalieri: in this case, is also used one year of parallel measurements, from 01/09/2012 to 31/08/2013. We have to remind that in this field trial there is only installed one AWS that was calibrated with a portable climatic chamber in 2012. Thus, the objective to use this parallel measurement (applying or not the calibration results) is only to study if the adoption of the metrological procedures can improve the reliability of the temperature time-series. As there is only one AWS, the differences are only due to the application of this procedure, thus, is not necessary to cover a large period, to for example analyse the possible influence of different weather situations.

### **3.2.3 – Assessing the differences AWS – MAN at hourly scale (data used for the Chapter 6)**

To assess the hourly differences between the AWS and MAN observations, hourly temperatures of Ebro Observatory from the period 01/07/2013 – 30/06/2015 are used. For the hourly measurements a liquid-in-glass thermometer is used, with the same characteristics as the maximum and minimum liquid-in-glass thermometers.

In the case of the AWSc, the instantaneous hourly observations that came from the minutal observations computed by the mean of the 10s observations are used. In the case

of the MAN the observations taken by the LIG thermometer at different hours: at 6h, 7h, 9h, 12h, 13h, 15h and 18h UTC are used.

### **3.2.4 – The centennial air temperature time-series of Moncalieri (data used for the Chapter 7)**

The Moncalieri Observatory, located in Moncalieri (Torino), was set up in 1859 and temperature measurements began in 1865, extending to the present. This long record is taking for the assessment of the instrumental plus homogenisation uncertainties. There is not any long missing data period and for this study the period 1866 – 2012 is homogenised.

The monthly data are computed directly from the daily data according the WMO standards. The monthly data is not computed if there are 5 or less missed days or if the gap exceeds three consecutive days.

Many factors have likely affected the homogeneity of the Moncalieri's long climate records, although the station location has not changed. There were different change in instruments, their exposure and sheltering. The impact of Torino's urbanisation is considered to be negligible. It is important to take into account that between 1961 to 1989 the observations were taken by non-professional staff and the maximum-minimum LIG thermometers was unscreened, hanged directly on the window wall.

### 3.3 – Methodology

As in the case of the previous sub-section, this sub-section is also divided in four parts, describing the methodology used for each part of the thesis.

#### 3.3.1 – Methodology used to assessing the differences AWSu – MAN (Chapter 4)

The differences series  $\Delta T_{\max}$  and  $\Delta T_{\min}$  (for the three observatories AWSu – MAN) are first characterised with some basic descriptive statistics.

Firstly, for each HSP of each parallel AWSu – MAN its mean and root mean square deviation (RMSD) (Eq. 3.2) are computed:

$$\text{RMSD} = \sqrt{\frac{1}{N} \sum_{i=1}^n (\text{Temp AWSu} - \text{Temp MAN})^2} \quad (\text{Eq. 3.2})$$

The distribution of the differences is visually assessed using histograms and the AWSu-MAN empirical distribution is illustrated by the use of boxplots (Wilks, 2011). To check if the differences between seasons are statistically significant, it's used the ANOVA table with Fisher's test as a contrast

To assess if the differences are dependent on the temperature, the observations are stratified into three groups depending on the values of MAN  $T_{\max}$  and  $T_{\min}$ :

- For  $T_{\max}$ :  $T_{\max} \text{ MAN} < 15 \text{ }^\circ\text{C}$ ;  $15 - 30 \text{ }^\circ\text{C}$ ;  $> 30 \text{ }^\circ\text{C}$
- For  $T_{\min}$ :  $T_{\min} \text{ MAN} < 10 \text{ }^\circ\text{C}$ ;  $10 - 20 \text{ }^\circ\text{C}$ ;  $> 20 \text{ }^\circ\text{C}$

The relationship between  $\Delta T_{\max}$  and  $\Delta T_{\min}$  and other variables is evaluated in two ways:

- Computing the Spearman's correlation test between  $\Delta T_{\max}$  and  $\Delta T_{\min}$  and  $T_{\max}$  and  $T_{\min}$ , the daily temperature range (DTR), the number of daily sunshine hours and the daily wind speed.
- Empirical distribution of  $\Delta T_{\max}$  and  $\Delta T_{\min}$  for the whole year for summer and winter are analysed, stratifying the days according the sunshine hours and the wind speed. Thus, days are classified in four types: windy and overcast days, windy and clear days, calm and overcast days and calm and clear days. The thresholds (see Table 3.7) are different for the whole year and for winter and

summer. The different thresholds estimated from the empirical distribution of the different climate variables measured during each period (annual, winter or summer) and station (Ebro, Fabra or Murcia observatory).

*Table 3.7: Daily mean windspeed and sunshine hours thresholds for Ebro Observatory, Fabra Observatory and Murcia Observatory.*

	Ebro Observatory	Fabra Observatory	Murcia Observatory
Annual			
Windy (m/s)	10	8	6
Calm (m/s)	5	3	2
Clear (hours)	10	10	10.5
Overcast (hours)	5	4	6.5
Winter			
Windy (m/s)	12	10	5
Calm (m/s)	5	4	2
Clear (n° h)	8	8	9
Overcast (n° h)	3	2	4
Summer			
Windy (m/s)	8	7	6
Calm (m/s)	3	2	3
Clear (n° h)	12	12	13
Overcast (n° h)	8	7.5	10.5

For the sake of clarity, for some graphs, for every datalogger-sensor for Ebro and Fabra Observatory, only the largest and most continuous HSP are plotted.

### **3.3.2 – Methodology used to assess the influence of the introduction of the calibration procedures (methodology used for the Chapter 5)**

To assess the influence of the introduction of the calibration procedures first some basics statistics are computed; such as the mean (annual, summer and winter), the RMSD and the percentage of days in which the differences are inside the calibration uncertainty for Moncalieri and Castello Borello. For Ebro Observatory AWSc – MAN, AWSc – AWSu and AWSu – MAN the percentage of days in which the differences are inside the combined



calibration uncertainty (0.38 °C for AWSc – MAN and AWSu – MAN and 0.16 °C for AWSc – AWSu). The combined calibration uncertainty of temperature differences is the square root of the squared sum of the calibration uncertainty of each AWS or MAN. For example for the  $\Delta T_{\max}$  AWSc – MAN (Eq. 3.3):

$$|U| = \sqrt{(U_{AWSc})^2 + (U_{MAN})^2} \quad (\text{Eq. 3.3})$$

The distribution of the differences is assessed using histograms and is checked plotting the empirical distribution of the series, as for the previous section. For Castello Borello AWSc – AWSu is used to assess if the differences are dependent on the temperature, being the days also stratified depending on the range of temperature:

- For  $T_{\max}$ :  $T_{\max} \text{ MAN} < 10 \text{ }^\circ\text{C}$ ;  $10 - 20 \text{ }^\circ\text{C}$ ;  $> 20 \text{ }^\circ\text{C}$
- For  $T_{\min}$ :  $T_{\min} \text{ MAN} < 5 \text{ }^\circ\text{C}$ ;  $5 - 10 \text{ }^\circ\text{C}$ ;  $> 10 \text{ }^\circ\text{C}$

For Castello Borello the relationship of the differences with the recorded temperature, the DTR, the wind speed, the radiation and the relative humidity (RH) are studied.

To assess the impact of adopting the calibration curve results in Moncalieri have selected three extreme indices from the 27 core indices formulated by Expert Team on Climate Change Detection and Indices (ETCCDI) (<http://www.clivar.org/organization/etccdi/etccdi.php>). The ETCCDI indices chosen are:

- Number of Frost Days (FD): annual count of days when  $T_{\min}$  is  $< 0 \text{ }^\circ\text{C}$
- Number of Summer days (SU): annual count of days when  $T_{\max}$  is  $> 25 \text{ }^\circ\text{C}$
- Number of Tropical nights (TR): annual count of days when  $T_{\min}$  is  $> 20 \text{ }^\circ\text{C}$

### 3.3.3 – Methodology used to assess the differences AWS – MAN at hourly scale (methodology applied on the Chapter 6)

The assessment of the differences AWSc – MAN at the hourly scale faces a series of problems related to how and when the measures are taken at both systems. First, the MAN measurements in many cases are not routinely taken at the exact hour (in the case of the Ebro Observatory, for example the 6h observation is taken between 5:50 and 6:05 UTC). For Ebro Observatory, in cooperation with its personnel, we have available the exact time

of MAN observations, recorded on purpose for this project. This allows to select the same observation recorded at the AWS.

Yet another problem is the lack of consensus about how the instantaneous AWS measurements have to be taken to represent and exact point in time. The AWSc – MAN series considering different instantaneous AWS measurements are defined:

- The mean of 5 minutal observations centered to the instantaneous measurement time. For example the instantaneous AWS measurement at 12:00 UTC is computed with the mean of the observations from 11:58 to 12:02 UTC.
- The mean of the 5 minutal observations before the instantaneous measurement time. For example the instantaneous AWS measurement at 12:00 UTC is computed with the mean of the observations from 11:56 to 12:00 UTC.
- The mean of the 5 minutal observations after the instantaneous measurement time. For example the instantaneous AWS measurement at 12:00 UTC is computed with the mean of the observations from 12:00 to 12:04 UTC.

To analyse the differences, the mean, the RMSD and the percentage of observations in which the difference is inside the combined calibration uncertainty AWSc – MAN are computed. The empirical distribution of the differences is illustrated by boxplots.

### **3.3.4 – Methodology used for the homogenisation of Moncalieri centennial air temperature time-series and the estimation of the adjustment uncertainty budget (methodology applied on Chapter 7)**

This section encompasses two parts: the homogenisation of the Moncalieri monthly maximum and minimum temperature time-series and the methodology for the joint-estimation of the instrumental and homogenisation uncertainty budget.

#### **a. Homogenisation of Moncalieri monthly maximum and minimum temperature time-series:**

To carry out the homogenisation of the centennial monthly  $T_{max}$  and  $T_{min}$  records from Moncalieri Observatory HOMER method and software is used (Mestre *et al.*, 2013) available at <http://www.homogenisation.org>. This method includes the best features of series of methods, such as PRODIGE (Caussinus *et al.*, 2004), the

Adapted Caussinus Mestre Detection Algorithm for Homogenising Networks of Temperature Series (ACMANT) (Domonkos, 2011) and the Joint Segmentation Method (Picard *et al.*, 2011) approaches.

As other relative homogenisation methods, HOMER requires the use of highly correlated reference stations to compare with the candidate station (Moncalieri in our case). For this purpose, we rely on seven time-series, as shown in Figure 3.15: Alessandria (1866-2003), Moncalieri-Bauducchi (1993-2012), Cuneo (1866-2011, Romano *et al.*, 1994), Milan (1866-2003), Parma (1878-2003), Piacenza (1871-2003) and Torino (1866-2003, Di Napoli *et al.*, 2008). The application of HOMER has followed the guidance given by Mestre *et al.* (2013).

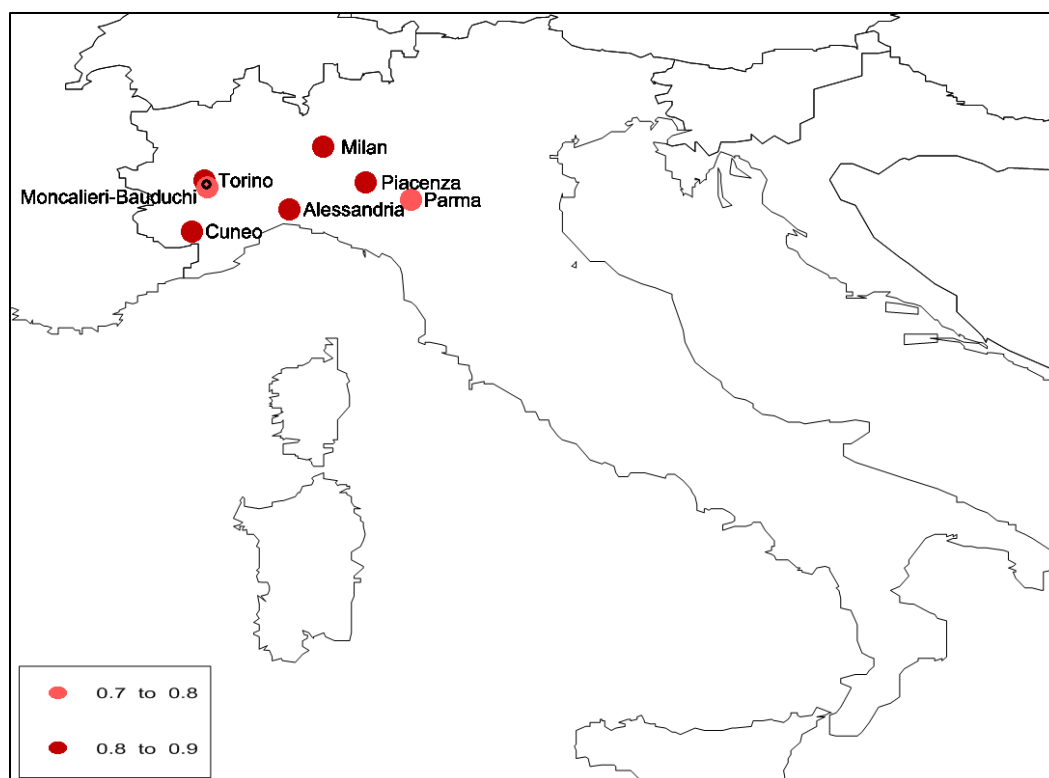


Figure 3.15: Localisation map of the seven reference stations for the homogenisation. The dot colour indicates the Pearson correlation ( $r$ ) between each reference station and the candidate station (Moncalieri). The empty black dot indicates the localisation of the candidate station.

In the detection and validation procedure of the BPs, the metadata gathered by Di Napoli *et al.* (1996) are used to verify if any physical cause could explain them. After the homogenisation of the monthly  $T_{max}$  and  $T_{min}$  series, the data of the period 1927-1989 has been traced to ITS-90 using the program ToITS-90 (Pavlašek, 2015).

However, the correction applied has not introduced significant changes in the data series.

#### **b. The joint-estimation of the instrumental plus homogenisation uncertainty budget**

There are many studies showing the importance and need of applying homogeneity adjustments to climate time-series, but unfortunately, little attention has been paid to estimate uncertainties associated with this procedure. Previous studies, have considered only Type B (sub-section 2.1.3) uncertainties in their research (Brohan *et al.* 2006 or Willet *et al.* 2013, 2014). Otherwise both authors consider only an estimation of the calibration and adjusted uncertainty for the whole dataset and not individually for each station and each measurement. This is useful if we are working in world or hemispherical datasets, but not for regional, local or if we are comparing two different stations.

In these late cases, there is the need to ensure a more complete traceability of individual time-series and apply adjustments for each one. In this thesis a preliminary approach to solve this complex problem is done, since many other different factors will determine the homogenisation and the measurement uncertainty. In this first approach is considered:

- Uncertainties related to the homogenisation procedure: for this source of uncertainty, the number of BPs, the length of the period between adjacent BPs, the correction and the accuracy of the homogenisation method are considered. For the accuracy of the method the RMSD taking 12 monthly benchmark networks (surrogate networks) generated under the action COST-HOME (Venema *et al.* 2012) is computed. This benchmark was considered appropriate because many networks are derived from southern European stations. The validated BPs are taken and HOMER is applied onto the 12 networks. Later, the RMSD are computed for all the networks and compare the differences of the results from HOMER's correction and the benchmark. For the detection capacity of the method, is also used this benchmark dataset and compute the Heidke Skill Score standard:

$$HSS_{std} = \frac{p - r_{std}}{1 - r_{std}}; \quad (Eq. 3. 4)$$

Where:  $r_{std} = \frac{a+c}{n} \frac{a+b}{n} + \frac{b+d}{n} \frac{c+d}{n}$ ;  $p = \frac{a+d}{n}$ ; a: true positive; b: false positives; c: false negatives; d: true negatives

Therefore, to compute the uncertainty related to the homogenisation procedure is estimated (Eq. 3.5):

$$U_h = \sqrt{RMSD^2 + (1 - HSS_{std})^2 + (n^{BP}/Y_p + Y_n)^2} \quad (Eq. 3.5)$$

where RMSD represents the root mean square deviation;  $HSS_{std}$  stands for Hedike Skill Score standard;  $n^{BP}$  indicates the number of the breakpoints;  $Y_p$  is the number of years after the BP, while  $Y_n$  is the number of years before the BP

- The calibration uncertainty of the reference stations for the homogenisation, the calibration uncertainty ( $U$ ) of all the reference stations used for calculating the adjustments is considered (Eq. 3.6):

$$U_r = (\sqrt{\sum U^2}) / n + 1 \quad (Eq. 3.6)$$

where  $U$  = calibration uncertainty of the reference series.  $n$  = number of reference series

- The instrumental uncertainty of the candidate station. It is computed considering the combined instrumental uncertainty of the period before and after each BP. For the estimation of the oldest thermometer uncertainty, it is followed the procedure developed by Knazovická and Strnad (2013), also under the MeteoMet project. So the instrumental uncertainty of the candidate station is expressed (Eq. 3.7):

$$U_c = (\sqrt{\sum U^2}) \quad (Eq. 3.7)$$

where  $U$  stands for instrumental uncertainty of the candidate series after and before the BPs

- To take into account all the uncertainty source in the homogenisation procedure and estimate the combined uncertainty budget, we adopt and apply to the adjusted time-series the equation (Taylor, 1997) (Eq. 3.8):

$$U_H = \sqrt{U_h^2 + U_r^2 + U_c^2} \quad (Eq. 3.8)$$

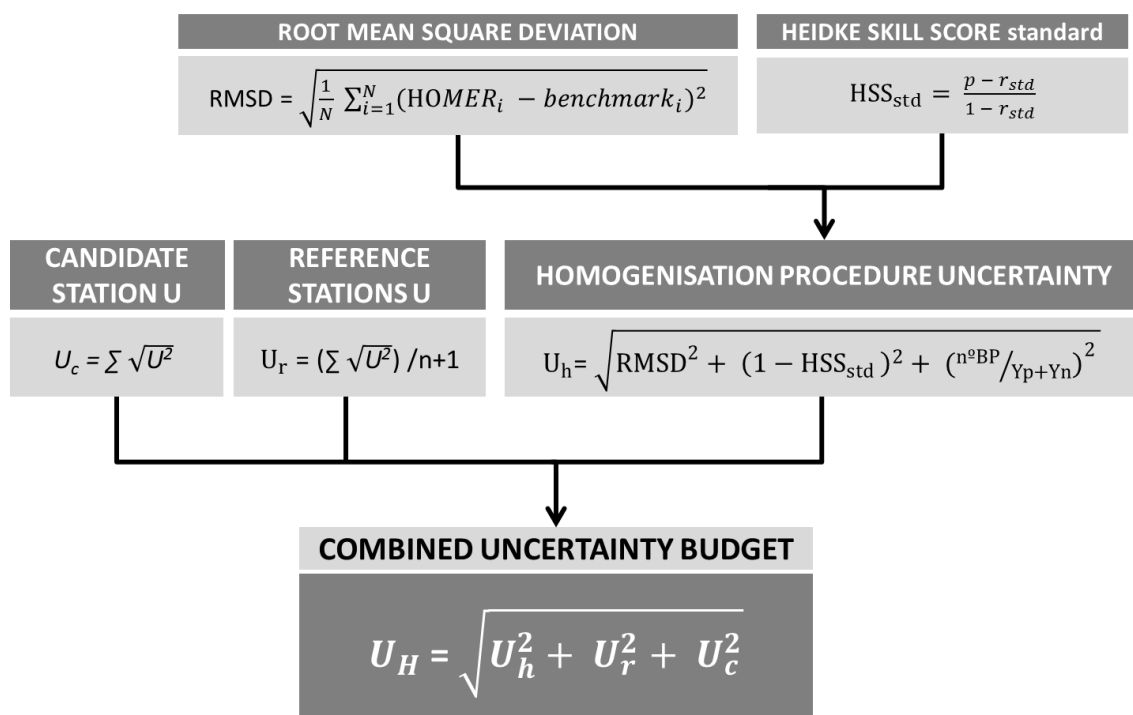


Figure 3.16: Diagram of the combined uncertainty budget methodology followed in this study

For the trend computation of the homogenised data the Ordinary Least Squares (OLS) (Eq. 3. 9) and Weighted Least Squares (WLS) are computed. The WLS (Eq. 3.10) give a weight of the difference observations, in this case takes into account the total joint-estimation homogenisation plus instrumental uncertainty to compute the trend. The both are used only for descriptive purpose.

$$Y_i = \beta_0 + \beta_1 X_i + \varepsilon_i \quad (\text{Eq. 3. 9})$$

$$\chi^2 = \sum_{i=1}^n w_i [Y_i - f(x'_i; \hat{\theta})]^2 \quad (\text{Eq. 3.10})$$

where  $w_i = \frac{1}{\sigma_i^2}$ ; and  $\sigma_i$  are the total uncertainties of each observation



## **Chapter 4 – Assessing the statistical characteristics of the AWSu – MAN differences**







## Chapter 4: Assessing the statistical characteristics of the AWSu – MAN differences

In this section, the results of the statistical analysis of the differences AWSu – MAN at daily scale are provided. For this analysis three parallel measurements: Ebro Observatory (01/07/1991 – 31/05/2015, sub-section 3.2.1.1), Fabra Observatory (01/01/1997 – 31/12/2010, sub-section 3.2.1.2) and Murcia Observatory (01/01/2004 – 31/12/2012, sub-section 3.2.1.3) are analysed. For each one, firstly is shown the results from the assessment of the paired temperature time-series recorded under the AWSu and MAN observing systems for each period followed by, their relationships with other climate variables.

### 4.1 – Ebro Observatory AWSu - MAN

During the 24<sup>th</sup> years (1991-2015) of paired temperature observations AWSu – MAN, there have been three changes of automatic data loggers and temperature sensors that have not been calibrated periodically according metrological standard procedures and comparison checks to detect a malfunction of the AWSu causing diverse inhomogeneities on this paired temperature time-series. Therefore, the main characteristic of the AWS bias is the dependence on a particular instrumentation setting, since each HSP shows a different bias magnitude and/or sign (Figure 3.12).

Table 4.1 provides some basic statistics (mean and RMSD) of  $\Delta T_{\max}$  and  $\Delta T_{\min}$  for each HSP. As is checked the differences (size and sign) depend on the HSP analysed, but the big differences are between the different data logger and temperature sensor installed (between SEAC, SOSS and ESOS periods), the mean of the differences between the different HSPs detected for a one period are more similar than between the different temperature measuring systems. The mean of the  $\Delta T_{\max}$  ( $\Delta T_{\min}$ ) series range between 0.3 °C for SOSS1 and SOSS2 (0.5 °C for SOSS3) and -1.1 °C for SEAC2 (-0.9 °C for SEAC2). RMSD estimates for the  $\Delta T_{\max}$  ( $\Delta T_{\min}$ ) oscillate between 0.2 °C for ESOS1 and ESOS2 (0.1 °C for ESOS2) and 1.2 °C for SEAC2 (1.0 °C also for SEAC2). For the SEAC and ESOS periods the largest differences are in the  $\Delta T_{\max}$ . The ESOS period shows the lowest differences, even

so, there is also variability in the bias considering the whole ESOS period, inasmuch as during these two years of parallel measurements there have been 2 BPs. Both BPs are related with a correction of the AWSu sensor derived by a comparison process.

*Table 4.1: Basic statistics estimated for each homogeneous sub-period (HSP) providing the number of parallel AWSu – MAN observations of Ebro Observatory, mean differences and root-mean square deviation (RMSD) for maximum temperature differences ( $\Delta T_{max}$ ) and minimum temperature differences ( $\Delta T_{min}$ ).*

		SEAC2	SEAC1	SOSS3	SOSS2	SOSS1	ESOS3	ESOS2	ESOS1
<b>N</b>		1415	1397	652	1055	1842	991	155	348
<b>Mean</b>	$\Delta T_{max}$ [°C]	-1.1	-0.7	0.2	0.3	0.3	-0.2	0.0	-0.1
	$\Delta T_{min}$ [°C]	-0.9	-0.8	0.2	0.5	0.3	-0.3	0.0	-0.1
<b>RMSD</b>	$\Delta T_{max}$ [°C]	1.2	0.8	0.3	0.4	0.4	0.3	0.2	0.2
	$\Delta T_{min}$ [°C]	1.0	0.9	0.2	0.6	0.4	0.4	0.1	0.4

The mean of the differences is not equal for all the HSPs and also the distribution of  $\Delta T_{max}$  and  $\Delta T_{min}$  varies depending on the HSPs. Figure 4.1 shows the histograms (the values are in Table A2.1 in the Annexes section) of  $\Delta T_{max}$  and  $\Delta T_{min}$  for all HSPs. For the SEAC and ESOS period for which the mean of the differences are negative, also the most part of the differences are negative, on the contrary, for the SOSS period the most part of the differences are positive. This indicates, the higher relationship between the temperature measuring system and differences AWSu – MAN.

For the SEAC period, for both HSPs and for the  $\Delta T_{max}$  and  $\Delta T_{min}$ , most part of the differences are larger than -0.5 °C, especially for  $\Delta T_{max}$ . And for SEAC2 most part of the differences are larger than -1 °C, this shows the higher impact of the introduction of the AWSu as consequence of the lower accuracy of the SEAC AWSu. This fact could be corrected (or at least minimised) with the correct application of the metrological standards, as shown in section 3.1.1.2).

The bias sign for all the HSPs of the SOSS period is different when compared with other periods and HSPs, for these, for most part of the cases the bias is positive and also smaller than for the SEAC period.

The SOSS2 sub-period is the sub-period in which the differences are larger, especially for  $\Delta T_{min}$ , for which the proportion of cases with differences larger than 0.5 °C is 40 %. This is consistent with the results of the mean and RMSD of this period.

For the ESOS sub-periods, the differences are negative as in the SEAC sub-periods, but in these cases, most of the differences are lower than  $\pm 0.5$  °C. And as in the case of the SOSS period, the larger differences are in  $\Delta T_{min}$ . This is also consistent with the results of the mean and RMSD.

The distribution of the differences shows the complexity of this bias, the higher dependence of the type of sensor and as a result the complexity to minimise or correct the bias.

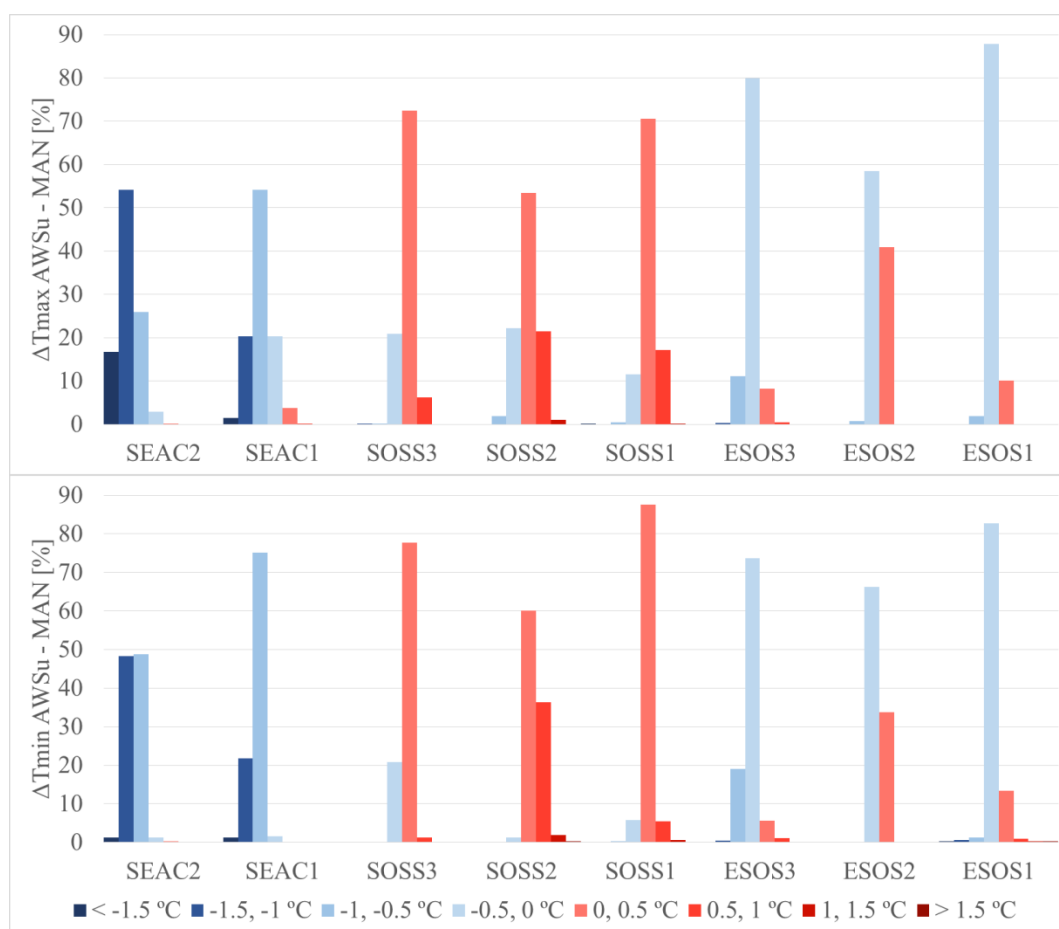


Figure 4.1: Histogram of the daily maximum and minimum temperature differences AWSu – MAN of Ebro Observatory ( $\Delta T_{max}$  and  $\Delta T_{min}$ ) for the 8 HSPs detected.

With the  $\Delta T_{\max}$  and  $\Delta T_{\min}$  time-series, the differences are not constant across the year, but follow a cycle. Figure 4.2 provides seasonal boxplots of  $\Delta T_{\max}$  and  $\Delta T_{\min}$  series (mean and RMSD in Table A2.2). In this case, only one HSP is shown for every period (the largest and most continuous HSP for each period: SEAC2, SOSS2 and ESOS3). For all the HSPs and for  $\Delta T_{\max}$  and  $\Delta T_{\min}$  series (except ESOS2, is not computed due to lack of data for all seasons), the differences across the seasons, are significant according the Fisher ANOVA test. So, the  $\Delta T_{\max}$  and  $\Delta T_{\min}$  depends on the season, the differences are not equal along the year and for a future minimisation/correction of the bias this fact have also to be considered.

For the initial SEAC period, the AWS bias is negative and the largest in magnitude for both  $\Delta T_{\max}$  and  $\Delta T_{\min}$  series. Summer (June-August) is characterised by larger negative differences than winter (December-February) months. During the SOSS period, the AWS bias is positive for both  $T_{\max}$  and  $T_{\min}$  and its magnitude is lower, the higher differences occur in winter. In the last ESOS period,  $\Delta T_{\max}$  and  $\Delta T_{\min}$  are smaller, the seasonal cycle is reduced respect to the other periods but is still significant.

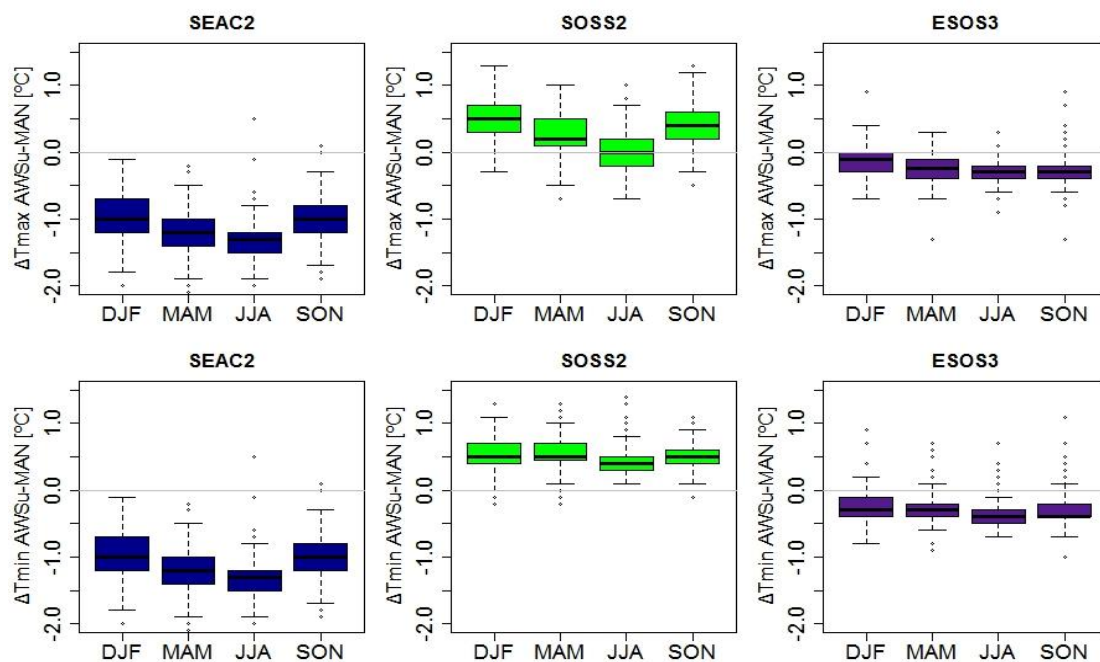


Figure 4.2: Seasonal boxplots (DJF winter, MAM spring, JJA summer and SON autumn) for maximum (upper plots) and minimum (lower plots) temperature difference series AWSu-MAN of Ebro Observatory for one HSP for every period (the largest and most continuous

*HSP) the ESOS3 (for the ESOS period), SOSS2 (for the SOSS period) and SEAC2 (for the SEAC period) sub-periods.*

Previously, we see that there are significant differences depending on the season so one hypothesis can be that these differences are due to differences depending on the different seasonal temperature range or that these differences are due to different weather situations characteristics of each season.

Figure 4.3 presents boxplots of  $\Delta T_{\max}$  and  $\Delta T_{\min}$  according to the different range of temperatures. In general, differences increase for the upper/lower temperatures, especially for the higher temperatures of both biases ( $\Delta T_{\max}$  and  $\Delta T_{\min}$ ) for SEAC2 and lower temperature of both biases for SOSS2. The differences of the current period depending on the different range of temperatures are smaller.

These differences dependent on the recorded temperature are another prove of the low accuracy of the sensors, especially the sensors of the periods SEAC and SOSS and the not application of the standard calibration procedures. It is obvious that with the introduction of the AWS, it was very likely that we can find differences. And these differences between the different AWS indicates that maybe there are something wrong, and also, the very high dependence between the temperature and the HSP analysed shows that is not only a problem of different device characteristics. There are something more, and taking into account, how the calibration works and the results of this procedure, one can conclude with a high confidence, that the introduction of the calibration procedure can reduce the differences and correct the AWS measurements.

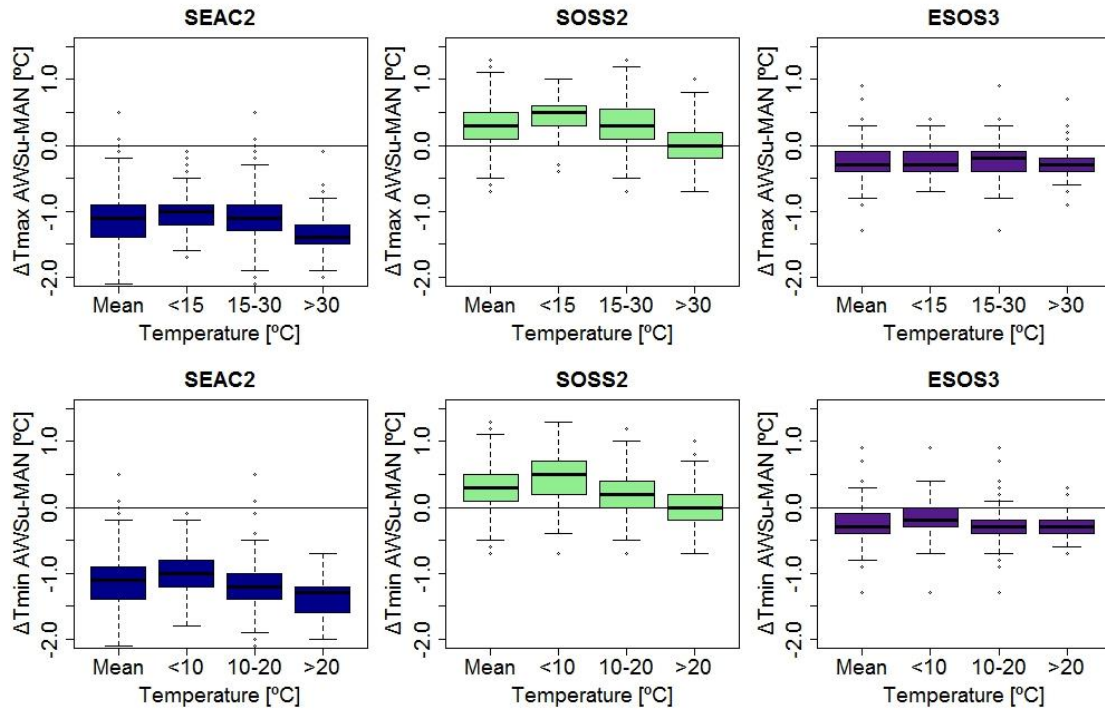


Figure 4.3: Boxplots for maximum (upper plots) and minimum (lower plots) temperature difference series AWSu-MAN of Ebro Observatory of SEAC2, SOSS2 and ESOS3 for those days in which daily maximum temperatures ( $T_{max}$ ) is lower than 15 °C, 15-30 °C and upper than 30 °C and days in which daily minimum temperatures ( $T_{min}$ ) is lower than 10 °C, 10-20 °C and upper than 20 °C, it is also shown the mean of the  $\Delta T_{max}$  and  $\Delta T_{min}$  for the whole period.

Another important point to consider for the analysis of the automatization bias is the relationship of the bias with other variables. Previous studies, indicate, that there is a relationship between the bias and the daily mean wind speed and the radiation (Hubbard *et al.*, 2004 or Milewska *et al.*, 2002). It is important to determine the relationship between AWS bias characteristics and other climate variables, since this can provide more information to help to minimise the AWS bias.

In this way, the relationship between the AWSu-MAN daily temperature differences and some variables is analysed, Table 4.2 gives Spearman's correlation coefficients ( $\rho$ ) estimated between  $\Delta T_{max}$  and  $\Delta T_{min}$  and the MAN  $T_{max}$  and  $T_{min}$ , daily temperature range (DTR), daily mean wind speed (WS) and sunshine hours.

Table 4.2: Spearman’s correlation coefficients ( $\rho$ ) estimated among the maximum ( $\Delta T_{max}$ ) and minimum ( $\Delta T_{min}$ ) temperature differences AWSu-MAN of Ebro Observatory and  $T_{max}$  –  $T_{min}$  MAN ( $T_{max}$  MAN,  $T_{min}$  MAN) observations, daily temperature range (DTR), daily mean wind speed (WS) and daily number of sunshine hours (sunshine) for the SEAC2, SOSS2 and ESOS3 sub-periods. In bold are the coefficients that are statistically significant at the 95 % confidence level.

	SEAC2		SOSS2		ESOS3	
	$\Delta T_{max}[^{\circ}C]$	$\Delta T_{min}[^{\circ}C]$	$\Delta T_{max}[^{\circ}C]$	$\Delta T_{min}[^{\circ}C]$	$\Delta T_{max}[^{\circ}C]$	$\Delta T_{min}[^{\circ}C]$
$T_{max}$ MAN	<b>-0.4</b>		<b>-0.5</b>		<b>-0.1</b>	
$T_{min}$ MAN		<b>-0.3</b>		<b>-0.3</b>		<b>-0.3</b>
DTR	<b>-0.1</b>	<b>0.2</b>	<b>-0.2</b>	0.0	<b>0.3</b>	0.0
WS	<b>-0.4</b>	<b>-0.2</b>	<b>-0.3</b>	<b>-0.1</b>	<b>-0.1</b>	-0.1
Sunshine	<b>-0.3</b>	0.0	<b>-0.3</b>	<b>-0.1</b>	0.1	-0.1

The main conclusion is that the recorded temperature is the variable that has a high influence on the differences for the both cases ( $\Delta T_{max}$  and  $\Delta T_{min}$ ). In general, for all the period and for the  $\Delta T_{max}$  and  $\Delta T_{min}$  the DTR has not an influence. Regarding the wind speed and the number of sunshine hours, have a little influence, but only on the  $\Delta T_{max}$  for the SEAC and SOSS periods, but it is important to highlight that in both cases the  $\rho$  is not high.

Figure 4.4 shows for the three sub-periods (SEAC2, SOSS2 and ESOS3) the  $\Delta T_{max}$  (left) and  $\Delta T_{min}$  (right plots) stratified depending on the wind speed and the number of sunshine hours (Table A2.3 the mean of the  $\Delta T_{max}$  and  $\Delta T_{min}$  for each sub-period and type of day). Therefore, according to the wind speed and sunshine hours, the days are classified into 4 groups (Table 3.7 to see the values): the first one, for windy and with a few hours of sunshine days. The second is formed by windy and many hours of sunshine days. The third one group for calm and a few hours of sunshine days, while the last one, involves calm and many hours of sunshine hours. For the whole period and for winter and summer.

As for the correlation results, the  $\Delta T_{max}$  are more affected than the  $\Delta T_{min}$  for all the sub-periods depending on the different weather type days. The  $\Delta T_{max}$  in winter are most



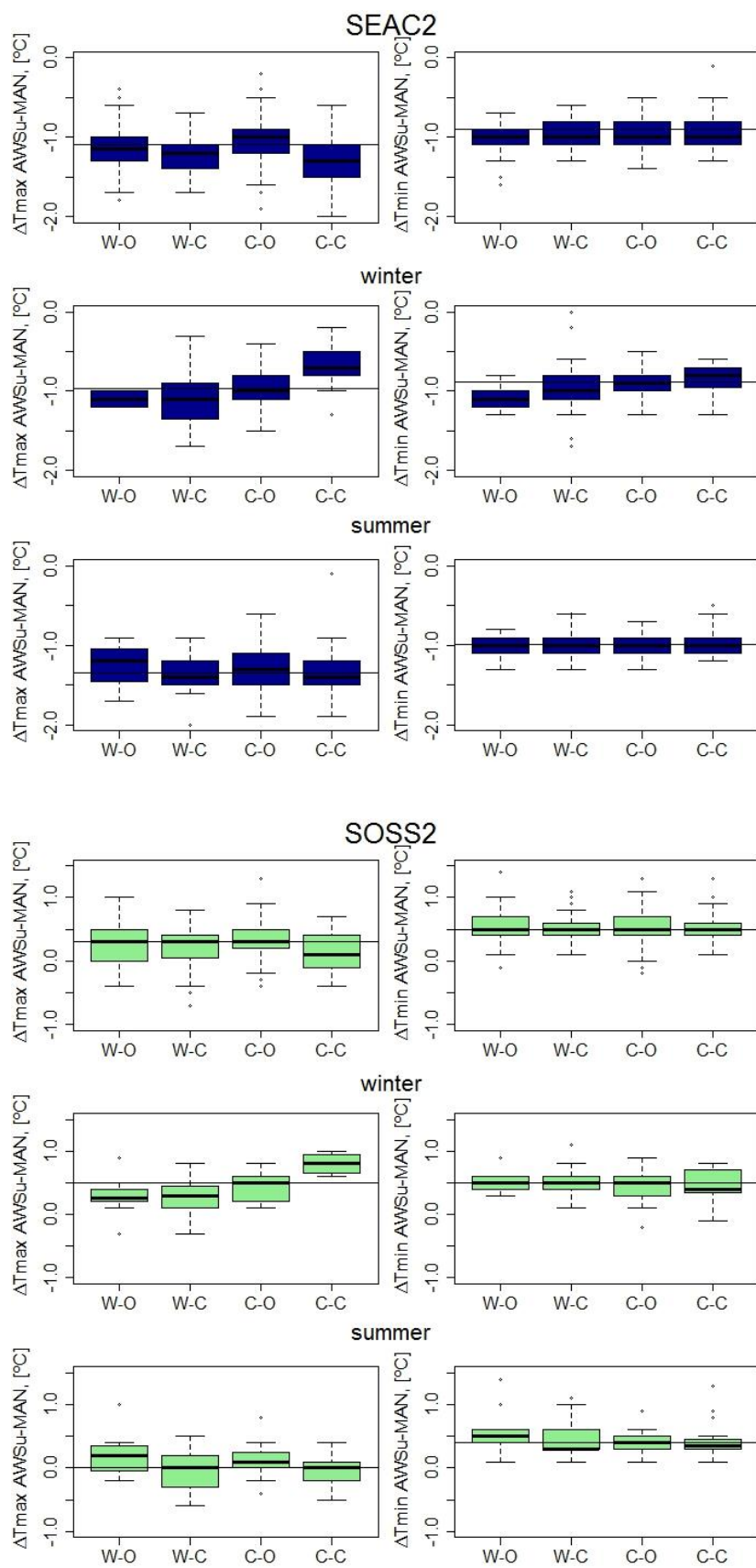
affected for the covariables than in summer and for the whole sub-period. The higher differences are in winter  $\Delta T_{\max}$  between the windy and overcast days and the calm and clear days.

For the SEAC2 sub-period, also the winter  $\Delta T_{\max}$  are the most affected by the covariables, so the mean winter  $\Delta T_{\max}$  of the windy and overcast days is  $-1.1\text{ }^{\circ}\text{C}$ , opposite, for the calm and clear days is  $-0.7\text{ }^{\circ}\text{C}$ .

As for the other analysis, the characteristics of the differences AWSu-MAN of the period SOSS are different than for the other two periods. In this case, also the winter  $\Delta T_{\max}$  are the most affected by the covariables, but in this case the highest positive differences are for the calm and clear days ( $\Delta T_{\max}$  mean of this days is  $0.8\text{ }^{\circ}\text{C}$ ) and the lowest differences for the windy and overcast days ( $\Delta T_{\max}$  mean is  $0.3\text{ }^{\circ}\text{C}$ ).

The relationship between the differences and the covariables of the ESOS period is similar than for the SEAC period but as for the other cases with lowest differences. So, in this case, also the winter  $\Delta T_{\max}$  differences are the most affected by the wind and the sunshine hours, and as for the SEAC2 sub-period, for the ESOS3 sub-period, the highest negative differences are for the windy and overcast days ( $\Delta T_{\max}$  mean  $-0.3\text{ }^{\circ}\text{C}$ ). Oppositely, for the calm and clear winter days the mean of  $\Delta T_{\max}$  differences is positive,  $0.1\text{ }^{\circ}\text{C}$ .

4 – Assessing the statistical characteristics of the AWSu – MAN differences



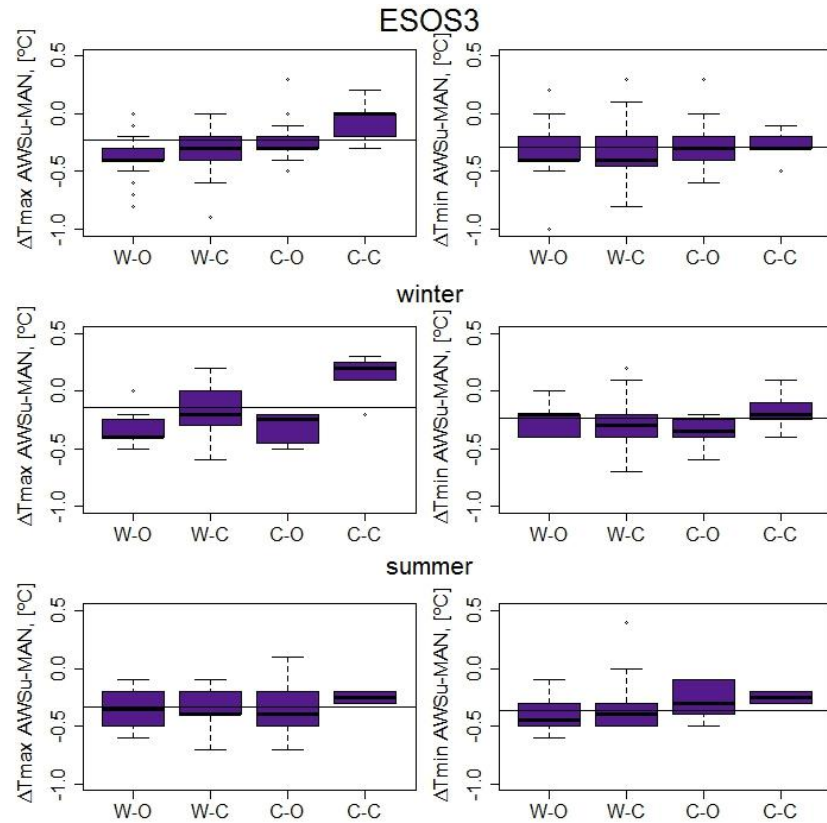


Figure 4.4: Boxplots for maximum (left plots) and minimum (right plots) temperature difference series AWSu-MAN of Ebro Observatory of SEAC2, SOSS2 and ESOS2 according the stratification of the days depending the wind speed and the sunshine hours. W-O (windy and overcast days), W-C (windy and clear days), C-O (calm and overcast days) and C-C (calm and clear days). On methodology (Page 93) to see the wind speed and sunshine hours thresholds.

Even with the stratification of days according the covariables, the covariables have not a higher influence on the differences AWSu-MAN of Ebro Observatory than the recorded temperature. The sign and shape of the differences are not equal for all the HSPs. This may be because the two temperature measuring systems are always into the same Stevenson Screen and in the same relative position. This fact, supports the importance of the calibration and the adoption of the standard metrological procedures, because is the recorded temperature the variable that have a highest effect on the bias. Because only, calibrating correctly the AWS according the metrological standard procedures, it is possible to analyse independently the different temperature points, to then optain the calibration curve with which it can be possible to correct the different temperature measurements.

## 4.2 – Fabra Observatory AWSu – MAN

The parallel daily temperature measurements AWSu-MAN of the Fabra Observatory analysed in this thesis come from 1996 to 2010, 15 years of parallel measurements. But as in the case of the Ebro Observatory, during these 15 years of paired observations, there have been also three different data loggers and temperature sensors and, in this case, also a change of the AWSu screen. As in the case of the Ebro Observatory, there are also different BPs during these periods, maybe for some corrections of the measurements or changes of the sensor due to a malfunction. So, as in the case of the Ebro Observatory, the main characteristic of the AWS bias and the common factor between the both observatories is the dependence of the bias with the temperature measurement system and for Fabra Observatory also with the AWSu screen. (Figure 3.13, page 88).

Figure 3.13, shows that the higher differences are also in  $\Delta T_{\max}$  and especially during the MCV periods for which, besides to the different temperature measurement system, each one is into different screens. Table 4.3 provides some basic statistics (mean and RMSD) of  $\Delta T_{\max}$  and  $\Delta T_{\min}$  for each HSP. For  $\Delta T_{\max}$  there are larger differences depending on the HSP, so the higher differences are in the MCV1.2 (mean 3.7 °C and RMSD 4.0 °C) and the lower and negative differences in Vaisala period (mean -0.1 °C and RMSD 0.6 °C). This points to the big influence on the bias of the sensors sheltering. For  $\Delta T_{\min}$  the differences between the HSPs are lower, being the higher differences in MCV2.3 (mean -0.8 °C and RMSD 0.9 °C) and the lower differences are also found during the Vaisala period (mean -0.2 °C and RMSD 0.3 °C).

It is important to highlight the different sign of the differences, for  $\Delta T_{\max}$  (positive, AWSu measurements higher than MAN) and  $\Delta T_{\min}$  (negative, AWSu measurements lower than MAN) when the AWSu sensor was inside a multiplate screen and the MAN inside the Stevenson Screen. This can be due to the different conditions inside the screens, the Stevenson Screen is bigger and is made of wood, while, the multiplate screen is smaller and is made of plastic or fiberglass. This means that the conditions inside the two screens are different and the responses of the two screens to the environment changes are different.

Due to this, under this thesis and under the MeteoMet/REG5 project a new sensor has been installed in Ebro Observatory (with exactly the same characteristics that the previous) but inside a Young screen to analyse separately which is the influence of the change on the temperature measurement system and which is the influence of the screen change.

Unfortunately, in many meteorological networks, automation of weather stations was not only the change of the measuring instrument / system but also, it has been accompanied by a change of the screen. For this reason, is so important to isolate the different factors of the transition and analyse the influence of each factor independently, with a complete knowledge about the complexity of the transition in order to correct or at least minimise the bias.

Table 4.3: Basic statistics estimated for each homogeneous sub-period (HSP) providing the number of parallel AWSu – MAN observations of Fabra Observatory, mean differences and root-mean square deviation (RMSD) for maximum temperature differences ( $\Delta T_{max}$ ) and minimum temperature differences ( $\Delta T_{min}$ ).

		MCV1.2	MCV1.1	MCV2.3	MCV2.2	MCV2.1	Vaisala
N		669	545	504	515	457	1249
Mean	$\Delta T_{max}$ [°C]	3.7	1.1	0.5	1.8	1.5	-0.1
	$\Delta T_{min}$ [°C]	-0.6	-0.3	-0.8	0.0	-0.4	-0.2
RMSD	$\Delta T_{max}$ [°C]	4.0	1.7	1.2	2.1	1.9	0.6
	$\Delta T_{min}$ [°C]	0.8	0.7	0.9	0.4	0.6	0.3

As in the case of Ebro Observatory, not only the mean, but also the distribution of the bias depends on the HSP. Figure 4.5 shows the histograms of  $\Delta T_{max}$  and  $\Delta T_{min}$  for each HSPs (the values are in Table A2.4). The main characteristic of the AWSu-MAN serie is the high differences of the MCV1 and MCV2 sub-periods, especially on  $\Delta T_{max}$ .

The histograms show that the higher differences are in the MCV1.2, in the same way that mean and RMSD, especially for the  $\Delta T_{max}$ , for which more than 90% of the differences are larger than 1.5 °C. Opposite, the differences on  $\Delta T_{min}$  are also high (50% of the differences smaller than -0.5 °C), but negative. This different sign on the differences can be as consequence of the different shelter. The multiple screens are smaller so the inertia of the shelter is lower than with the Stevenson Screen. This means that the multiple screen response quickly to the atmospheric change. On the other side, we have to consider if the multiple screen is ventilated or not, for the not ventilated, the air circulation is smaller than in the case of the ventilated (as in the case of the Stevenson Screen), but in this case,

the air quantity inside the multiplate screen is lower. So, in sunny and calm days (days with high solar radiation and lower wind speed), for which the natural air mixing is not so much, we can expect to have higher temperatures during day time, due to the continuous heating, and lower temperatures during the night time by heat loss and terrestrial radiation, in multiplate screens than in the Stevenson Screen.

During the MCV2 sub-periods, the distribution of the differences also indicates high positive differences for  $\Delta T_{\max}$  and not so high negative differences for  $\Delta T_{\min}$ . Regarding the  $\Delta T_{\max}$  is the MCV2.2 sub-period for which the differences are higher, for this sub-period, more than 55 % of the differences are higher than 1.5 °C, which is a very high percentage. Especially, if we consider that about 90 % of the  $\Delta T_{\max}$  are larger than 0.5 °C. The  $\Delta T_{\min}$  of this period are also high, in this case, is the MCV2.3 the sub-period with the maximum differences, more than 75 % of the differences are smaller than -0.5 °C.

For the Vaisala period, the differences are lower for both extreme daily temperatures. For this case, the most part of the differences are between -0.5 and 0.5 °C, and for both cases, mostly positives. For both extreme series, the most part of the differences out of this range are negative and between -1 and -0.5 °C. This different differences sign especially on the  $\Delta T_{\max}$  and the smaller differences can be explained because in this period, both the AWSu and the MAN are recorded inside the Stevenson Screen. Otherwise, it could be a complete change on the temperature measurement system and a change on the manufacturer and this also can influence the change on the differences.

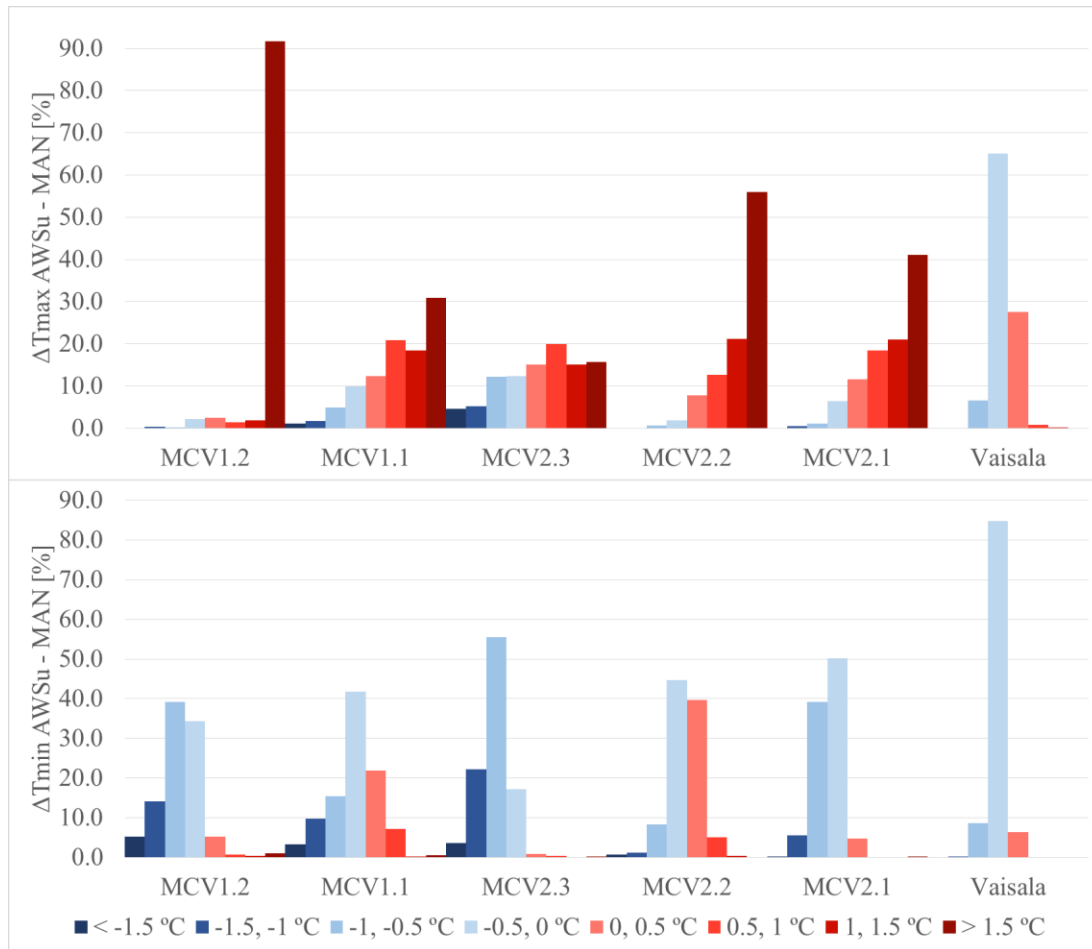


Figure 4.5: Histogram of the daily maximum and minimum temperature differences AWSu-MAN of Fabra Observatory ( $\Delta T_{max}$  and  $\Delta T_{min}$ ) for the 6 HSPs detected.

Another important point for describing the bias is the seasonality, being especially important to minimise or to correct the bias in the future. The seasonality is a good indicator of the characteristics of the bias, because it gives us information about the factors that we have to consider.

In this case, in concurrence with Ebro Observatory, the differences for all the sub-periods and for  $\Delta T_{max}$  and  $\Delta T_{min}$  across the season are statistically significant according the Fisher ANOVA test.

The  $\Delta T_{max}$  are the most influenced (Figure 4.6), as for the other characteristics, the differences are more similar between the MCVs sub-periods than with the Vaisala period. In the case of the MCV sub-period, in all the cases the higher differences are in summer and the lower in winter (also considerably minor in autumn). In the case of the  $\Delta T_{min}$ , there are differences between the sub-periods of the MCV1 and MCV2. For the oldest sub-periods,

the most part of the  $\Delta T_{min}$  are negative in all the seasons. Is not the case of  $\Delta T_{min}$  of the MCV2, because for this sub-periods, there are differences on the sign of the bias according the season. So, especially for winter the differences are positive and for spring-summer negative. As is explained, in this sub-period the AWSu and the MAN are not inside the same screen, so this can have an influence on the different sign of the differences according the season.

In the Vaisala period, the differences along the seasons are important, so in the case of the  $\Delta T_{max}$ , in winter the differences are negative but for summer, the most part of the differences are positive. For  $\Delta T_{min}$ , in all the seasons the most part of the differences are negative, but is for winter and autumn when the differences are larger.

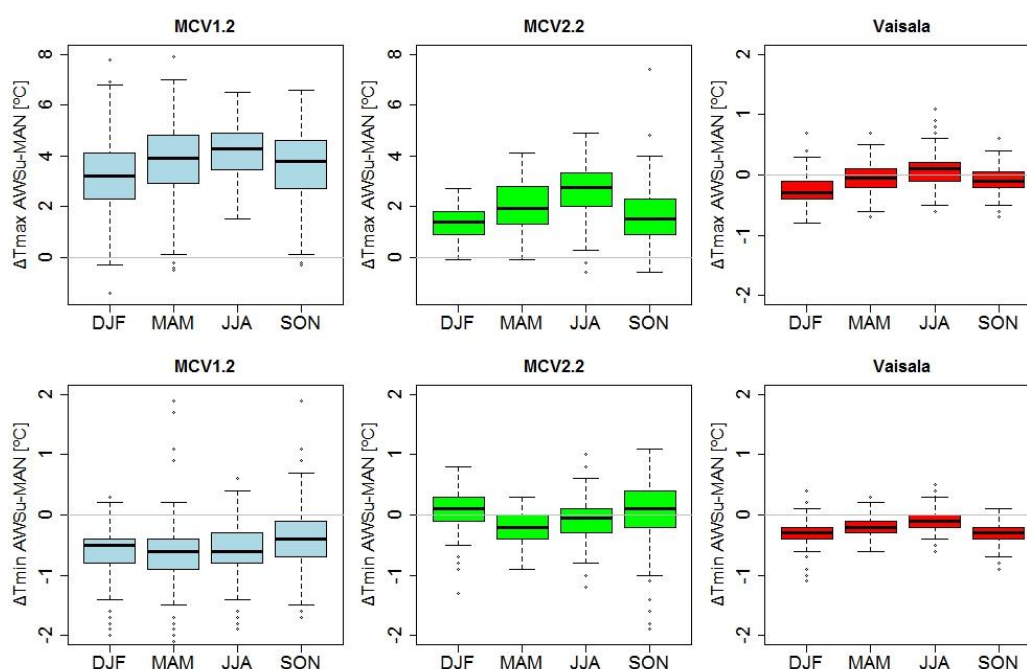


Figure 4.6: Seasonal boxplots of the  $\Delta T_{max}$  (upper plots) and  $\Delta T_{min}$  (lower plots) for the MCV1.2, MCV2.2 and Vaisala sub-periods, Fabra Observatory.

We have seen in the Ebro Observatory data, that the recorded temperature has an influence on the differences. In the case of the Fabra Observatory AWSu-MAN, for the MCVs periods, the influence on the  $\Delta T_{min}$  is negligible, but not for  $\Delta T_{max}$ . In the case of  $\Delta T_{max}$ , for all sub-periods of MCV1 and MCV2 for lower  $T_{max}$  ( $< 15$  °C) the differences are lower than for the high  $T_{max}$  ( $> 30$  °C) for which the mean of the  $\Delta T_{max}$  are higher than the mean of all  $\Delta T_{max}$  (Figure 4.7).



In the case of the Vaisala period, the both ( $\Delta T_{max}$  and  $\Delta T_{min}$ ) are different depending on the recorded temperature. Thereby, the sign of  $\Delta T_{max}$  depends on the recorded temperature, for lower  $T_{max}$ , the mean of the difference are negative and for higher  $T_{max}$ , the mean of the differences are positive and lower than for lower  $T_{max}$ . In case of  $T_{min}$ , the differences also depend on the recorded  $T_{min}$  but in this case, the mean of the differences is also negative. So, for  $T_{min}$ , higher negative differences when the  $T_{min}$  of the MAN observations is lower than 10 °C.

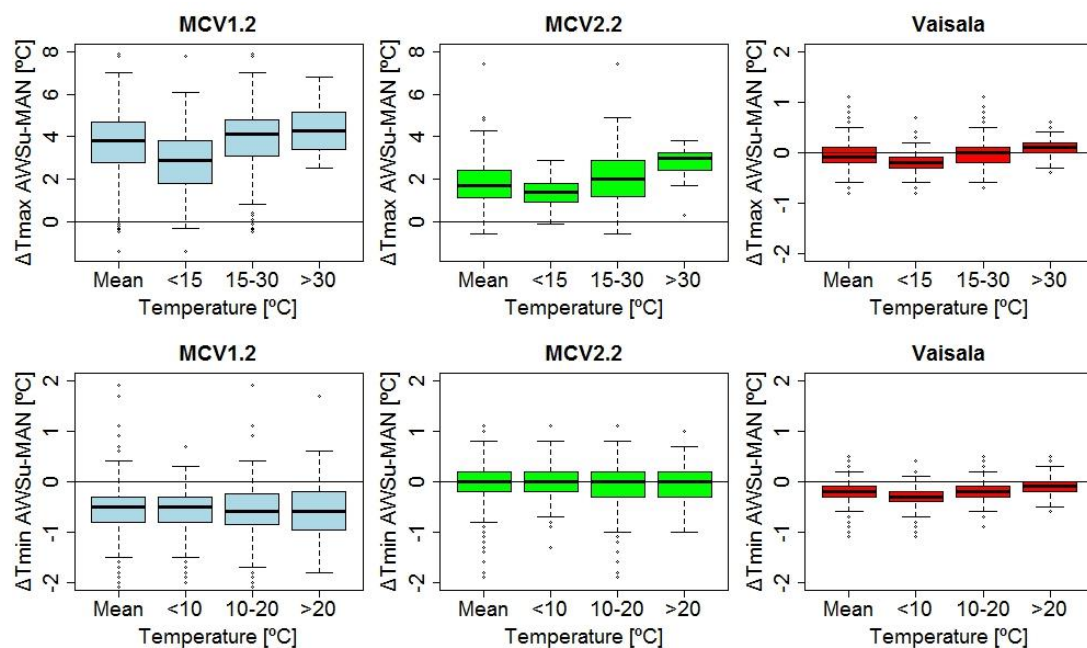


Figure 4.7: Boxplots for maximum (upper plots) and minimum (lower plots) temperature difference series AWSu-MAN of Fabra Observatory of MCV1.2, MCV2.2 and Vaisala for those days in which daily maximum temperatures ( $T_{max}$ ) is lower than 15 °C, 15-30 °C and upper than 30 °C and days in which daily minimum temperatures ( $T_{min}$ ) is lower than 10 °C, 10-20 °C and upper than 20 °C.

At this point, it is checked that the  $\Delta T_{max}$  and  $\Delta T_{min}$  of the MCVs sub-periods are significantly different than for the Vaisala period and than for the Ebro Observatory sub-periods. We know that for these sub-periods, we not only are comparing two observations take it by different measurement systems, but also by paced in different shelter. It was expectable that for the MCVs sub-periods, the correlation with covariables will be higher than for the Vaisala period.

Table 4.4 shows the spearman’s correlation coefficients between  $\Delta T_{max}$ ,  $\Delta T_{min}$  and  $T_{max}$  and  $T_{min}$  recorded temperatures, DTR, wind speed and sunshine hours. Opposite to the expected, the Spearman’s correlation coefficients for the MCVs sub-periods are not very high. But if the days are stratified depending on a combination of high and lower wind speed and sunshine hours, effectively, the MCVs sub-periods are more affected (Figure 4.8), especially for the MCV2.2 and  $\Delta T_{max}$ .

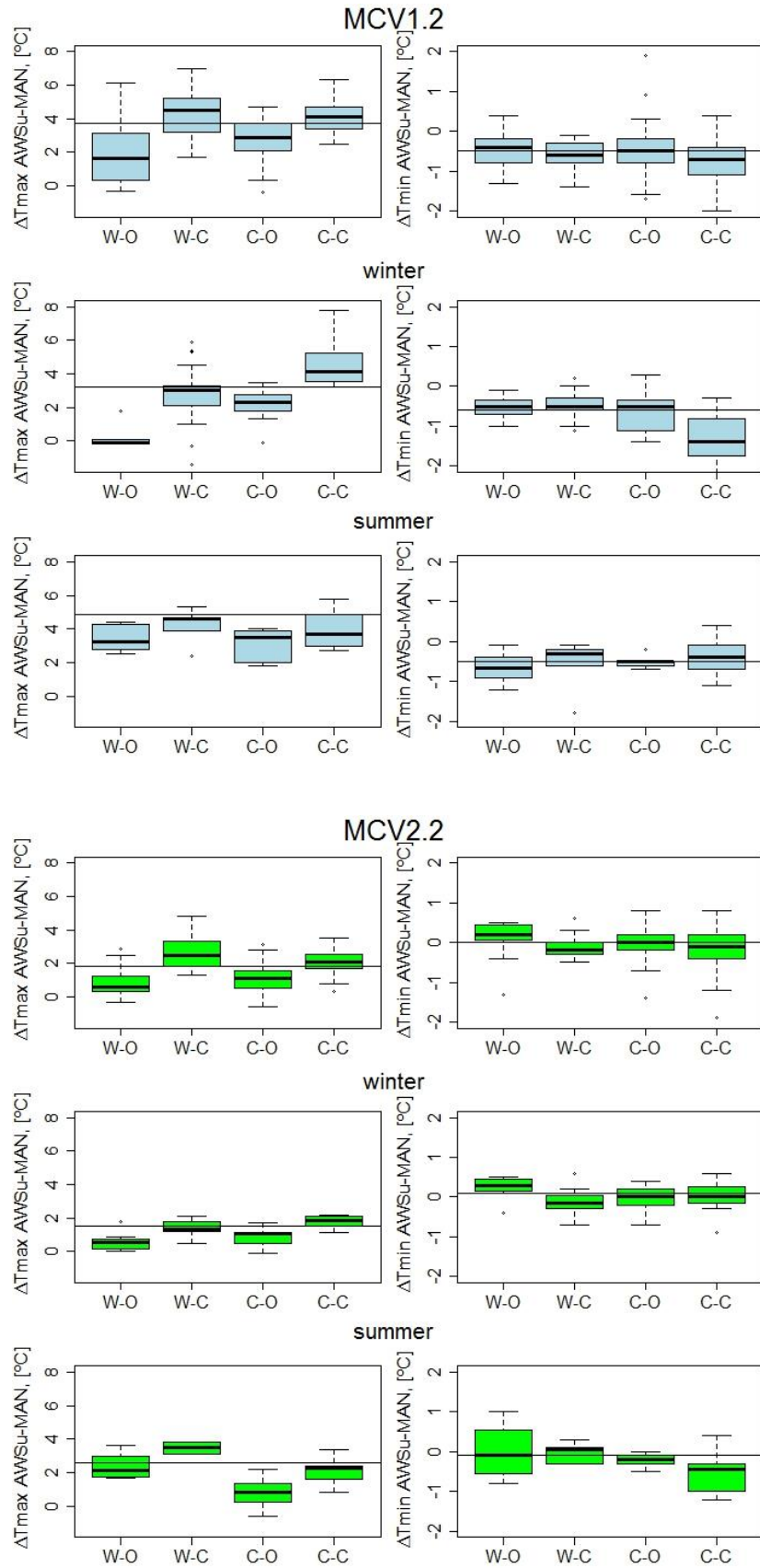
The winter  $\Delta T_{max}$  are most affected by the combination of wind and sunshine than the summer  $\Delta T_{max}$  for MCV1.2. There are higher differences on winter  $\Delta T_{max}$  between the wind and overcast days than the calm and clear days. For the calm and clear days, the winter  $\Delta T_{max}$  are always higher than the mean, opposite the  $\Delta T_{max}$  of windy and overcast days are always lower than the mean. In the case of  $\Delta T_{min}$ , only for winter the difference of the calm and clear days is lower than the mean.

For MCV2.2, the  $\Delta T_{max}$  are especially affected by the sunshine. Thereby, for the whole year, the clear days (windy and calm) the  $\Delta T_{max}$  are higher than the mean. In summer are the windy and calm days the days with highest  $\Delta T_{max}$ . In the case of  $\Delta T_{min}$ , in winter for the windy and overcast days the differences are positive. In summer, the higher differences are at calm and clear days.

For the Vaisala period, there are not differences on the  $\Delta T_{max}$  and  $\Delta T_{min}$  depending on the stratification of the days according the wind speed and sunshine hours.

Table 4.4: Spearman’s correlation coefficients ( $\rho$ ) estimated among the maximum ( $\Delta T_{max}$ ) and minimum ( $\Delta T_{min}$ ) temperature differences and  $T_{max} - T_{min}$  MAN ( $T_{max}$  MAN,  $T_{min}$  MAN) observations, daily temperature range (DTR), wind speed (WS) and sunshine hours (sunshine) for the MCV1.2, MCV2.2 and Vaisala sub-periods, Fabra Observatory. In bold are the coefficients that are statistically significant at the 95 % confidence level.

	MCV1.2		MCV2.2		Vaisala	
	$\Delta T_{max}[^{\circ}\text{C}]$	$\Delta T_{min}[^{\circ}\text{C}]$	$\Delta T_{max}[^{\circ}\text{C}]$	$\Delta T_{min}[^{\circ}\text{C}]$	$\Delta T_{max}[^{\circ}\text{C}]$	$\Delta T_{min}[^{\circ}\text{C}]$
$T_{max}$ MAN	<b>0.3</b>		<b>0.5</b>		<b>0.5</b>	
$T_{min}$ MAN		0.0		0.0		<b>0.3</b>
DTR	<b>0.3</b>	-0.1	<b>0.5</b>	<b>-0.1</b>	<b>0.4</b>	<b>0.3</b>
WS	<b>-0.2</b>	<b>0.1</b>	0.0	0.1	<b>-0.3</b>	<b>-0.2</b>
Sunshine	<b>0.4</b>	<b>-0.2</b>	<b>0.5</b>	-0.1	<b>0.3</b>	<b>0.2</b>



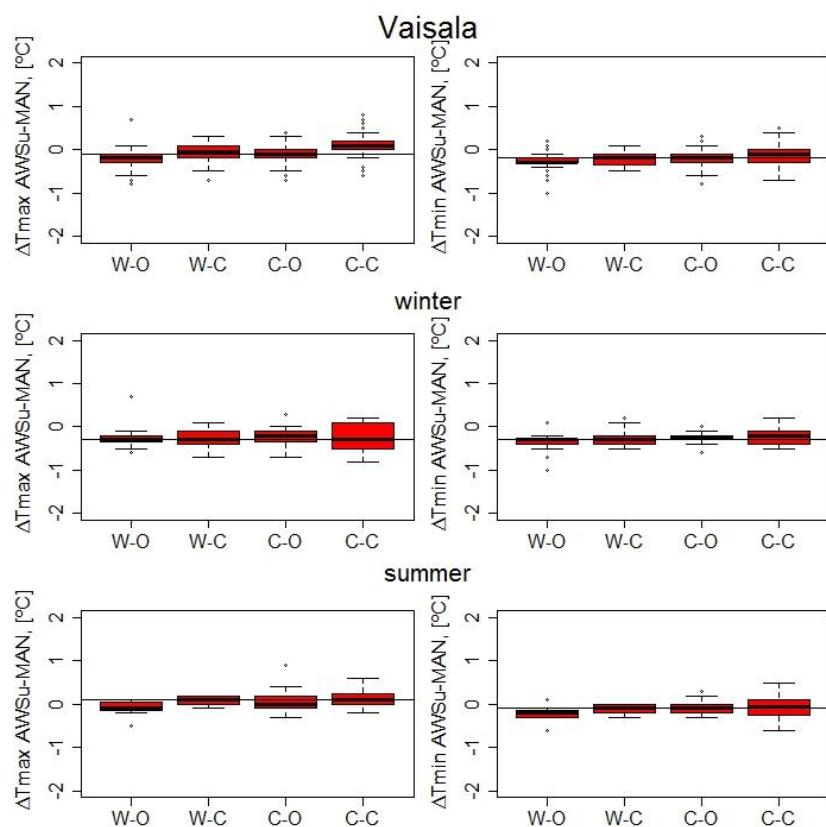


Figure 4.8: For the MCV1.2, MCV2.2 and Vaisala sub-periods (Fabra Observatory) the boxplots of  $\Delta T_{\max}$  (left plots) and  $\Delta T_{\min}$  (right plots) according the stratification of the day depending on the wind speed and the sunshine hours. W-O (windy and overcast days), W-C (windy and clear days), C-O (calm and overcast days), C-C (calm and clear days). See Table A2.5 (page 203) for the values.

### 4.3 – Murcia Observatory AWSu – MAN

Eight years of parallel measurements of AWSu-MAN (2004-2012) have been used for Murcia observatory. As in the case of Ebro and Fabra Observatories, AWSu-MAN parallel measurements show during these 8 years different BPs, describing 4 HSPs. Also for this daily parallel temperature time-series, the main characteristic of the AWS bias is the dependence of the bias with the instrumentation, with the changes on the AWSu (Figure 3.14, page 90).

Table 4.5 shows the mean and RMSD for  $\Delta T_{max}$  and  $\Delta T_{min}$  for the 4 HSPs detected. In general, the differences are positive except for the  $\Delta T_{max}$  of SEAC3 for which the mean of  $\Delta T_{max}$  is  $-0.4\text{ }^{\circ}\text{C}$ . The higher differences for the both daily temperature extremes are in this SEAC3 sub-period, the RMSD of  $\Delta T_{max}$  is  $0.7\text{ }^{\circ}\text{C}$  ( $1.0\text{ }^{\circ}\text{C}$  for  $\Delta T_{min}$ ). The lower differences for the both ( $\Delta T_{max}$  and  $\Delta T_{min}$ ) are for SEAC1.

*Table 4.5: Basic statistics estimated for each homogeneous sub-period (HSP) providing the number of parallel AWSu – MAN observations of Murcia Observatory, mean differences and root-mean square deviation (RMSD) for maximum temperature differences ( $\Delta T_{max}$ ) and minimum temperature differences ( $\Delta T_{min}$ ).*

		SEAC4	SEAC3	SEAC2	SEAC1
<b>N</b>		980	673	694	845
<b>Mean</b>	$\Delta T_{max}$ [ $^{\circ}\text{C}$ ]	0.1	-0.4	0.4	0.0
	$\Delta T_{min}$ [ $^{\circ}\text{C}$ ]	0.5	0.9	0.3	0.2
<b>RMSD</b>	$\Delta T_{max}$ [ $^{\circ}\text{C}$ ]	0.4	0.7	0.5	0.4
	$\Delta T_{min}$ [ $^{\circ}\text{C}$ ]	0.6	1.0	0.5	0.4

With the mean and RMSD is obvious that there are differences on the bias depending on the HSP, especially the SEAC3 sub-period. Another important point in order to explain the bias is the distribution of the differences. For the parallel measurements AWSu-MAN of Murcia Observatory, the most part of the  $\Delta T_{max}$  and  $\Delta T_{min}$  for all the HSPs -except for the SEAC3- are between  $-0.5$  and  $0.5\text{ }^{\circ}\text{C}$  (Figure 4.9).

For the older HSP, the SEAC4, most than 80 % of the  $\Delta T_{max}$  are between  $-0.5$  and  $0.5\text{ }^{\circ}\text{C}$ , the  $\Delta T_{max}$  outside this range are mostly negative, but the larger differences are positive, being  $\Delta T_{max}$  higher than  $1.5\text{ }^{\circ}\text{C}$ . For the  $\Delta T_{min}$  of this period, the differences are larger,

the percentage of the differences inside the interval  $-0.5\text{ }^{\circ}\text{C} - 0.5\text{ }^{\circ}\text{C}$  is 51 % and the greatest part of the differences are inside the range 0.5 and  $1.0\text{ }^{\circ}\text{C}$  (44.9 %), so mainly, the differences are positive.

As it is explained before, the SEAC3 is the sub-period in which the bias is larger, for both series ( $\Delta T_{\text{max}}$  and  $\Delta T_{\text{min}}$ ). For  $\Delta T_{\text{max}}$ , the most part of the differences are negative and around 50 % are smaller than  $-0.5\text{ }^{\circ}\text{C}$ . For  $\Delta T_{\text{min}}$ , the most part are positive, and more than 80 % of the differences are larger than  $0.5\text{ }^{\circ}\text{C}$ .

For the SEAC2 sub-period, and for both variables, the most part of the differences are positive and the percentage of cases in which  $\Delta T_{\text{max}}$  and  $\Delta T_{\text{min}}$  are larger than  $0.5\text{ }^{\circ}\text{C}$  is more than 25 %.

The SEAC1 sub-period, which is the most recent, shows, as for the other parallel temperature series AWSu-MAN analysed, that the differences are lower than for the other sub-periods and the main part of them are inside the range  $-0.5$  and  $0.5\text{ }^{\circ}\text{C}$ , about the 85 % in both cases.  $\Delta T_{\text{max}}$  outside this range are mostly negative, while the opposite happens in the case of  $\Delta T_{\text{min}}$  which the differences outside the interval are mostly positive.

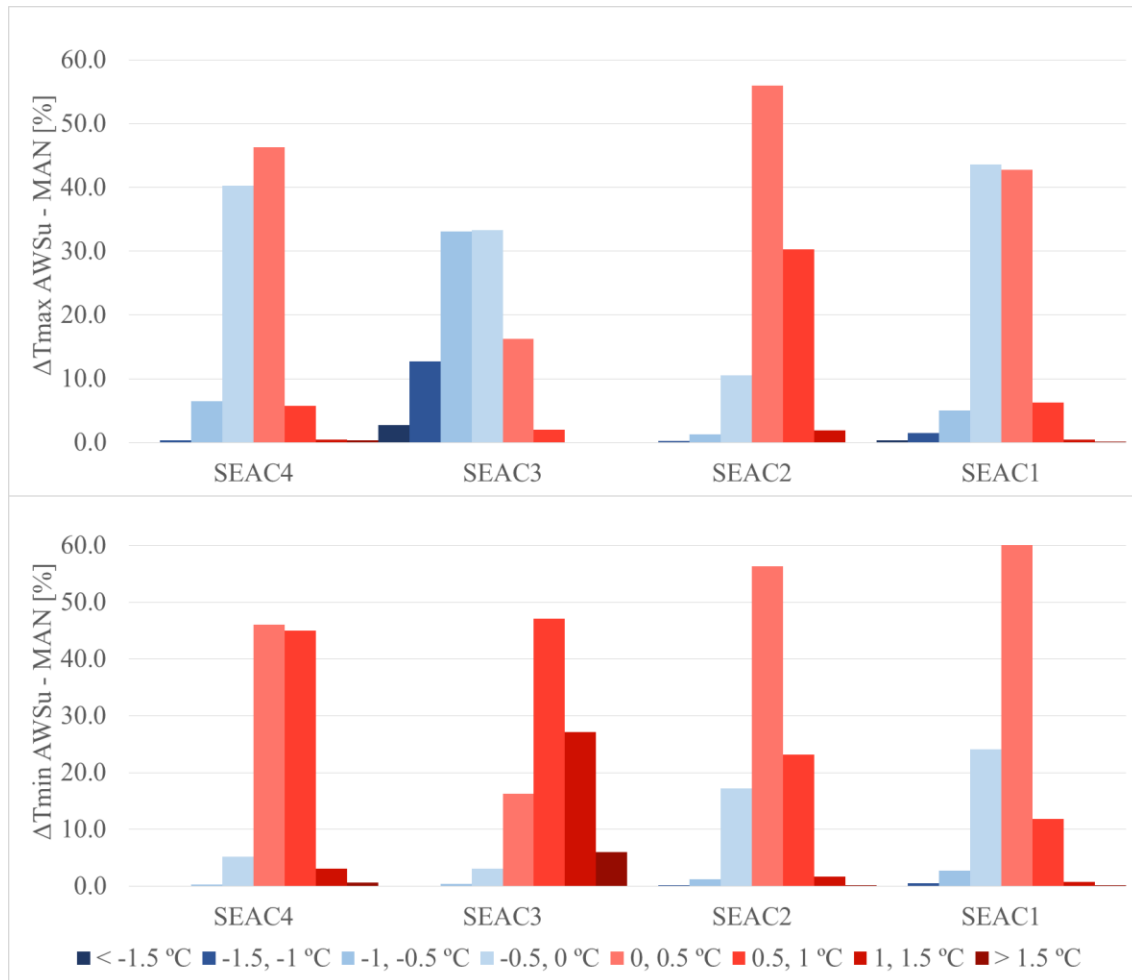


Figure 4.9: Histogram of the daily maximum and minimum temperature differences AWSu - MAN of Murcia Observatory ( $\Delta T_{max}$  and  $\Delta T_{min}$ ) for the 4 HSPs detected, SEAC4, SEAC3, SEAC2 and SEAC1, Table A2.6, page 204 to see the values.

Also, as for the other observatories analysed, the AWS bias has an important seasonality. In the case of the Murcia AWSu-MAN, except for the SEAC1  $\Delta T_{max}$ , the differences across the seasons are significant according the Fisher ANOVA test.

Figure 4.10 shows seasonal boxplots for  $\Delta T_{max}$  and  $\Delta T_{min}$  for each HSP detected. For SEAC4 the main characteristic of  $\Delta T_{max}$  is that for summer the differences are positive and for winter mostly negative and for  $\Delta T_{min}$  the differences for all the seasons are mainly positive but larger for spring and summer. For SEAC3,  $\Delta T_{max}$  in summer are larger than for the other seasons, especially than for winter, the season in which the differences are lower. As it has been shown before, the differences of  $\Delta T_{min}$  of this period are mainly negative and for these variables, as different as for  $\Delta T_{max}$  the larger differences are in summer. For SEAC2 sub-period, for  $\Delta T_{max}$  as for SEAC4 the larger positive differences

are in summer, and in this sub-period also for autumn. For  $\Delta T_{min}$ , the larger differences are also larger in summer. In the case of SEAC1, the differences across the season are lower, especially for  $\Delta T_{max}$ , for which the differences are not significant.

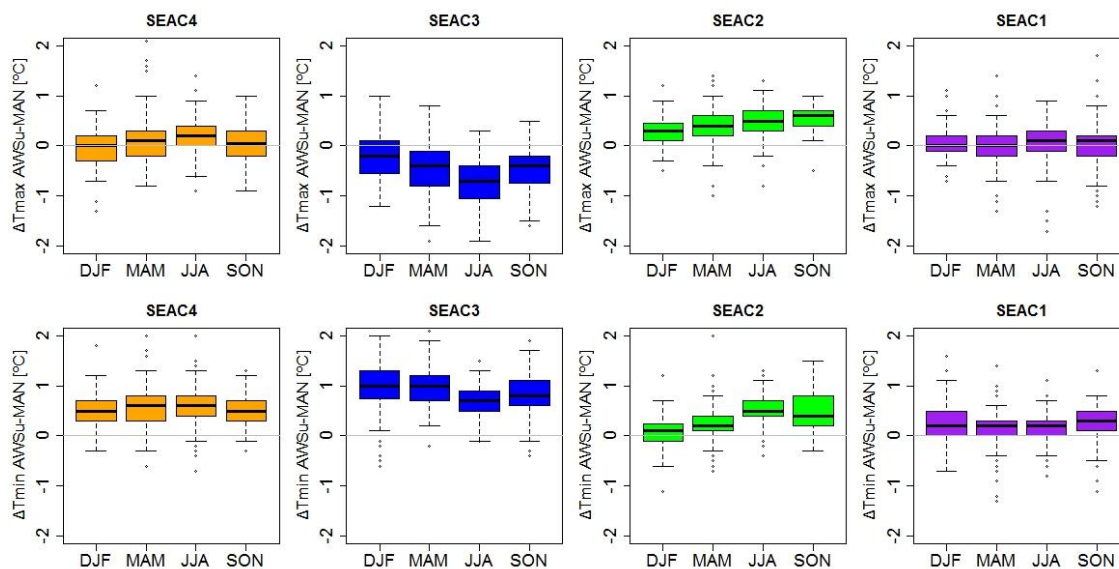


Figure 4.10: Seasonal boxplots of the  $\Delta T_{max}$  (upper plots) and  $\Delta T_{min}$  (lower plots) for the four HSPs detected in Murica Observatory.

Figure 4.11 shows the boxplots of the  $\Delta T_{max}$  and  $\Delta T_{min}$  depending on different  $T_{max}$  and  $T_{min}$  temperature range for the four detected HSPs. It is for the sub-periods SEAC3 and SEAC2 when there are more differences on the bias depending on the range of temperatures. Thereby, the  $\Delta T_{max}$ , in the case of  $T_{max}$  lower than 15 °C, of SEAC3 are mostly positive and for the other ranges of temperatures are negative. Contrary, the differences  $\Delta T_{min}$  for all ranges of  $T_{min}$  are mainly negative, but for the cases of  $T_{min}$  lower than 10 °C the differences are lower and some part positive. As for  $T_{max}$ , as higher is the  $T_{min}$  register, higher  $\Delta T_{min}$ .

For the SEAC2 sub-period, there are also significant differences on the  $\Delta T_{max}$  and  $\Delta T_{min}$  depending on the  $T_{max}$  and  $T_{min}$  registered but in this case, the sign of the differences is mainly positive but the magnitude differs. For the both cases, lower temperatures (lower  $T_{max}$  and  $T_{min}$ ) means lower differences, especially for  $\Delta T_{max}$ .

For the other two periods, the differences are not so influenced by the recorded temperature. For the SEAC4 sub-period the  $\Delta T_{max}$ , but especially the  $\Delta T_{min}$  are slightly higher for high temperatures. The dependence  $\Delta T - T$  of the SEAC1 is similar to the SEAC4. These results



are consistent with the significant Spearman correlation coefficients (Table 4.6), especially for the SEAC3 but also for the SEAC2 between the  $\Delta T_{\max}$  ( $\Delta T_{\min}$ ) and  $T_{\max}$  ( $T_{\min}$ ).

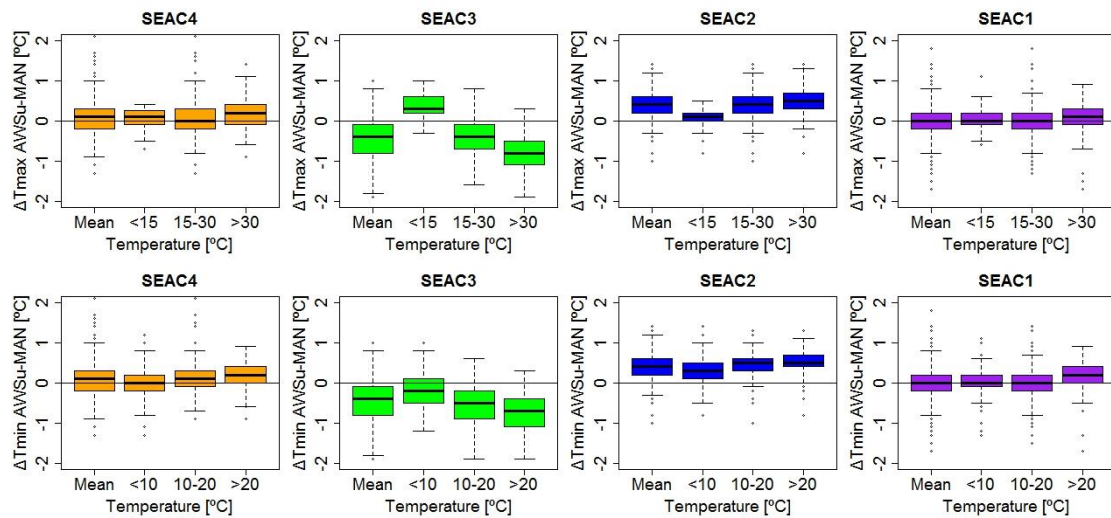


Figure 4.11: Boxplots for maximum (upper plots) and minimum (lower plots) temperature difference series AWSu-MAN of Murcia Observatory of the four HSPs detected for those days in which daily maximum temperatures ( $T_{\max}$ ) is lower than 15 °C, 15-30 °C and upper than 30 °C and days in which daily minimum temperatures ( $T_{\min}$ ) is lower than 10 °C, 10-20 °C and upper than 20 °C.

The AWSu-MAN differences of Murcia Observatory are also affected by the covariables. Table 4.6 shows the Spearman's correlation coefficients between  $\Delta T_{\max}$  and  $\Delta T_{\min}$  and the recorded temperature, the DTR, the wind speed and the daily number of sunshine hours. In general, the correlation of the wind speed and the sunshine with the differences AWSu-MAN, are similar than the results found to the AWSu-MAN of Ebro Observatory. As for this case, the highest correlations are for the relation between the differences and the recorded temperature and the DTR, while for wind speed and sunshine hours the correlations are lower. The  $\Delta T_{\max}$  of the SEAC3 are the more correlated with the sunshine hours.

Table 4.6: Spearman’s correlation coefficients ( $\rho$ ) estimated among the maximum ( $\Delta T_{max}$ ) and minimum ( $\Delta T_{min}$ ) temperature differences and  $T_{max} - T_{min}$  MAN ( $T_{max}$  MAN,  $T_{min}$  MAN) observations, daily temperature range (DTR), wind speed (WS) and sunshine hours (sunshine) for the SEAC4, SEAC3, SEAC2 and SEAC1 sub-periods, Murcia Observatory. In bold are the coefficients that are statistically significant at the 95 % confidence level.

	SEAC4		SEAC3		SEAC2		SEAC1	
	$\Delta T_{max}$	$\Delta T_{min}$	$\Delta T_{max}$	$\Delta T_{min}$	$\Delta T_{max}$	$\Delta T_{min}$	$\Delta T_{max}$	$\Delta T_{min}$
	[°C]	[°C]	[°C]	[°C]	[°C]	[°C]	[°C]	[°C]
$T_{max}$ MAN	0.1		<b>-0.7</b>		<b>0.4</b>		<b>0.3</b>	
$T_{min}$ MAN		-0.1		<b>-0.5</b>		<b>0.5</b>		<b>0.1</b>
DTR	<b>-0.2</b>	<b>0.3</b>	<b>-0.5</b>	<b>0.3</b>	<b>0.2</b>	<b>0.2</b>	<b>0.1</b>	<b>0.1</b>
WS	<b>-0.2</b>	<b>-0.2</b>	<b>-0.2</b>	<b>-0.2</b>	<b>-0.2</b>	0.0	<b>-0.2</b>	<b>-0.2</b>
Sunshine	<b>0.1</b>	<b>0.2</b>	<b>-0.5</b>	0.0	<b>0.2</b>	<b>0.3</b>	<b>0.1</b>	-0.1

But as for the other cases, if the days are stratified depending on the wind speed and the sunshine hours, the relation of these two variables with the differences is higher, especially if we consider what is happening for the extreme seasons, winter and summer. Figure 4.12 shows the boxplots for all the HSPs detected with the  $\Delta T_{max}$  and  $\Delta T_{min}$  according the days stratification, for the whole year, as well as for winter and summer.

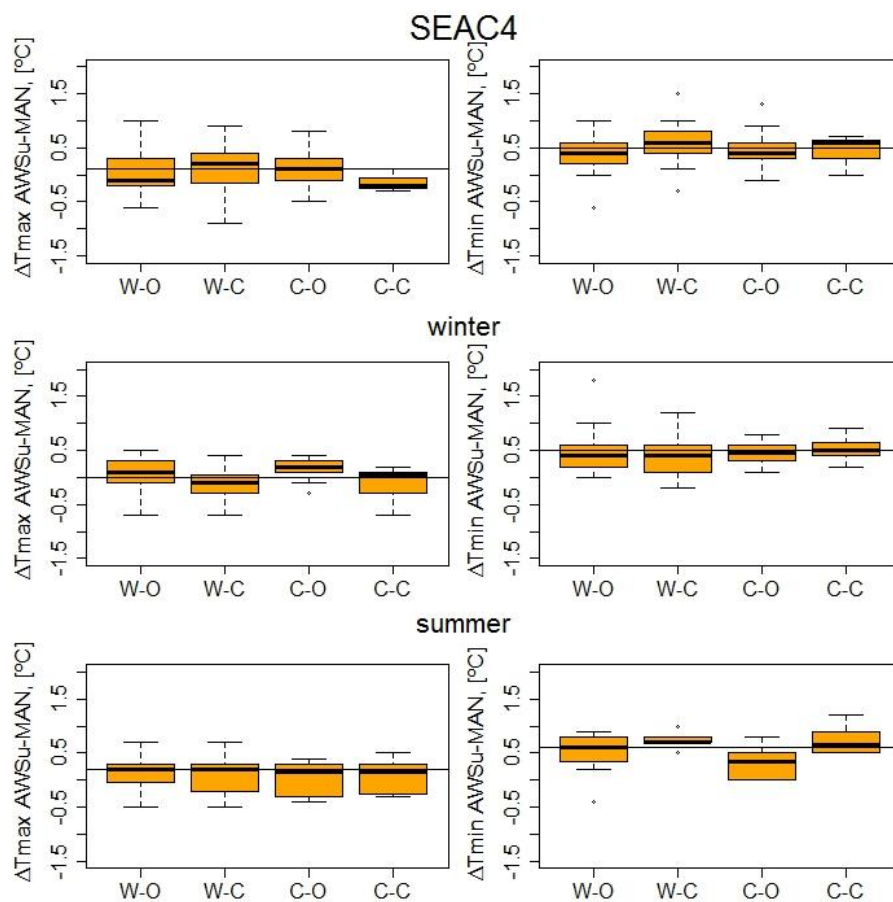
As for the other cases, winter is the season in which the differences AWSu-MAN are more influenced by the wind speed and the sunshine hours, but as for the other parallel series, this influence is not equal for all the HSPs and for different sub-periods, the same type of weather days can give larger or lower differences.

For the SEAC4 sub-period, the winter  $\Delta T_{max}$  of the windy and clear days are negative, and oppositely the calm and overcast days positive. The SEAC3 sub-period as is showed before is the most affected, especially in winter. In general, for this period, the  $\Delta T_{max}$  of the windy and overcast days are positive and the highest negative differences are found -for windy and clear days. For the  $\Delta T_{min}$  the differences are lower, except for winter, for which the maximum positive differences are for the calm and clear days.

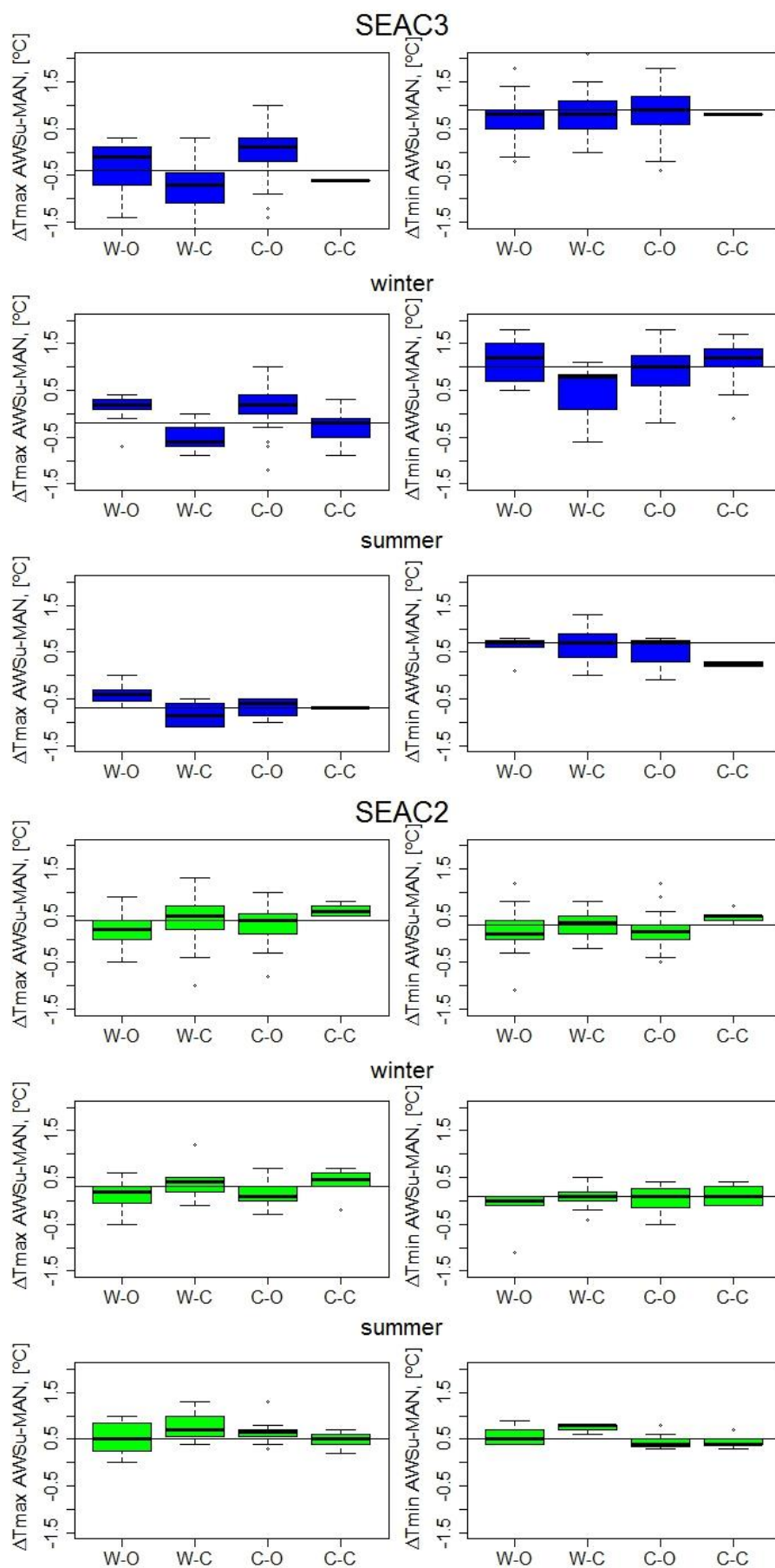
For the SEAC2 there are also differences depending on the stratifications days, especially for the  $\Delta T_{max}$ . So, in general, for the whole year and winter, the windy and overcast days

and the calm and overcast days have lower differences and the calm and clear days have the highest positive differences. For summer, the calm and overcast and the windy and clear days are the days with the maximum positive differences.

On the SEAC1 sub-period, there are also differences depending on the windy and sunshine conditions. And this difference depends on the season, so for winter the windy and overcast days have negative and larger  $\Delta T_{max}$  and opposite this type of days in summer means larger and positive  $\Delta T_{max}$ . Regarding the  $\Delta T_{min}$  of this period, the influences of the covariables are lower.



## 4 – Assessing the statistical characteristics of the AWSu – MAN differences



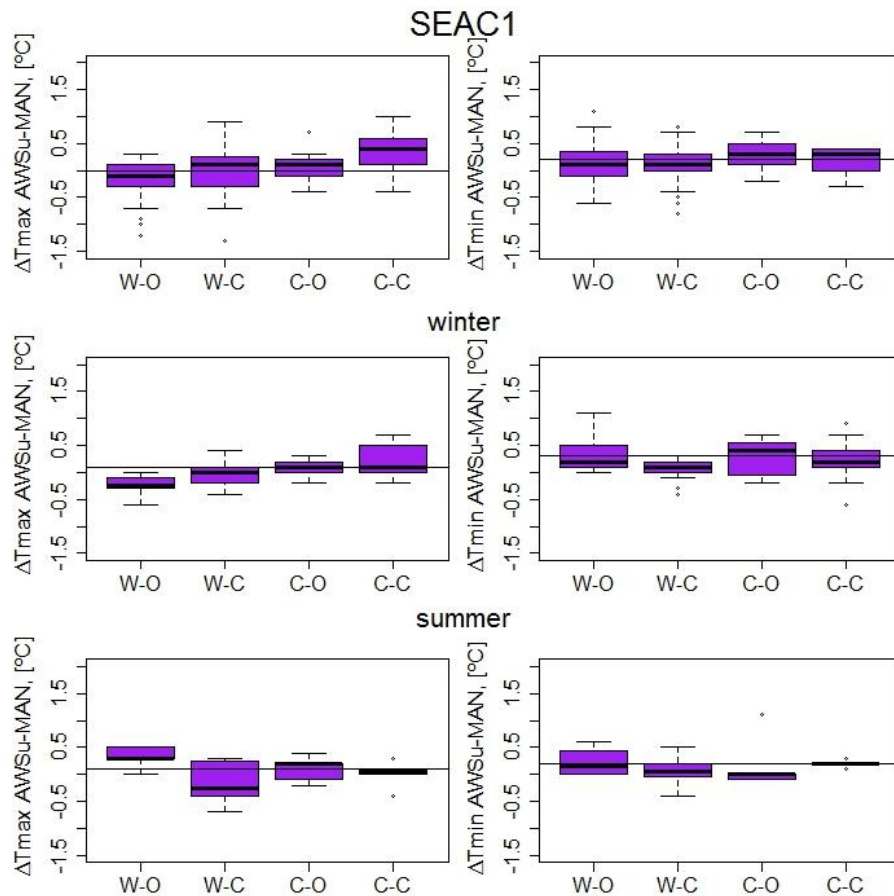


Figure 4.12: Boxplots of  $\Delta T_{max}$  (left plots) and  $\Delta T_{min}$  (right plots) for the four sub-periods determinate according the stratification of the day depending the wind speed and the sunshine hours. W-O windy and overcast days, W-C windy and clear days, C-O calm and overcast days and C-C calm and clear days. Page 93 to see the thresholds.

## Chapter 4 summary

- I. There is a clear dependence of AWSu bias on a particular instrumentation setting, since each HSP of every parallel temperature series analysed shows different bias magnitude and/or sign. Therefore any bias description or correction attempt must carefully account for internal inhomogeneities.
- II. In general, the AWSu-MAN differences are not equal for all the seasons, so for the majority of the HSP there is a clear seasonal cycle.
- III. The distribution of the differences depends also on the HSP analysed for the three observatories, in general the current HSP have lower differences
- IV. The recorded temperature has a high impact on the differences. So the  $\Delta T_{\max}$  and  $\Delta T_{\min}$  depends on the  $T_{\max}$  or  $T_{\min}$  observed. This shows the impact of a not calibration regarding the metrological standard procedures.
- V. In general, the covariables independently have not a high impact on the differences. But the stratification of the days depending on the wind speed and the sunshine hours has an impact on the bias.
- VI. For Fabra Observatory, when the AWSu-MAN observations are take it in different shelters the differences are higher. This shows the need to study the AWS bias isolated.
- VII. To correct or at least minimise the AWSu-MAN bias it will be necessary to take into account the dependence of the  $\Delta T_{\max}$  and  $\Delta T_{\min}$  with the HSP and the seasonal cycle of the differences. These high differences with the AWSu and the bias and the shortness of the HSPs make difficult the possible application of the current homogenisation methods.



## **Chapter 5 – Can the metrological approach improve the quality of the temperature time-series? – Daily data**







## Chapter 5: Can the metrological approach improve the quality of the temperature time-series? – Daily data

In the previous chapter, is demonstrated that the main characteristic of the AWSu – MAN differences is the higher dependence of the bias with the AWSu. This can be caused by the not adoption of the standard metrological procedures.

The introduction of AWS has been a breakthrough and has brought us many advantages, but in order to fully exploit the advantages of these measurement systems, firstly is necessary to understand very well the complexity of the new temperature measurements and apply all procedures required to ensure the reliability of the measures.

In this chapter, is used the data registered by the three field trials, to answer two question: the first one is if the adoption of the standard calibration procedures can improve the reliability of the temperature time-series and secondly if with this is also possible at least minimise the AWS bias. This chapter is organised in three parts, on the first part is analysed the data take it on Moncalieri, in the second the data take it in Castello Borello, with this two field trials, the first question is assessed and on the third and last section, the data measured in Ebro Observatory is used to answer the second question.

### 5.1 – The impact of the adoption of the calibration curve – Moncalieri field trial

In this field trial, the AWS previously installed was calibrated regarding the metrological procedures, so in this field trial, there is only one AWS. Therefore, in here are provided the results of assessing the impact of introducing (AWS<sub>c</sub>) or not (AWS<sub>u</sub>) the calibration curve, as it is described in sub-section 3.1.2 (see page 78 for details of this field trial and the results of the calibration procedure applied to the AWS<sub>u</sub> in use). This means that the recorded observations are subjected to the application, or not, of the derived calibration curve. Thanks to this strategy, is possible isolate the influence of the application of the calibration curve and, therefore not assess the impact of other variables on the difference

series (AWS<sub>c</sub> – AWS<sub>u</sub>). It is only analysed to what degree the application of the calibration procedures affects the data series of daily  $T_{\max}$  and  $T_{\min}$  observations.

Figure 5.1 shows daily differences of both daily  $\Delta T_{\max}$  and  $\Delta T_{\min}$  (AWS<sub>c</sub> – AWS<sub>u</sub>) estimated from the Moncalieri field trial 01/09/2012 – 31/08/2013. The differences are lower for  $\Delta T_{\min}$  and in winter than in  $\Delta T_{\max}$  and in summer, as according to the results of the calibration curve, that indicates higher corrections for lower temperatures.

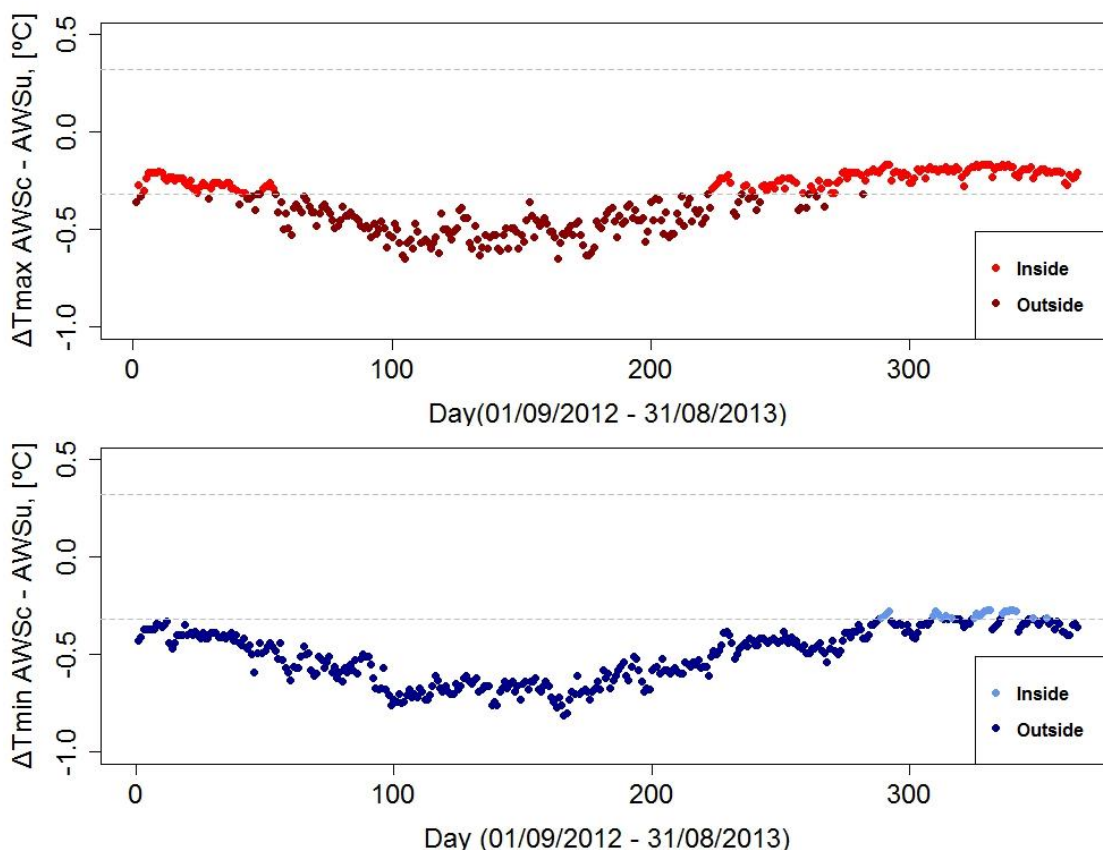


Figure 5.1: Daily maximum (upper plot) and minimum (bottom) temperature differences applying (AWS<sub>c</sub>) or not (AWS<sub>u</sub>) the results of the calibration curve in Moncalieri Observatory. Dotted grey lines surround the calibration uncertainty range ( $\pm 0.32$  °C). Red and blue (dark red and dark blue) circles identify differences inside (outside) the calibration uncertainty.

Table 5.1 provides annual and seasonal (winter and summer) averages of daily  $\Delta T_{\max}$  and  $\Delta T_{\min}$  along with the RMSD and the percentage of observations in which the differences are inside the calibration uncertainty for the whole year, summer and winter. These statistics confirm that the largest differences are estimated for winter and for  $\Delta T_{\min}$ . The mean of the  $\Delta T_{\max}$  for the whole year is  $-0.36$  °C and for  $\Delta T_{\min}$   $-0.50$  °C, for both cases

the mean of the yearly differences are outside the calibration uncertainty. And if is analysed what happen for the extreme seasons, is showed that for winter the mean of  $\Delta T_{min}$  is  $-0.68$  °C, being of  $-0.53$  °C for  $\Delta T_{max}$ .

Also the RMSD shows that the highest differences are for  $\Delta T_{min}$ , as a result, only the 6.9 % of the  $\Delta T_{min}$  are inside the calibration uncertainty, this means that the 93.1 % of the measurements of the AWSu without applying the calibration curve are potentially wrong.

These are very high differences, that shows not only to give traceability to the temperature time-series, also for the reliability of this time-series, the metrological procedures should be adopted.

*Table 5.1: Annual and seasonal (winter and summer) mean differences (°C) applying (AWS<sub>c</sub>) or not (AWS<sub>u</sub>) the calibration curve for daily maximum ( $\Delta T_{max}$ ) and minimum ( $\Delta T_{min}$ ) temperatures, along with the Root Mean Square Deviation (RMSD), the percentage of differences falling into the calibration uncertainty ( $\%|0.32|$  °C) and the number of parallel observations (n) for the period 21/09/2012 – 20/09/2013.*

	n	$\Delta T_{max}$ [°C]	$\Delta T_{min}$ [°C]
Mean (annual)	365	-0.36	-0.50
Mean (winter)	90	-0.53	-0.68
Mean (summer)	92	-0.20	-0.34
RMSD (annual)	365	0.38	0.52
$\%  0.32 $ °C	-	46.9	6.9

Figure 5.2 shows the histogram of the  $\Delta T_{max}$  and  $\Delta T_{min}$ . The most part of the differences and the higher mean differences are for  $\Delta T_{min}$ , and also for this variable is when the proportion of differences larger than  $-0.5$  °C is higher. For  $\Delta T_{max}$ , the proportion of the differences larger than  $-0.5$  °C also is important but least. This is an important fact, that shows how the not introduction of the calibration results can affects our data.

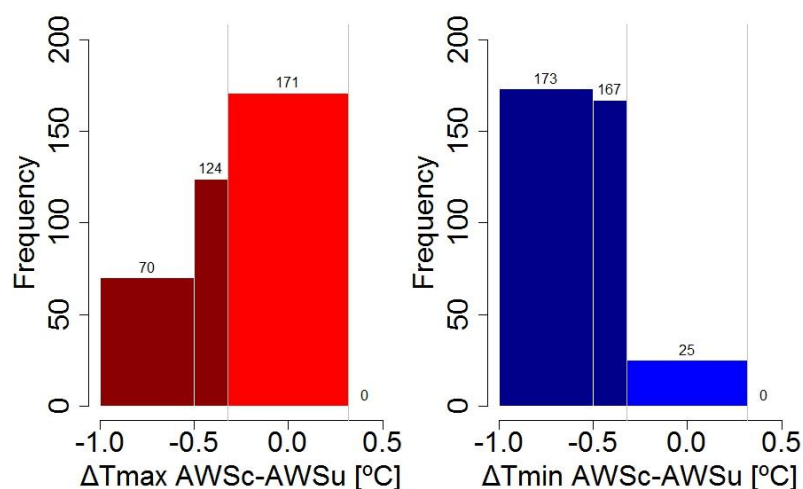


Figure 5.2: Histogram of the daily maximum and minimum temperature differences applying (AWSc) or not (AWSu) the calibration curve of Moncalieri Observatory observations ( $\Delta T_{max}$  and  $\Delta T_{min}$ ). In dark red and dark blue (for  $\Delta T_{max}$  and  $\Delta T_{min}$ ) the  $\Delta T_{max}$  and  $\Delta T_{min}$  outside the calibration uncertainty ( $0.32\text{ }^{\circ}\text{C}$ )

From Table 5.1 it is evident that the largest differences are estimated for winter for the two variables, with December for  $\Delta T_{max}$  and February for  $\Delta T_{min}$  showing the largest differences (Figure 5.3). In winter months plus March and November for  $\Delta T_{max}$  all the differences fall outside the calibration uncertainty. For  $\Delta T_{min}$  only some paired observations in summer fall inside the calibration uncertainty.

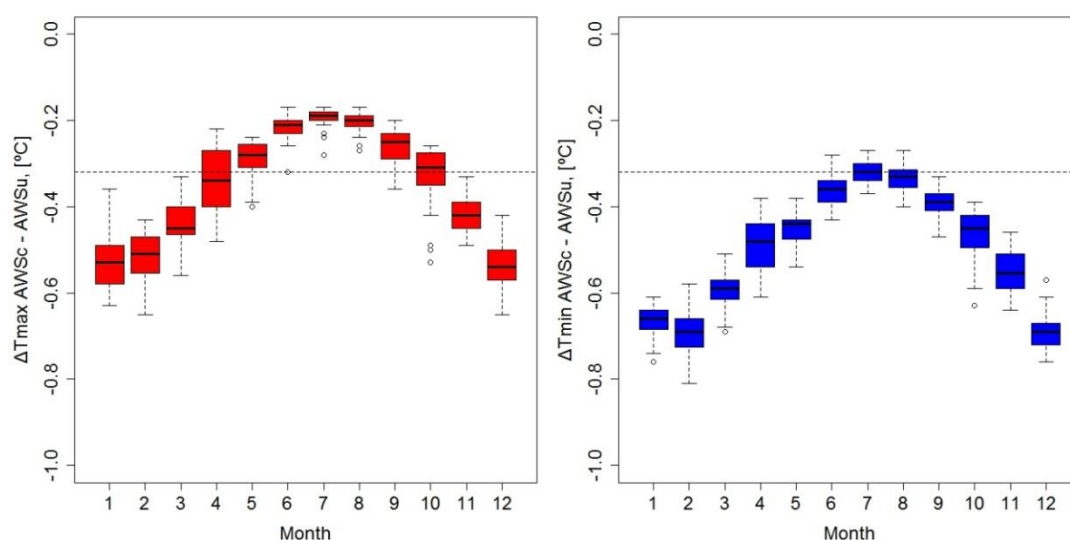


Figure 5.3: Boxplot of monthly maximum ( $\Delta T_{max}$ ) and minimum ( $\Delta T_{min}$ ) temperature differences applying (AWSc) or not (AWSu) the results of the calibration curve from the period 01/09/2012 to 31/08/2013 at the Moncalieri Observatory. Dotted line indicates the calibration uncertainty  $\pm 0.32\text{ }^{\circ}\text{C}$ .

We see that the adoption or not of the calibration curve has an impact on the temperature time-series, has an impact on the seasonality, and also has an impact on some of the extreme indices. Table 5.2 provides the results of our comparison between the adoption or not of the calibration curve for the yearly  $T_{max}$  and  $T_{min}$  annual average and for some some ETCCDI indices.

The fact of adopting or not the results of the application of the calibration curve has also an impact on the yearly  $T_{max}$  and  $T_{min}$  average. For both cases also the yearly average of the daily extremes are outside the calibration uncertainty and obviously, the  $\Delta T_{min}$  are more affected.

In the case of the three ETCCDI analysed indices: the Frost Days (FD), Summer Days (SU) and the tropical nights (TR), for the Moncalieri AWSc-AWSu only the FD was affected, without applying the results of the calibration curve, the number of FD are less than considering this. This is because this index is based on the cold extremes, the most affected by the calibration curve.

*Table 5.2: Annual averaged results for daily maximum ( $T_{max}$ ) and minimum ( $T_{min}$ ) temperatures and the number of Frost days (FD), Summer days (SU) and tropical nights (TR) calculated applying (AWSc) or not (AWSu) the calibration curve of the observations taken at Moncalieri Observatory.*

	AWSu	AWSc
Daily $T_{max}$ mean for the whole year (°C)	19.22	18.86 ± 0.32
Daily $T_{min}$ mean for the whole year (°C)	9.55	9.04 ± 0.32
Frost Days (no. days)	43	58.5 ± 8.5
Summer Days (no. days)	122	120 ± 3
Tropical Nights (no. days)	29	28 ± 1

These results indicate the importance of adopting a standard calibration procedure to most robustly record temperatures, also have to take into account that a single sensor is used, thus, the differences are only due to the application or not of the calibration curve. There are not any other factors that can affect these differences.

## 5.2 – The differences between AWSc and AWSu – Castello Borello field trial

In Castello Borello (Italy) was installed an AWS calibrated regarding the metrological standard procedures (see sub-section 3.1.3.2 for details). Therefore, for this field trial the parallel measurements AWSu – AWSc come from 21/09/2013 to 20/09/2014. The objective of analysing these data is to check if the introduction of the standard metrological procedures has an impact on the temperature time-series. For this purpose it is assumed that one year of data is quite enough. It is justified because, as for the previous sub-section, the objective of this analysis is not the correction of the differences, but the description of the impact.

In here, contrasting with the analysis of Moncalieri Observatory, for this analysis the observations taken by two different AWS are used. One AWS previously installed by the SMI only calibrated by the manufacturer (AWSu), and another AWS installed under the MeteoMet/REG5 project and calibrated at INRiM (AWSc). This AWSc is manufactured by Rotronic and to try to avoid the influence of other factors, both sensors (AWSu and AWSc) are placed inside the same Stevenson Screen and in the same relative position.

The analysis of the  $T_{max}$  and  $T_{min}$  paired series AWSc – AWSu ( $\Delta T_{max}$  and  $\Delta T_{min}$ ) indicates that the introduction of AWSu has a negative effect on the quality of temperature time-series, especially remarkable during spring and summer months in this setting, as shown in Figure 5.4. As for Moncalieri Observatory, also the  $\Delta T_{min}$  are more affected

5 – Can the metrological approach improve the quality of the temperature time-series? – Daily data

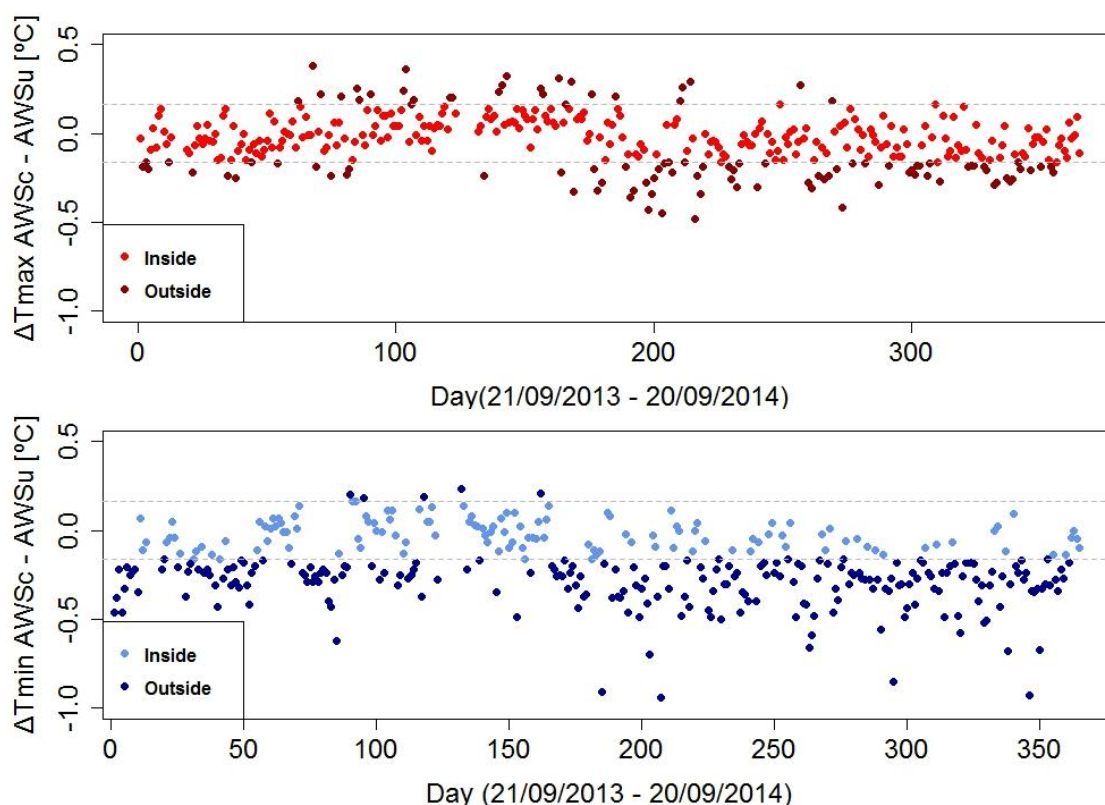


Figure 5.4: Daily maximum (upper plot) and minimum (bottom) temperature differences between the AWS calibrated and the AWSu uncalibrated (AWS<sub>c</sub> – AWS<sub>u</sub>) of Castello Borello field trial. Dotted grey lines surround the calibration uncertainty range ( $\pm 0.16$  °C). Red and blue (dark red and dark blue) circles identify differences inside (outside) the calibration uncertainty.

In this regard, from Table 5.3 is shown the 67.4 % of the  $\Delta T_{\max}$  are inside the calibration uncertainty but only the 34.5 % of  $\Delta T_{\min}$  are inside the  $\pm 0.16$  °C. This indicates that the calibration procedure has a high impact on the quality of climate series, because most of the differences fall outside the calibration uncertainty, meaning that most of the measurements taken by the AWS<sub>u</sub> sensor are potentially inaccurate, especially for  $T_{\min}$  observations. The RMSD of  $\Delta T_{\max}$  (0.15 °C) are inside the calibration uncertainty but not the RMSD of  $\Delta T_{\min}$  (0.28 °C), also these statistics show that the  $\Delta T_{\min}$  differences are higher.



Table 5.3: Annual and seasonal (winter and summer) mean differences ( $^{\circ}\text{C}$ ) between the AWS calibrated (AWS<sub>c</sub>) or the AWS not calibrated (AWS<sub>u</sub>) for daily maximum ( $\Delta T_{\text{max}}$ ) and minimum ( $\Delta T_{\text{min}}$ ) temperatures, along with the Root Mean Square Deviation (RMSD) and the percentage of differences falling into the calibration uncertainty ( $\%|0.16| \text{ }^{\circ}\text{C}$ ) for the period 21/09/2013 – 20/09/2014.

	$\Delta T_{\text{max}}$	$\Delta T_{\text{min}}$
Mean (year) [ $^{\circ}\text{C}$ ]	-0.1	-0.2
Mean (winter) [ $^{\circ}\text{C}$ ]	0.06	-0.10
Mean (summer) [ $^{\circ}\text{C}$ ]	-0.10	-0.27
RMSD [ $^{\circ}\text{C}$ ]	0.15	0.28
$\%  0.16  \text{ }^{\circ}\text{C}$	67.4	34.52

As for Moncalieri, it is also analysed the distribution of the differences  $\Delta T_{\text{max}}$  and  $\Delta T_{\text{min}}$ . Figure 5.5 shows the distribution of  $\Delta T_{\text{max}}$  and  $\Delta T_{\text{min}}$ . In this case, the proportion of cases inside the calibration uncertainty, for both variables is higher, especially for  $\Delta T_{\text{max}}$  and also for this field trial, the differences outside this calibration uncertainty, in general, are less than  $0.5 \text{ }^{\circ}\text{C}$ . Only for  $\Delta T_{\text{min}}$  about the 6% of the differences are larger than  $\pm 0.5 \text{ }^{\circ}\text{C}$ .

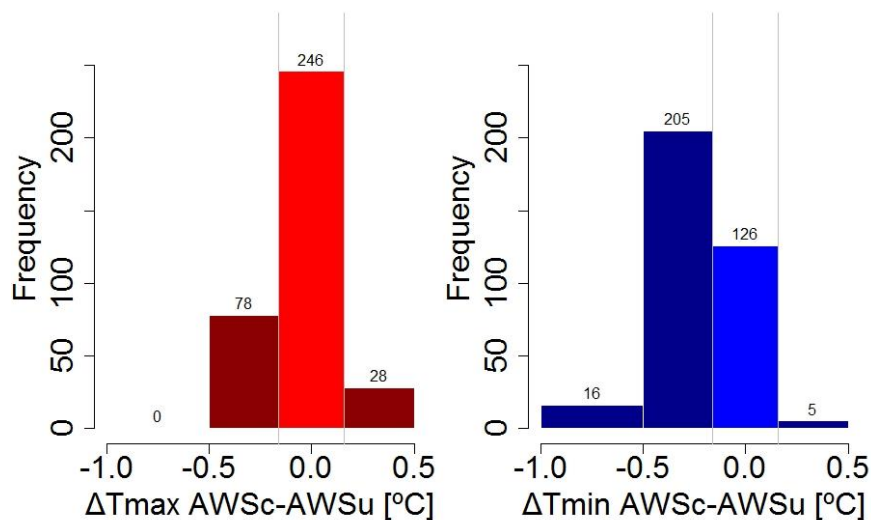


Figure 5.5: Histogram of the daily maximum and minimum temperature differences between the AWS calibrated (AWS<sub>c</sub>) and the not calibrated (AWS<sub>u</sub>) of Castello Borello field trial observations ( $\Delta T_{\text{max}}$  and  $\Delta T_{\text{min}}$ ). In dark red and dark blue (for  $\Delta T_{\text{max}}$  and  $\Delta T_{\text{min}}$ ) the  $\Delta T_{\text{max}}$  and  $\Delta T_{\text{min}}$  outside the calibration uncertainty ( $0.16 \text{ }^{\circ}\text{C}$ )

In contrast to Moncalieri AWSc – AWSu differences, for Castello Borello, summer is the season in which the differences are higher, otherwise, for this field trial, the sign of the differences is not always negative. Figure 5.6 shows the monthly boxplots of  $\Delta T_{\max}$  and  $\Delta T_{\min}$ , for which is evident that the lowest differences are estimated for summer for both variables, the lowest differences are for summer plus September for  $\Delta T_{\min}$ .

This is in concordance with Table 5.3 is evident that the largest differences for Castello Borello are estimated for summer for the two variables, with July also for the both variables showing the largest differences (Figure 5.6). For summer months plus September all the  $\Delta T_{\min}$  fall outside the calibration range, in the case of  $\Delta T_{\max}$ , as is seen the differences are lower and for all the months the most part of the differences fall inside the calibration range.

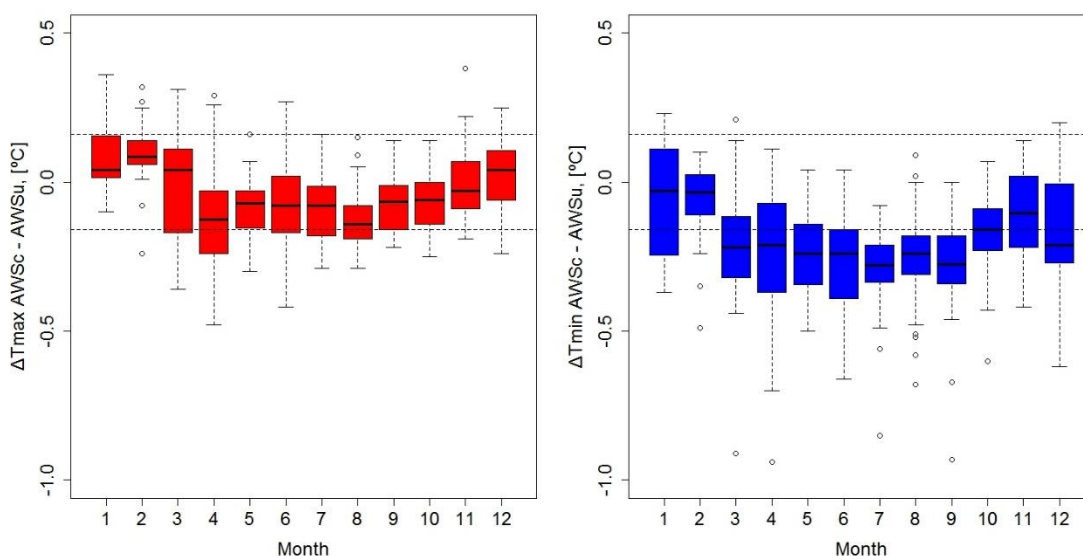


Figure 5.6: Boxplot of monthly maximum ( $\Delta T_{\max}$ ) and minimum ( $\Delta T_{\min}$ ) temperature differences between the AWS calibrated (AWSc) and the AWS uncalibrated (AWSu) from the period 21/09/2013 – 20/09/2014 at the Castello Borello Observatory. Dotted line indicates the AWSc calibration uncertainty  $\pm 0.16$  °C.

As expected, the differences depend on the recorded temperature, thereby, Figure 5.7 shows the  $\Delta T_{\max}$  and  $\Delta T_{\min}$  stratifying the days depending on the  $T_{\max}$  and  $T_{\min}$ . Especially, for  $\Delta T_{\min}$  higher temperatures means higher negative differences. For  $T_{\min}$  upper than 10 °C the most part of the differences are negative and also outside the calibration uncertainty. This linearity of the differences according the recorded temperatures can be caused by the non-calibration of the AWSu.

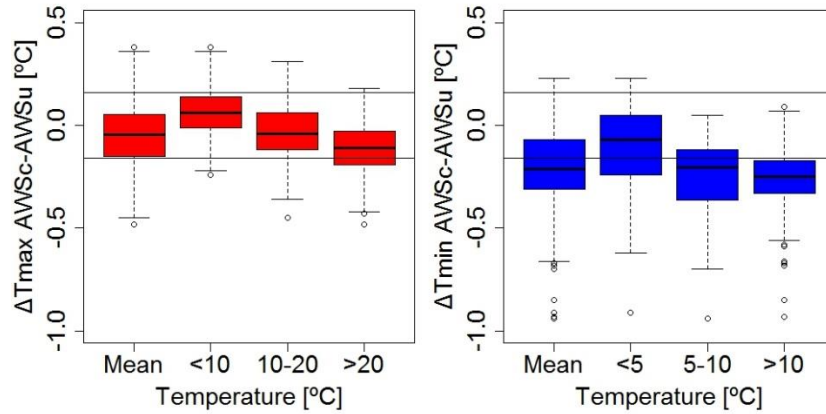


Figure 5.7: Boxplot for maximum (left plot) and minimum (right plot) temperature difference series AWSc – AWSu of Castello Borello field trial for those days in which daily maximum temperatures ( $T_{max}$ ) is lower than 10 °C, 10-20 °C and upper than 20 °C and days in which daily minimum temperature ( $T_{min}$ ) is lower than 5 °C, 5-10 °C and upper than 10 °C.

We see that differences between both sensors readings are mainly determinate by the recorded temperature, but these differences are also influenced by other climate variables, such as RA, WS and RH. In this regard, Table 5.4 provides the spearman’s correlation coefficients estimated for  $\Delta T_{max}$  and  $\Delta T_{min}$  and the recorded  $T_{max}$  and  $T_{min}$  temperature, the DTR, the WS, the RA and the RH.

For  $\Delta T_{max}$ , the higher correlation is with the recorded  $T_{max}$ , and the results of the Spearman’s correlation test are in accordance with what is shown in the previous test and graphs. Opposite, the  $\Delta T_{min}$  are also affected by the recorded  $T_{min}$  but also is affected by other covariables, as the relative humidity and the DTR.

Table 5.4: Spearman's correlation coefficients ( $\rho$ ) estimated among the maximum ( $\Delta T_{max}$ ) and minimum ( $\Delta T_{min}$ ) temperature differences  $AWSc - AWSu$  and  $T_{max} - T_{min}$  of  $AWSc$  observations, daily temperature range (DTR), wind speed (WS), radiation (RA) and relative humidity (RH) for the Castello Borello field trial observations. In bold are the coefficients that are statistically significant at the 95 % confidence level.

	$\Delta T_{max}$ [°C]	$\Delta T_{min}$ [°C]
$T_{max}$ $AWSc$	<b>-0.5</b>	
$T_{min}$ $AWSc$		<b>-0.4</b>
DTR	<b>-0.3</b>	<b>-0.5</b>
WS	<b>-0.3</b>	<b>-0.4</b>
RA	<b>-0.3</b>	<b>-0.4</b>
RH	<b>0.1</b>	<b>0.5</b>

The main characteristic of the differences is the dependence on the recorded temperature, the linearity of the differences with the recorded temperature. This shows the need of the calibration, with this field trial and with the Moncalieri's field trial, is shown that the not adoption of the standard metrological procedures affects the quality not only of the daily data, but also the statistics computed with the  $AWSu$  series.

### 5.3 – The Ebro Observatory field trial, a triple analysis between AWSc, AWSu and MAN

In chapter 4 is proved that the main characteristic of the automatization of weather stations is the dependence of the bias with the HSP studied. For the three parallel measurements series AWSu - MAN (Ebro Observatory, Fabra Observatory and Murcia Observatory), when there is metadata available, every change on the AWSu or every comparison procedure applied on the AWSu means a break on the difference series (AWSu-MAN). It is known that unfortunately this is the most common way on the introduction of the AWS. On the other side, with the previous field trials, the introduction of the metrological procedures has a high impact on the measurements. And the main of this thesis is to try to isolate what implies the automatization of the AWS on the temperature time-series.

Therefore, to assess the real impact of introducing an AWS, it is required to isolate this transition to other factors than can also affect the measurements. For this, it is considered that for study correctly this transition is necessary to take into account two points. The first one, the AWS installed should be calibrated regarding the standard metrological procedures, to ensure that the AWS measurements are corrects and the second point is that the both instruments should be inside the same screen under the same observation conditions. Only considering these two points is possible to assess the real characteristics of the AWS bias, what implies measure the temperature with the two different measurement systems.

To assess this, in Ebro Observatory (Spain, see page 73 for details) was installed an AWS calibrated according the standard metrological procedures at INRiM (to see the details of the calibration procedure see page 75). The three-way comparisons (AWSc – MAN – AWSu) comprise the period 01/06/2013 – 31/05/2015. The objective of this sub-section is to try to analyse which are the real characteristics of the AWS bias (without any other influence factor) with the comparison AWSc – MAN and secondly to try to see the influence of the introduction of the AWSc with the comparison AWSc – AWSu.

Figure 5.8 illustrates the daily maximum and minimum temperature differences over the last two years (01/06/2013 – 31/05/2015) of paired readings AWSc – MAN, AWSc – AWSu and AWSu – MAN. Our findings indicate that remarkable differences exist between the AWSc and AWSu, for this case, the means of  $\Delta T_{max}$  is 0.34 °C (0.33 °C for  $\Delta T_{min}$ ) and for the both variables less than 25 % of the differences are inside the

combined calibration uncertainty, this means that most of the 75 % of the AWSu observations are potentially wrong.

Respects to the AWSc-MAN differences, the differences are smaller, the mean of  $\Delta T_{\max}$  is 0.15 °C and 0.16 °C for  $\Delta T_{\min}$ , the both means are inside the combined calibration uncertainty. And the most important for both cases, around the 90 % of the paired observations are inside the combined calibration uncertainty. This means that the AWS bias is smaller if the temperature is recorded by a calibrated AWS.

If the differences AWSc – MAN with AWSu – MAN are compared, they are apparently of similar magnitude. For the whole period, the mean of  $\Delta T_{\max}$  and  $\Delta T_{\min}$  AWSu – MAN are also inside the combined calibration uncertainty and the percentage of paired observations inside this range is larger than 75 % for the both. But, we cannot forget that only in two years we have 2 BPs in AWSu series and especially, the first one has a big impact. This means that using AWSu we are introducing a series of errors and we cannot ensure the measurement traceability. Only with the introduction of the calibration procedures is possible to eliminate the BPs in the AWS – MAN series. This stability of the differences makes it possible to apply a correction function or at least a minimise the bias.

*Table 5.5: Statistical results (mean, RMSD and percentage of observations falling inside the combined calibration uncertainty  $\%|U|$ ) for the daily maximum ( $\Delta T_{\max}$ ) and minimum ( $\Delta T_{\min}$ ) differences series estimated from the calibrated AWS (AWSc) minus manual (MAN), AWSc minus uncalibrated AWS (AWSu) and AWSu minus MAN. The combined calibration uncertainty is  $\pm 0.38$  °C for AWSc-MAN and AWSu-MAN and  $\pm 0.16$  °C for AWSc – AWSu*

		N	Mean [°C]	RMSD [°C]	% U
AWSc - MAN	Tmax	725	0.2	0.2	89.2
	Tmin	721	0.2	0.2	91.5
AWSc – AWSu	Tmax	643	0.3	0.6	22.4
	Tmin	641	0.3	0.4	12.5
AWSu - MAN	Tmax	643	-0.2	0.6	83.1
	Tmin	641	-0.2	0.3	75.0

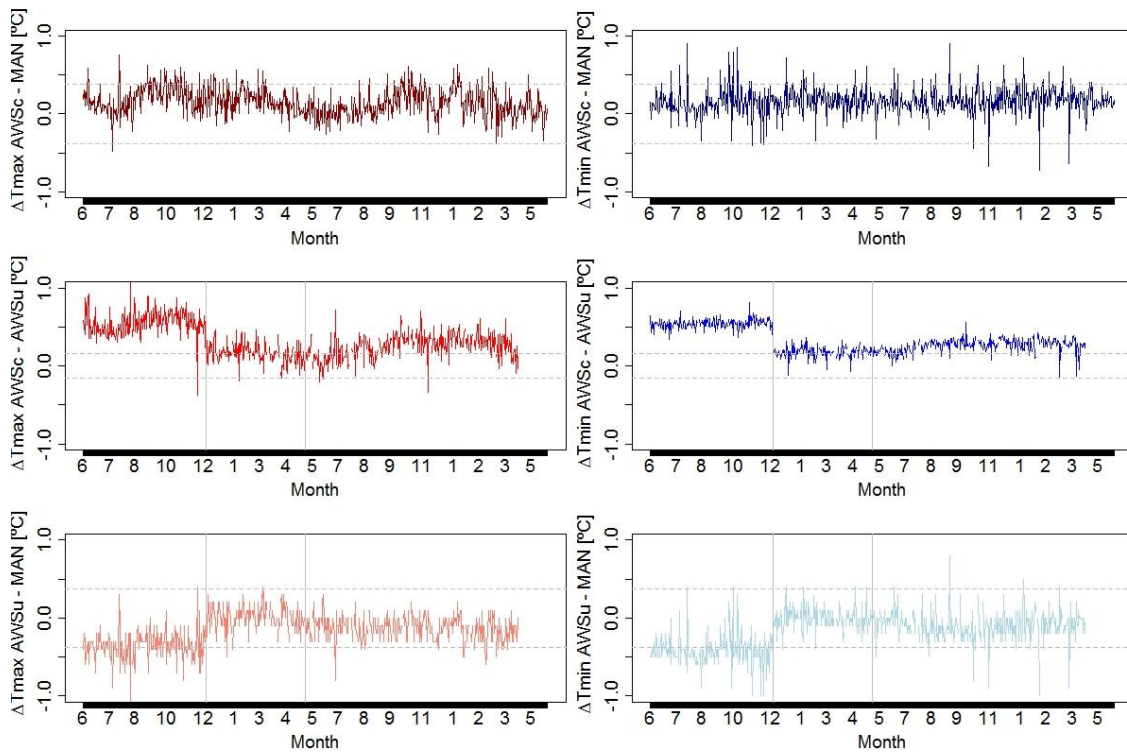


Figure 5.8: Paired daily maximum (left plots) and minimum (right plots) temperature differences AWSc - MAN (upper plots), AWSc - AWSu (middle plots) and AWSu - MAN (bottom plots) at the Ebro Observatory during the period 01/06/2013 to 31/05/2015. Horizontal dashed grey lines represent the combined calibration uncertainty and vertical grey lines correspond to changes on AWSu.

Figure 5.9 provides histograms for  $\Delta T_{max}$  and  $\Delta T_{min}$  estimated from AWSc - MAN, AWSc - AWSu and AWSu - MAN difference series. As it is seen previously, most of the AWSc - MAN observations are inside the combined calibration uncertainty, the observations that are outside this range are mostly positive. Conversely, the proportion of differences outside the combined calibration uncertainty for AWSc - AWSu series is much larger, although most fall between 0.16 °C and 0.5 °C but a high proportion (most of the 20 % for the two variables) are higher than 0.5 °C. This means a high difference, between both AWS and this causes that the error of AWSu in some cases is too large. Due to this, is necessary to highlight that at the end the fact to have a little differences between the AWSc and MAN is normal, and something that is expected. Because a complete different measurement systems, with different characteristics are compared, but with the comparison AWSc - AWSu in the case that the both AWS works properly, is expect to have differences 0 (all the differences inside the combined calibration uncertainty). The

differences outside this range means that the AWSu are not working properly in some situations.

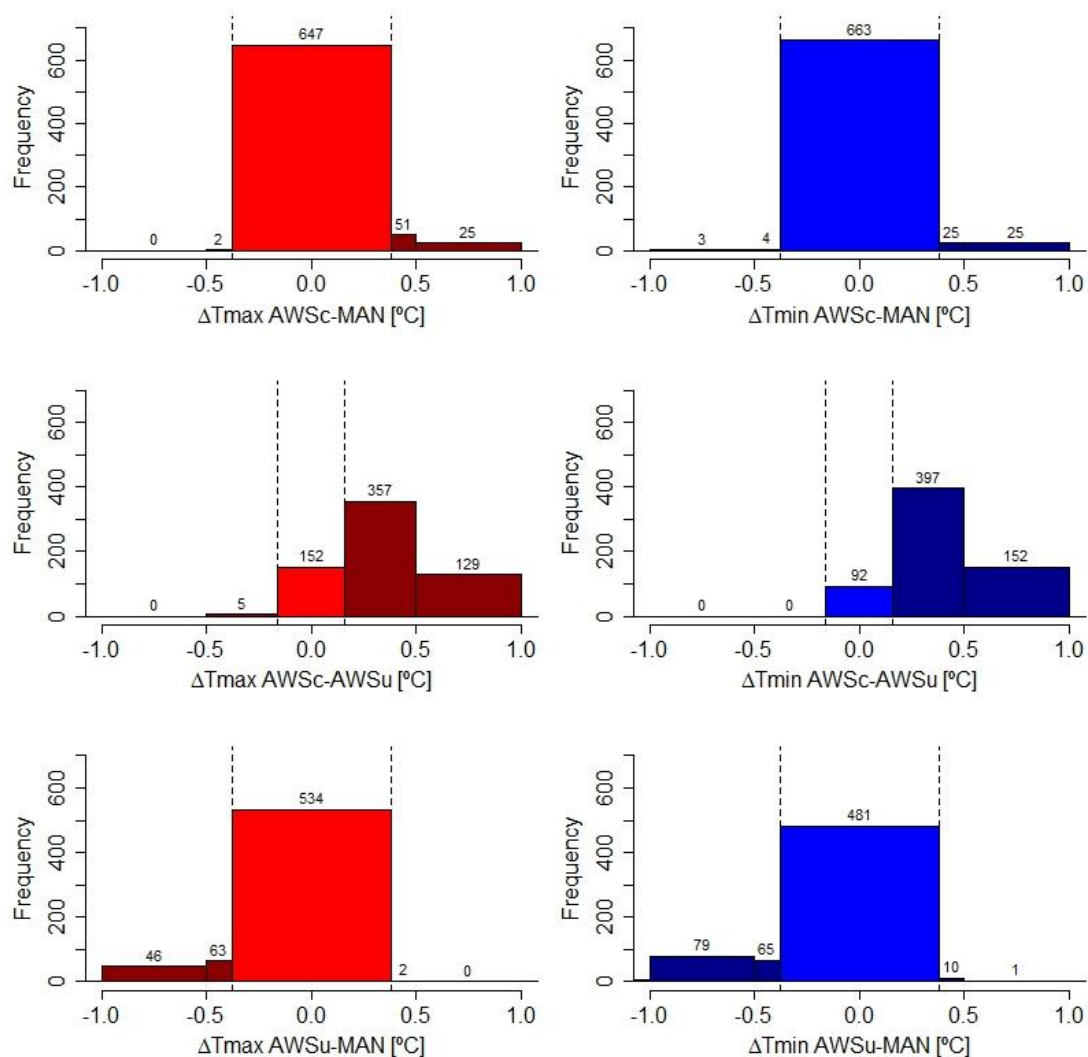


Figure 5.9: Histogram of the daily maximum (left plots) and minimum (right plots) temperature differences between AWSc - MAN (upper plots), AWSc - AWSu (middle plots) and AWSu - MAN (bottom plots) at the Ebro Observatory during the period 01/06/2013 to 31/05/2015. In dark red and dark blue (for  $\Delta T_{max}$  and  $\Delta T_{min}$ ) the  $\Delta T_{max}$  and  $\Delta T_{min}$  outside the calibration uncertainty ( $0.38\text{ }^{\circ}\text{C}$  for AWSc - MAN and  $0.16\text{ }^{\circ}\text{C}$  for AWSc-AWSu)

Otherwise, the  $\Delta T_{max}$  and  $\Delta T_{min}$  between AWSc-AWSu and AWSu-MAN are statistically different for the different seasons. On Figure 5.10 the seasonal boxplots for  $\Delta T_{max}$  and  $\Delta T_{min}$  of AWSc-MAN, AWSc-AWSu and AWSu-MAN are presented. For the differences between AWSc-AWSu, the larger differences for  $\Delta T_{max}$  and for  $\Delta T_{min}$



occur in spring and are positive. In the case of the AWSu-MAN the larger differences are also in spring but they are negative.

For the AWSc – MAN, there are not significant differences on the  $\Delta T_{max}$  and  $\Delta T_{min}$  regarding the season. Only the  $\Delta T_{max}$  in winter are less than for summer and annual. But for all the seasons the mean of the differences are inside the combined calibration uncertainty.

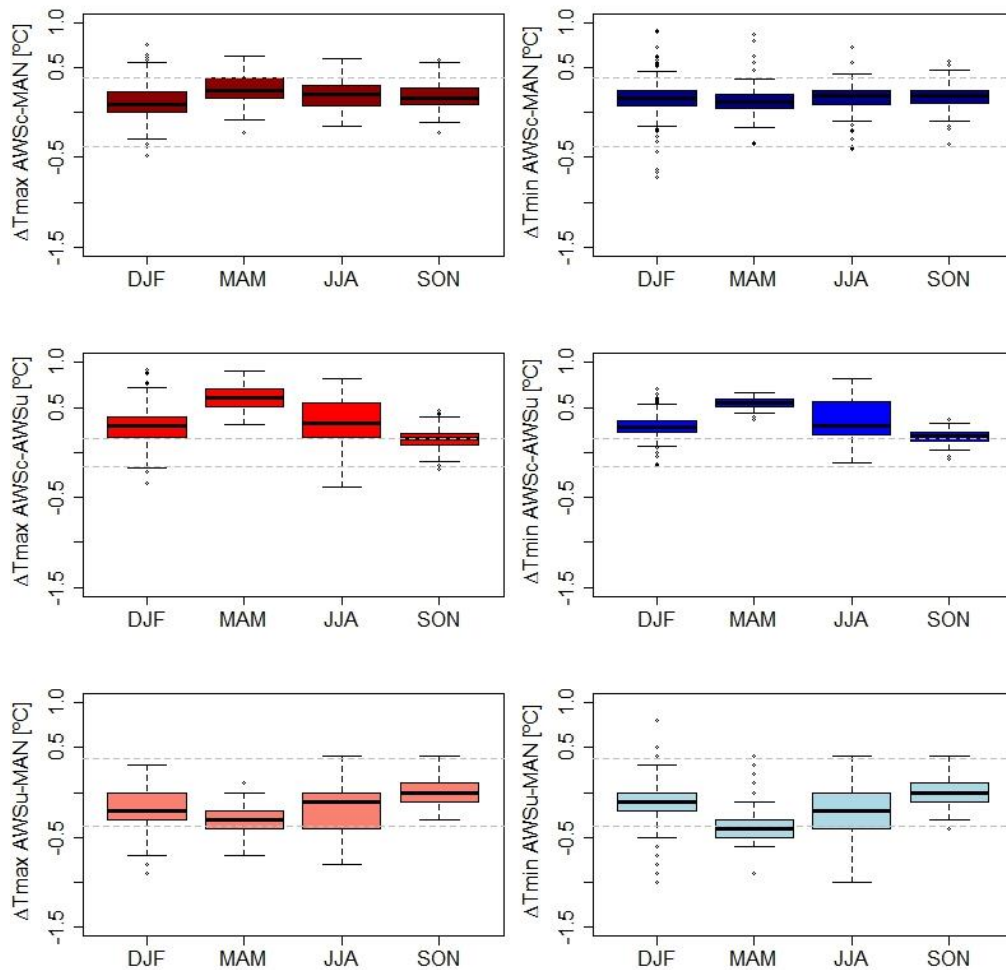


Figure 5.10: Boxplot of seasonal maximum ( $\Delta T_{max}$ , left plots) and minimum ( $\Delta T_{min}$ , right plots) temperature differences between AWSc - MAN (upper plots), AWSc - AWSu (middle plots) and AWSu – MAN (bottom plots) at the Ebro Observatory during the period 01/06/2013 to 31/05/2015. In dark red and dark blue (for  $\Delta T_{max}$  and  $\Delta T_{min}$ ) the  $\Delta T_{max}$  and  $\Delta T_{min}$  outside the calibration uncertainty (0.38 °C for AWSc – MAN and 0.16 °C for AWSc-AWSu).

The fact that the differences  $AWSu - AWSc$  and  $AWSu - MAN$  present a marked seasonality, but the differences  $AWSc - MAN$  does not show this behaviour, means that the bias depends on other factors. In chapter 4 we also see that the common characteristic of the bias between the different HSPs and between the different observatories is the seasonality of the differences and the dependence of the differences with the recorded temperature that is observed. This indicates that something is wrong or not too correct with the  $AWSu$ .

## Chapter 5 summary

- I. The adoption of the metrological standard procedures is an important step to generate climate data of high standards, quality and traceable to international standards.
- II. The application or not of the calibration curve in Moncalieri field trial affects the quality of the daily data, and also the indices computed without the application of the calibration curve.
- III. The application of any correction due to a comparison procedure to the AWSu series, without a whole calibration procedure, has the potential to introduce a continuous BPs on the series.
- IV. The not adoption of the metrological standard procedures not only affects the daily mean observations, also affects the extremes. So the not application of this procedures, also can affect the analysis of extremes events
- V. Although using AWSc, there are a little difference in comparison of the MAN observations, this can due to the very different inertia and response of the MAN and AWS systems.
- VI. The transition to AWS observing systems has increased the spatial and temporal resolution of climate data but has also the potential to introduce biases to climatic records. Therefore, the adoption of standard metrological procedures will assist a smooth transition between MAN and AWS observing systems.

## **Chapter 6 - Assessing the differences AWSc – MAN at hourly scale**





## Chapter 6: Assessing the differences AWSc – MAN at hourly scale

In the previous chapter, it is shown that the introduction of the AWSc can minimise and smooth the transition from the MAN observations at daily scale, there remain some differences, but we cannot forget, that the two measurement systems are very different, so this is what is expected. But there are increasing the studies that use temperature at hourly scale, for this in this chapter will be analysed the differences AWSc – MAN at hourly scale.

The first consideration that is making here is that we expect to have high differences than at daily scale, because in the instantaneous measurements the difference characteristics between both temperature measurement systems are more important.

This chapter is organised into two parts: in the first part the hourly AWSc-MAN correcting and not correcting the observation time are compared and in the second part the AWSc hourly measurements with different observation periods are computed.

### 6.1 – Adapting the AWSc hourly temperature to the MAN observing times

The AWSc – MAN differences at hourly scale are larger than at daily scale, as is said this is what is expected because at this scale many other factors can influence on the difference, like the different response time, the different sensitive element characteristics and also the different observation time.

In general, in the case of the AWS the observations are taken always at the same exact time (hour, minute and second), this is not the case of the MAN observations, thus can also have an influence on the hourly differences. For this, on Table 6.1 are compared for the 7 hourly MAN observations the differences AWSc – MAN correcting the observing time ( $\Delta T_h$ ) or not correcting this ( $\Delta T_{nh}$ ). And only for the 18h the differences are larger when the observing time is corrected. For the early measurements (at 6h and 7h) and at 18h the differences are lower in both cases and also the percentage of differences inside the combined calibration uncertainty are higher, Table 6.1. For both cases, the maximum

differences between the AWSc (correcting the hour and not) and the MAN hourly observations is at 15h when, normally, the temperatures is reaching its daily maximum value.

On the other side, the differences between  $\Delta T_h$  and  $\Delta T_{nh}$  are higher at 9h, this is because is in this hour when the gradient is higher, so a minimum change on observing time have a high influence. Thus, is for this observing times when is more crucial to adapt the both measurement time.

Table 6.1: Statistical results (mean, RMSD and percentage of observations falling inside the combined calibration uncertainty  $\%|U|$ ,  $0.38\text{ }^\circ\text{C}$ -) for the hourly temperature differences at 6h, 7h, 9h, 13h, 15h and 18h U.T.C AWSc – MAN, correcting the AWSc observing times to the MAN observations ( $\Delta T_h$ ) or without applying this correction ( $\Delta T_{nh}$ )

		Mean [°C]	RMSD [°C]	% U	Winter mean [°C]	Summer mean [°C]
6h	$\Delta T_h$	0.19	0.31	93.0	0.19	0.18
	$\Delta T_{nh}$	0.31	0.39	68.6	0.23	0.44
7h	$\Delta T_h$	0.16	0.25	93.5	0.19	0.18
	$\Delta T_{nh}$	0.20	0.42	68.4	0.22	0.24
9h	$\Delta T_h$	0.21	0.31	82.3	0.13	0.30
	$\Delta T_{nh}$	0.41	0.50	47.6	0.34	0.48
12h	$\Delta T_h$	0.40	0.51	51.3	0.35	0.42
	$\Delta T_{nh}$	0.49	0.62	38.4	0.44	0.47
13h	$\Delta T_h$	0.42	0.54	48.2	0.35	0.45
	$\Delta T_{nh}$	0.41	0.62	44.5	0.40	0.48
15h	$\Delta T_h$	0.45	0.57	42.5	0.37	0.48
	$\Delta T_{nh}$	0.46	0.67	48.1	0.38	0.43
18h	$\Delta T_h$	0.27	0.71	75.5	0.19	0.36
	$\Delta T_{nh}$	0.20	0.70	85.9	0.17	0.25

Figure 6. 1 shows for the  $\Delta T_h$  and  $\Delta T_{nh}$  and also the differences between the AWSc without correcting the hour and the AWSu the boxplots for each 7 hourly times. As is shown with the previous statistics, taking the differences between the AWSc and the MAN for the both cases, the higher differences are at midday. Taking the AWScnh – AWSu the higher hourly differences are at first hours at morning and at late afternoon. This is because the minimum temperatures are the most affected.

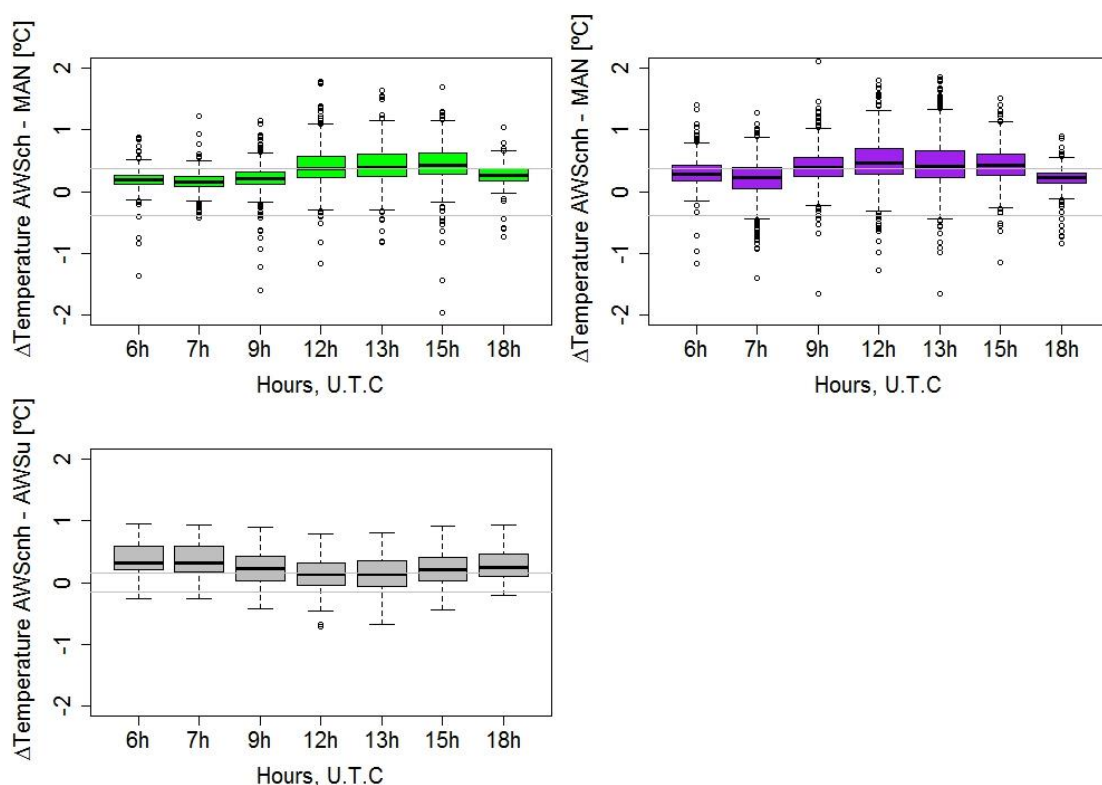


Figure 6. 1: Boxplots for the hourly differences at 6h, 7h, 9h, 12h, 13h, 15h and 18h UTC for the differences AWSc – MAN correcting the AWSc observing times to the MAN observations  $\Delta T_{th}$  (upper left), without applying this correction  $\Delta T_{nh}$  (upper right) and AWSch and AWSu.

Figure 6.2 shows the hourly differences for winter and summer (in Table 6.1 the mean), in all the cases (as for the daily differences) and for all the hours, the higher differences are in summer. In general, in winter the differences correcting or not the time are lower than for summer, and is also in winter at 9h when the differences correcting or not the hours are higher.

For summer, the differences without time correction are also higher except for the 18h and higher than for the whole year.



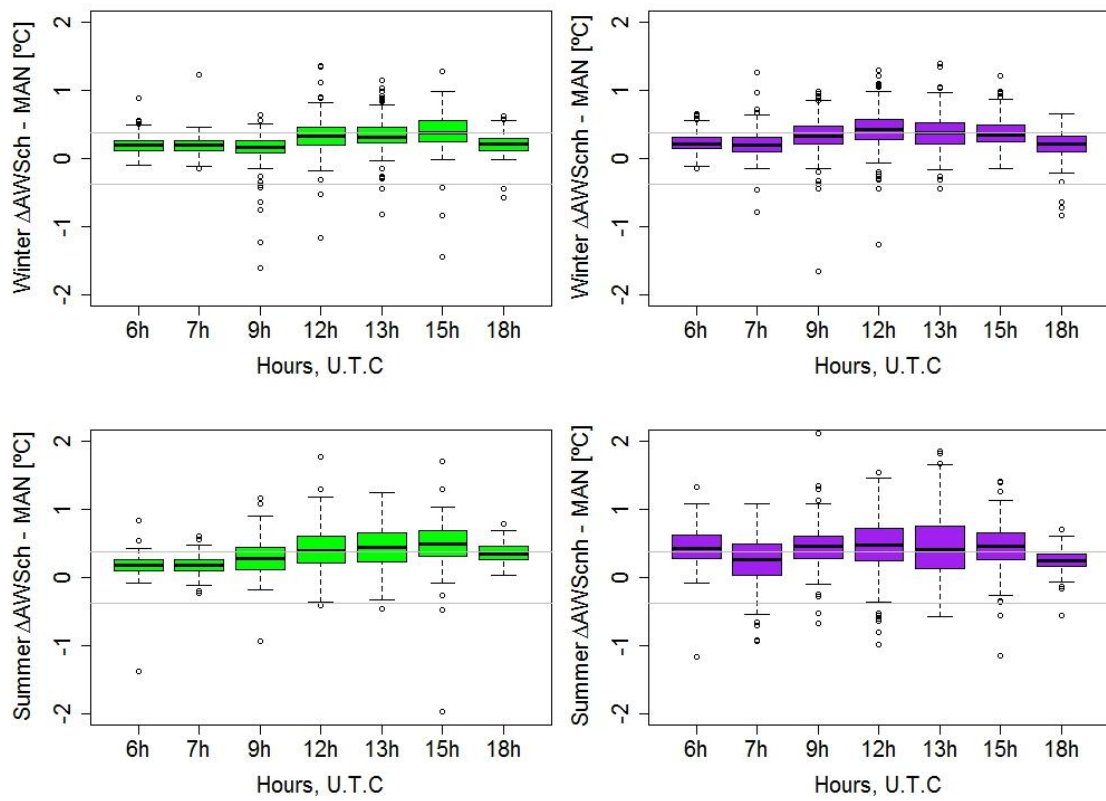


Figure 6.2: Winter (upper plots) and summer (bottom plots) boxplots for the hourly differences at 6h, 7h, 9h, 12h, 13h, 15h and 18h UTC for the differences  $\Delta WSc - MAN$  correcting the  $\Delta WSc$  observing times to the  $MAN$  observations  $\Delta Th$  (left) and without applying this correction  $\Delta Tnh$  (right)

## 6.2 – Adapting the AWSc hourly temperature to the MAN observing times

Previously, has been shown that taking the AWSc with the observing times adapted to the MAN observations, can reduce the AWSc-MAN bias at hourly scale, but this fact is difficult to have in another observatories, for this, in here the hourly AWSc computed in different ways are compared with the MAN (see sub-section 3.3.3, page 95 for more details).

The data are split, in one, the 5 minutal observations centered to the exact observing time are taken, in another 5 minutal observations before the observing time are taken and in the last one 5 minutal observations after the observing time. Table 6.2 shows the mean of the hourly differences at 6h, 7h, 9h, 12h, 13h, 15h and 18h AWSc – MAN for different AWSc hourly computation. For all the hours, noither the centred mean of the 5', nor the mean of the 5' before the exact hour and nor the mean after the 5' have less difference that using the AWSch, except for the 18h. As is expected for the morning and midday hours, the minimum differences are when we compare AWSc mean of the 5 minutal observations before to the hour and for the afternoon is when we take the 5' after the hour.

These differences between the morning observations and afternoon observations are due to the different characteristics of the observing systems. In general, the response time of the AWS is shorter than the response time of the MAN measuring instruments.

*Table 6.2: Mean for the hourly temperature differences at 6h, 7h, 9h, 13h, 15h and 18h U.T.C AWSc – MAN for the AWSch, AWSchh, AWSc taking the 5' mean centered, AWSc taking the mean of the 5' before and AWSc taking the mean of the 5' after.*

	AWSch [°C]	AWSchh [°C]	Mean 5' [°C]	Before 5' [°C]	After 5' [°C]
6h	0.19	0.31	0.31	0.28	0.29
7h	0.16	0.20	0.20	0.15	0.25
9h	0.21	0.41	0.41	0.35	0.47
12h	0.40	0.49	0.48	0.46	0.50
13h	0.42	0.41	0.46	0.45	0.47
15h	0.45	0.46	0.46	0.47	0.39
18h	0.27	0.21	0.21	0.25	0.17

On Figure 6.3 is shown the hourly boxplots for the seven hourly MAN measurements, of the differences between the AWSch, the centered mean of the 5 observations AWSc at each hour, the 5 minutal observations AWSc before the exact hour and the 5 minutal observations AWSc after the exact hour.

In the last table is shown that taking the 5-minute mean centered to the each observing time does not reduce the bias in any of the 7 hourly observations considered. Taking the AWSc 5' before not improve the differences computed taking the AWSc corrected at the MAN observing hour, but reduces the differences for the first hours of the day, and only taking the mean of the 5' after observations reduce the AWSc – MAN reduce the differences at 18h.

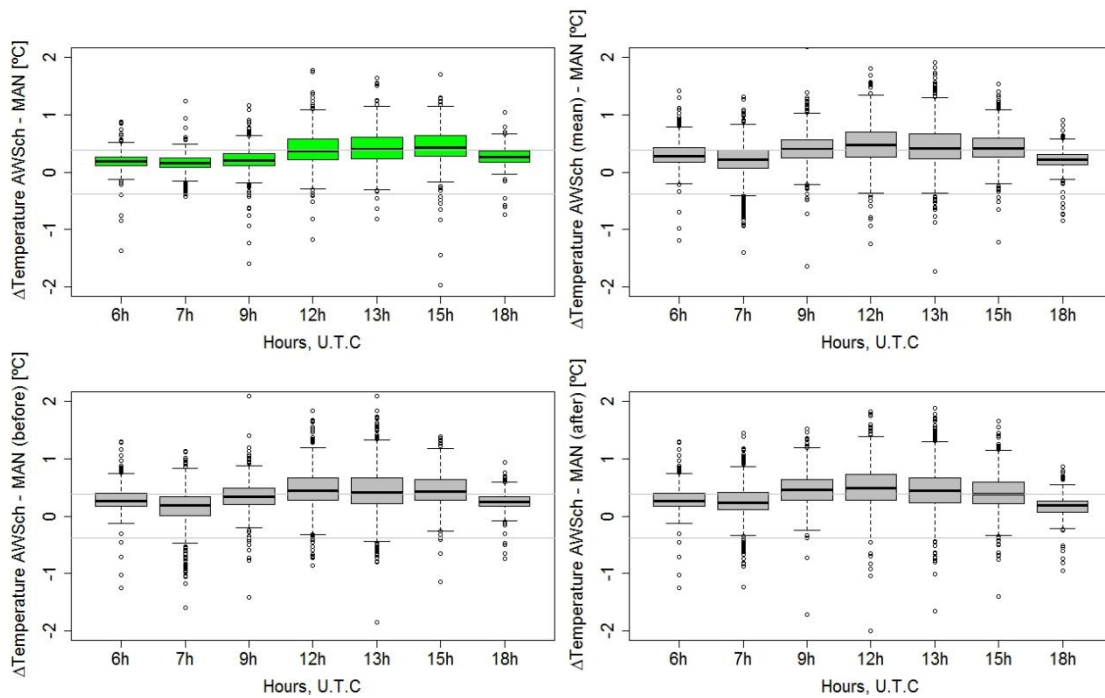


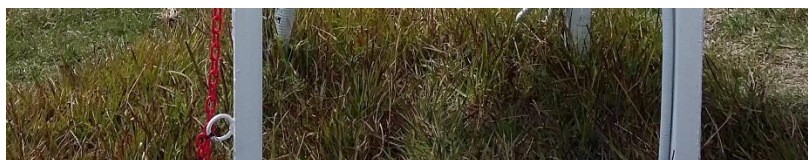
Figure 6.3: : Boxplots for the hourly temperature differences at 6h, 7h, 9h, 13h, 15h and 18h U.T.C AWSc – MAN for the AWSch (upper-right plot), AWSc taking the 5' mean centered (upper-left plot), AWSc taking the mean of the 5' before (bottom-left plot) and AWSc taking the mean of the 5' after (bottom-right).

## Chapter 6 summary

- I. The AWSc – MAN at hourly scale are larger than at daily scale, as consequence as to the different measuring systems characteristics and other factors
- II. Another factor that increases the differences at hourly scale is the differences in observing times. The AWS generally takes the observations at the exact observing time but in the case of the MAN observations, this became more difficult.
- III. If the AWSc are corrected to the MAN observing times, in general the differences were reduced but remain higher than at the daily scale, especially when the gradient between the instantaneous measurements are higher (at mid-morning). Because in this hours, the different characteristics of the device like the response time, the hysteresis are more important and increase this differences
- IV. As for daily differences, the hourly differences are not equal for the whole year. In general the hourly differences in summer are higher than in winter.
- V. Taking the previous different ways to compute the instantaneous AWSc measurements, only for the 18h can reduce the differences respect to take the AWSc corrected to the MAN hour. But taking for the morning observations the mean of the 5 minutal observations before the hour and for the afternoon observations the 5 minutal observations after the hour can reduce the AWSc – MAN differences without correcting the AWSc hour to the MAN
- VI. At hourly scale, the AWSc reduce the bias respects to the AWSu but not at the same level that at daily scale, this means that even though the application of the metrological standard procedures improve the quality and reliability also of the hourly data, the application of this procedures can smooth but not reduce at all the hourly differences. At this scale is when the differences of the measurement system characteristics are more important.



## Chapter 7 – Giving traceability to the historical temperature series





## Chapter 7: Giving traceability to the historical temperature series

This last results chapter is organised in two sub-sections. The first sub-section, discusses the results of homogenisation of the centennial-long monthly maximum and minimum temperature series of Moncalieri (1866 – 2012) by applying the HOMER method and the estimated uncertainty budget related to the adjustments calculated for each HSP detected.

In the second sub-section, is provided a first estimation of the combined uncertainty budget, taking into account the instrumental plus homogenisation uncertainty and the impact in time-series variations.

### **7.1 - Homogenisation results of the Moncalieri monthly maximum and minimum temperature series**

The monthly maximum and minimum temperature series of Moncalieri Observatory of the period 1866 - 2012 have been subjected to a homogenisation procedure with HOMER. Different BPs were detected and some of them could be related to physical causes according the metadata provided by Di Napoli and Mercali (1996).

Figure 7.1 is an example of the pairwise seasonal output, is the comparison between the candidate monthly maximum temperatures with their reference series providing the potential BPs identified.



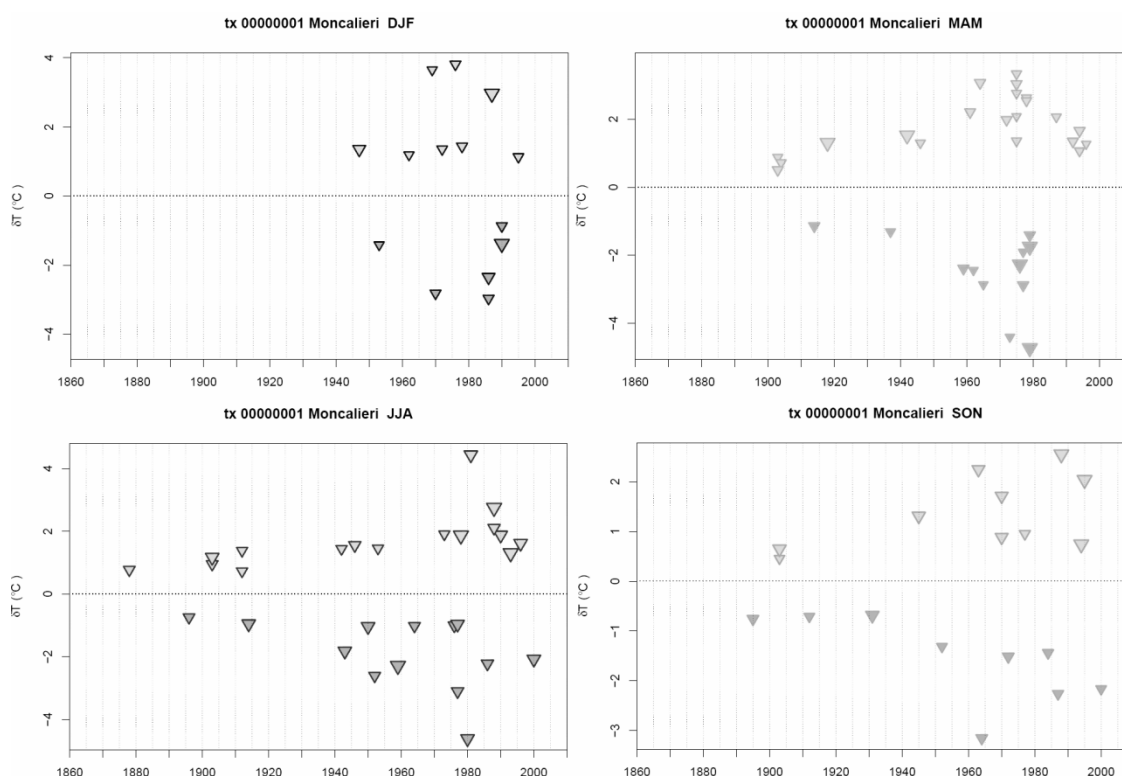


Figure 7.1: Seasonal breakpoint detection results of pairwise detection of HOMER for Moncalieri maximum ( $T_{max}$ ) temperature series. Triangles are the potential breakpoints (BPs).

After the whole application of HOMER (Mestre *et al.*, 2013) have been identified 13 BPs for  $T_{max}$ , some of them can be explained by the available metadata. Table 7.1 provides the HSP periods and the causes of the BPs.

Also in Table 7.1 is provided the estimated homogenisation plus instrumental uncertainty budget, from this, is clear that the highest adjustment uncertainty are for the HSPs estimated between 1961 and 1992, when the observations were taken by amateur observers and the LIG thermometers where unscreened.

*Table 7.1: Uncertainty budget estimated from the adjusted monthly maximum temperature (Tmax) for every Homogeneous Sub-Period (HSP) identified by the homogenisation assessment applied to Moncalieri monthly data 1866-2012, along with the causes documented by the metadata. Uh is the uncertainty related to the homogenisation procedure, Ur is the calibration uncertainty of the reference stations, Uc is the instrumental uncertainty of the candidate stations, UH is the total homogenisation uncertainty plus instrumental.*

	U <sub>h</sub> (°C)	U <sub>r</sub> (°C)	U <sub>c</sub> (°C)	U <sub>H</sub> (°C)	Cause BP
01/1866 - 11/1879	0.60	0.33	0.74	1.01	-----
12/1879 - 05/1901	0.70	0.33	0.74	1.07	Instrument change
06/1901 - 07/1903	0.80	0.33	0.74	1.14	Undocumented
08/1903 - 03/1919	0.61	0.33	0.74	1.02	Change in thermometer exposure
04/1919 - 10/1929	0.90	0.33	0.48	1.06	Change in thermometer exposure
11/1929 - 11/1932	1.00	0.33	0.48	1.16	Change in observing times
12/1932 - 11/1939	0.60	0.33	0.48	0.83	Undocumented
12/1939 - 11/1952	0.54	0.33	0.48	0.80	Undocumented
12/1952 - 11/1961	0.51	0.33	0.48	0.78	Instrument change
12/1961 - 11/1975	0.48	0.33	1.55	1.66	Starts of non-professional measurements
12/1975 - 11/1988	0.50	0.33	1.55	1.66	Undocumented
12/1988 - 02/1992	0.67	0.33	1.55	1.72	Undocumented
03/1992 - 11/1994	0.47	0.33	0.37	0.68	End of non-professional measurements
12/1994 - 11/2001	0.45	0.33	0.37	0.67	Undocumented
12/2001 - 12/2012	-	-	-	0.32	AWS introduction

In the case of the monthly minimum temperatures, five other HSP were detected. Table 7.2 shows the HSPs period, the cause of the BPs and the uncertainty budget.

Table 7.2: As Table 7.1, but for monthly minimum temperature series of Moncalieri Observatory.

	$U_h$ (°C)	$U_r$ (°C)	$U_c$ (°C)	$U_H$ (°C)	Cause BP
01/1866 - 11/1875	0.45	0.33	0.74	0.93	--
12/1875 - 11/1931	0.44	0.33	0.61	0.82	Undocumented
12/1931 - 11/1961	0.44	0.33	0.48	0.73	Undocumented
12/1961 - 02/1994	0.44	0.33	1.55	1.64	Starts of non-professional measurements
03/1994 - 12/2012	-	-	-	0.32	End of non-professional measurements

As is expected, when the measurements were taken by amateur observers, the total uncertainty was larger than for the other periods, because, one source of uncertainty considered to computing the  $U_c$  is the human's errors. The differences in  $U_h$  are determinate by the period before and after the BP and by the number of BPs. It has to be considered, that this is an exploratory estimation of the homogenisation plus instrumental uncertainties taking into account the Type A and Type B uncertainties and as impossible to calibrate the LIG used in the earliest measurements, the  $U_c$  and  $U_r$  have to be derived according metrological studies (Knazovickà and Strnad, 2013).

On the other side, there are other factors that are affecting the measurements and have to be considered in a future, for this this has to be considered as a preliminary assessment of a complex problem.

## 7.2 – Results from the joint estimation of instrumental plus homogenisation uncertainties for Moncalieri

In previous chapters the importance of adopting calibration procedures is explained. But this is not enough, and we also have to try to adopt these metrological approaches on our historical series, and try to start to estimate the uncertainties for every individual measurement that compose our temperature time-series. In here, are showed the results and impact in temperature variations and trends of adding the combined uncertainty budget to ensure a more complete traceability of the Moncalieri monthly temperature series.

Figure 7.2 shows the annual time variations for the Moncalieri annual adjusted maximum (upper plot) and minimum (bottom plot) series for the period 1866 – 2012, along with the uncertainty bars estimated individually for each year and the OLS and WLS trends. Both time-series show similar time variation, but for  $T_{max}$  the annually averaged series indicates larger interannual variability. Similar variations and temporal evolution in the Moncalieri adjusted  $T_{max}$  and  $T_{min}$  series at the annual scale have been identified by Brunetti *et al.* (2006) over the whole of Italy, by Abarca del Río *et al.* (2006) over France and Brunet *et al.* (2007) over mainland Spain.

The key difference between this study and the previous one is the estimation of annual uncertainty derived from the combined analysis of instrumental plus homogenisation uncertainties. This approach increases the data traceability and robustness over the whole period and, therefore, the reliability of any climate and climate change study that uses these data. In addition, is also with the Figure 7.2 that not all the annual values have similar uncertainties, as they are calculated individually for each HSP, for this the larger uncertainties bars are for the years between 1961 and 1991.

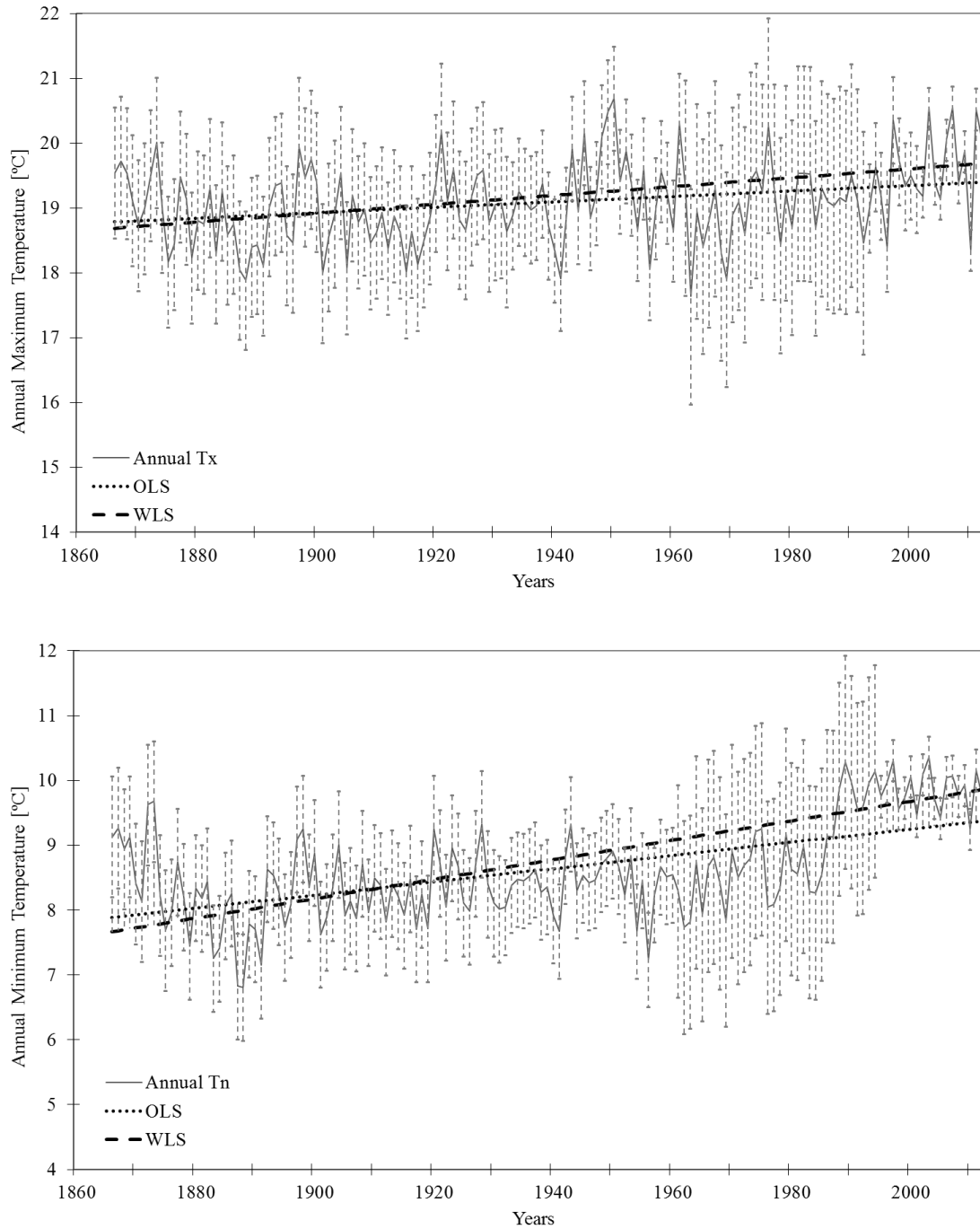


Figure 7.2: Annual evolution of the Moncalieri adjusted annual maximum (upper plots) and minimum (bottom plots) temperature series (grey thick line) for the 1866-2012 period, along with the homogenisation uncertainty bars for each year and the OLS (dotted line) and WLS (striped line) trends.

Table 7.3 give the trends for the periods 1866-2012, 1950-2012 and 1980-2012 for the annual maximum and minimum temperatures using OLS and WLS techniques. For all the trends except for the trend in annual minimum temperatures of the period 1950-2012 are significant at 95%. As for other variables, the annual minimum temperature trends are larger than the annual maximum temperature trend for both OLS and WLS estimation. For the computation of the WLS trend, are also taking into account the  $U_H$  of the annual means. In all cases, the trends (OLS and WLS) are different and larger when the total homogenisation uncertainty is considered. For the OLS trend of the annual maximum temperatures for the period 1980 – 2012 are  $0.248 \pm 0.099$  °C/decade and the WLS is  $0.276 \pm 0.019$  °C/decade or for the annual minimum temperature of the same period, the OLS trend is  $0.378 \pm 0.087$  °C/decade and the WLS is  $0.547 \pm 0.101$  °C/ decade. Despite the uncalibrated sensors and the breakpoints detected in the time-series, the relative trends emerging from original data (especially for  $T_{min}$  trend of 1866-2013) are positive and also consistent with the other ones observed in Italy and Europe, and with other proxies included the strong glacier retreat at observed in the near Alps. Such trend is all the way of different amplitude with respect to neighboring homogenised series (especially the monthly  $T_{max}$ ) due to the large amount of BPs and poor quality of observation carried on during the years. The use of calibrated instrument, now associated to the series, and a well-defined traceability and calibration frequency will solve this problem, making the series more reliable.

Table 7.3: Trend for the annual Maximum and Minimum Temperature of the periods 1866-2012, 1950-2012 and 1980-2012 using Ordinary Least Squares (OLS) and Weighted Least Squares (WLS). Significance trend at 95% in bold.

	Annual Tmax OLS [°C/dec.]	Annual Tmax WLS [°C/dec.]	Annual Tmin OLS [°C/dec.]	Annual Tmin WLS [°C/dec.]
1866 - 2012	<b>0.042 ± 0.012</b>	<b>0.068 ± 0.011</b>	<b>0.102 ± 0.012</b>	<b>0.150 ± 0.009</b>
1950 - 2012	<b>0.091 ± 0.044</b>	<b>0.097 ± 0.047</b>	0.341 ± 0.034	0.288 ± 0.036
1980 - 2012	<b>0.248 ± 0.099</b>	<b>0.276 ± 0.019</b>	<b>0.378 ± 0.087</b>	<b>0.547 ± 0.101</b>

The main result was to apply the calibration procedures in order to link in a continuous way the old homogenised data, with new, modern instrument providing accurate records.

## Chapter 7 summary

- I. Generally, the historical temperature time-series are affected by different bias breaking the homogeneity of the series, during the last decades there have done a very good work to improve the methods and procedures to homogenise these data, but not to compute the uncertainties related with these procedures.
- II. It is also important to give traceability to the historical temperature time-series, so only the combination of the instrumental plus homogenisation uncertainties can helps to this.
- III. The introduction of the instrumental plus instrumental uncertainty not only has an impact on the mean and on the individual observations, also on the trend.





## Chapter 8 : Conclusions, discussion and further work





## Chapter 8: Conclusion, discussion and further work

In this last chapter are provided the conclusions and discussion (first part) and ideas for the further work (second part).

This thesis deals with a complex problem, the characterisation of the bias introduced by automatisaton of the weather stations. Previously, other studies have explored this problem, but as shown in chapter 2, the main problem of these previous studies is that in the most part they are mixing other factors, rather than isolating only the AWS bias. For this, the novelty of this study is that tries to be a bridge between the metrology and the climatology and meteorology to assess the characteristics of the bias.

### 8.1. Conclusions and discussion

The measurement of the air-temperature is a complex procedure. Many factors are involved in the measurements, the two most important of which are the temperature measurement instrument or system and the shelter in which the instrument is placed. A small change in one of these factors can have a large impact on the air-temperature measurements.

It is known that the introduction of the AWS means a complete change in the temperature measurements, and with this the measurements are more complex, as there are more parts that contributes to the measurements and also the sensitive element is completely different. Thus, one can expect that the transition to this type of temperature measurement system can introduce a bias on the temperature time-series.

Other previous studies confirm this hypothesis, but in many cases the characteristics of this bias are not equal for different countries and networks. So, this shows that will be some other factors in this AWS transition that gives this high variability.

The first part of this thesis tries to identify characteristics of the bias using three parallel daily temperatures series in Spain. For this part, the main conclusion is that the transition to the AWS introduces a bias on the time-series and the distribution of the differences

shows the complexity of the bias. The main characteristic of the bias when the AWSs are not calibrated against the metrological standard procedures is the strong dependence of the bias magnitude and sign on the particular AWSu installed and on the particular corrections applied to the AWSu measurements due to comparison procedures. As a result, this increase the complexity to try to correct or at least minimise the bias.

These comparison procedures are only checks to know if the AWSu is working properly or not, so many times, these comparison procedures are accompanied with biases on the parallel AWSu – MAN series. Thus, the characteristics of the bias are not only changing with the different AWSu, they are also changing due to this procedure. This implies that every 6 months – 2 years, some correction can be applied to the AWSu or the AWSu can be replaced, introducing a bias in the air-temperature series. For these, before any study that tries to assess the AWS bias characteristics, firstly the temperature parallel measurements should be submitted to a break points detection test, to define the different homogenous sub-periods.

In any case, the bias tends to be larger for daily maximum temperature than for minimum temperature observations and this bias, in general, is dependent on the season. This seasonality of the differences is statistically significant for the three stations studied and for both, daily maximum and minimum temperature variables. This indicates that the recorded temperature has a high impact on the differences. Another conclusion of this first analysis is the higher dependence of the bias with the recorded temperature. The bias is larger or not depending on the higher/lower temperatures. This shows the impact of non calibration on the AWS-MAN bias. On the other side, the covariables independently have not a high impact on the differences, but when the days are stratified according the wind-speed and the number of sunshine hours, the characteristics of the bias are different regarding this type of days. Thus, to correct, or at least to minimise, the AWSu-MAN bias will be necessary firstly to assess the homogeneity of the parallel measurements and consider the dependence of the  $\Delta T_{max}$  and  $\Delta T_{min}$  with the recorded  $T_{max}$  and  $T_{min}$ . The highest differences of the bias regarding the AWSu and the HSP make it more difficult to homogenise with the current homogenisation methods.

Another important point is the higher influence on the bias due to the different sensors sheltering than to the AWS bias isolated. Seen with the parallel measurements in Fabra Observatory during the MCV periods in which the AWS was inside to a multiplate screen. The fact that the multiplate screens are smaller and is made of plastic or fiberglass and the

Stevenson Screen is bigger and made of wood, means that the conditions inside the two screens are not the same and especially, the response time of the two shelters to the environment changes are different. Otherwise, the degradation of the multiplate screen faster and according to Lopardo *et al.*, 2014 in three years the degradation of these type of screens affects the temperature measurements.

From chapter 5 the metrological standard procedures are introduced, to analyse if this procedures can improve the quality and reliability of the temperature time-series and secondly, to try to isolate the AWS bias to other factors. The first conclusion of this part of the study is that the introduction of the metrological standard procedures has a high impact on the temperature time-series, so from the national meteorological services these procedures have to be adopted periodically to generate climate data of high standards and quality. The application of calibration results not only affects the mean, but also has a high impact on the extremes and on the indices derived from these data. Another important fact is that the introduction of these procedures can smooth the impact of AWS transition and reduce the multiple BPs introduced by comparison procedure. Otherwise, although using AWSc, there continues to be a little difference with the MAN measurements, this can be due to the different inertia of the two measurements systems.

Chapter 6 deals with the AWS – MAN bias at the hourly scale. At this scale, as is shown, there are many other factors that affect the differences and although is better to use AWSc with this the differences are larger than at the daily scale. With the assessment of the AWS- MAN differences at the hourly scale, there are two problems: the first one is that there is not a consensus about how to compute the AWS observations so due to this it is more difficult to generalise the results. On the other side, the AWS and the MAN measurements are not observed instantaneously, so this introduces more noise in the assessment. The results show that the higher differences occur when the temperature gradient is higher, for the different characteristics of the both devices. Thus, at the hourly scale, the adoption of the standard metrological procedures does improve the measurements by reducing the bias, but it is not the only solution. It could be useful to continue assessing the differences at hourly scale, maintain or implement also the record of the observing time on the MAN observations.

And lastly, in this study is given a preliminary way to compute the homogenisation plus instrumental uncertainty for historical temperature time-series, to give traceability and reliability to these series. It is homogenised the monthly maximum and minimum air-

temperature time-series and this uncertainty is assessed for the centennial station of Moncalieri affected by different changes to the instruments, observing practice and shelters. The results indicate that this affects not only the individual data and the mean also the long-term trend.

In conclusion, this work contributes to assessment of temperature measurement characterisation that combines climatology and metrology, which can solve or at least minimise one part of the problem. However, this is only the beginning. There are many other factors that can affect the quality of the temperature measurements and many times the introduction of the AWS has been accompanied by a change in the shelter or a relocation of the station, or there will be different change on the surrounding environment. This makes it is necessary to continue studying the characteristics of the temperature measurements. Only with this is possible to improve the quality of long-term temperature time-series and so consequently improve the reliability of studies based on these data. It is indisputable that the climate is changing, but to give a better estimation at local and regional scale is necessary to continue working to improve data quality and reliability.

## 8.2 - Further work

The first thing required to extend this work is to continue assessing the AWSc-MAN differences at hourly scale. There are many other factors that are affecting the measurements and we have to try clarify and quantify their influence.

There are many other factors that are affecting the measurements, under this thesis the field trial of Ebro Observatory have been expanded in order to analyse the differences between the Stevenson Screens and the aspirated Young screen. The first results indicate that different shelters introduce a larger bias on the temperature data-series than the AWS bias, and the differences are mostly affected by other factors like the radiation, the wind speed and the humidity. But remains many other source that can affect the measurements and need to be studied, like the station replacement (for example from the cities to the airports, from the cities to countryside) or how the surroundings can affect the measurements, the type of vegetation close to the stations, the distance between the station and builds, the distance between the station and the sea or the rivers.

On the other side, the introduction of the standard metrological procedures improves the temperature data quality, but to adopt this procedure requires equipment. Under the MeteoMet project different prototypes or portable climatic chambers have been designed. But this procedure implies to have some trained staff. Otherwise, as is shown the calibration uncertainty is very high (especially due to the thermal inhomogeneity of the climatic chamber), so an improvement is also required for these chambers and the procedures employed to try to reduce this uncertainty to improve the studies derived to data.

Otherwise, in thesis is only estimated the instrumental plus homogenisation uncertainty, thus is also necessary to study the uncertainty derived by the shelter, the surroundings.

At the national and international scale many efforts are being made, which permits this field to continue on this way and at the end, ideally, to have a whole model of all the components that are involved on temperature measurements.





## References

- Aguilar E, Prohom M. 2011. RClimDex-extraQC (EXTRAQC Quality Control Software). User Manual, Centre for Climate Change, University Rovira i Virgili, Tarragona, Spain. [http://www.c3.urv.cat/data/manual/Manual\\_rclimdex\\_extraQC.r.pdf](http://www.c3.urv.cat/data/manual/Manual_rclimdex_extraQC.r.pdf)
- Aguilar E, Auer I, Brunet M, Peterson TC, Wieringa J. 2003. Guidelines on climate metadata and homogenization. *World Meteorological Organization, Geneva* **WMO-TD No.**
- Alexandersson H, Moberg A. 1997. Homogenization of Swedish Temperature Data. Part I: Homogeneity Test for Linear Trends. *International Journal of Climatology* **17**(1): 25–34. DOI: 10.1002/(SICI)1097-0088(199701)17:1<25::AID-JOC103>3.0.CO;2-J.
- Anyuan X, Yanjun Z, Zhihua R, Ying W. 2006. Influence of changes of sensor and shelter on air temperature observation, and analysis to its causes. *Instrument and observing methods* **94**.
- Ashcroft L, Gergis J, Karoly DJ. 2014. A historical climate dataset for southeastern Australia, 1788–1859. *Geoscience Data Journal* **1**(2): 158–178. DOI: 10.1002/gdj3.19.
- Ashcroft L, Karoly D, Gergis J. 2012. Temperature variations of southeastern Australia, 1860–2011. *Australian Meteorological and Oceanographic Journal* **62**(1): 227–245.
- Auchmann R, Brönnimann. 2012. A physics-based correction model for homogenizing sub-daily temperature series. *Journal Geophysical Research* **117**, D17119. DOI: 10.1029/2012JD018067
- Auer I, Böhm R, Jurkovic A, Lipa W, Orlik A, Potzmann R, Schöner W, Ungersböck M, Matulla C, Briffa K, Jones P, Efthymiadis D, Brunetti M, Nanni T, Maugeri M, Mercalli L, Mestre O, Moisselin JM, Begert M, Müller-Westermeier G, Kveton V, Bochnicek O, Stastny P, Lapin M, Szalai S, Szentimrey T, Cegnar T, Dolinar M, Gajic-Capka M, Zaninovic K, Majstorovic Z, Nieplova E. 2007. HISTALP—historical instrumental

climatological surface time series of the Greater Alpine Region. *International Journal of Climatology*. **27**: 17–46. doi: 10.1002/joc.1377

Bergstrom H, Moberg A. 2002. Daily Air Temperature and Pressure Series for Uppsala (1722-1998). *Climatic Change* **53**: 213–252.

Bertiglia F, Lopardo G, Merlone a., Roggero G, Cat Berro D, Mercalli L, Gilabert A, Brunet M. 2015. Traceability of Ground-Based Air-Temperature Measurements: A Case Study on the Meteorological Observatory of Moncalieri (Italy). *International Journal of Thermophysics* **36**(2-3): 589–601. DOI: 10.1007/s10765-014-1806-y.

Böhm R, Auer I, Brunetti M, Maugeri M, Nanni T, Schöner W. 2001. Regional temperature variability in the European Alps: 1760-1998 from homogenized instrumental time series. *International Journal of Climatology*. **21**(14): 1779–1801. DOI: 10.1002/joc.689.

Box JE. 2002. Survey of Greenland instrumental temperature records: 1873-2001. *International Journal of Climatology* **22**(15): 1829–1847. DOI: 10.1002/joc.852.

Böhm R, Jones PD, Hiebl J, Frank D, Brunetti M, Maugeri M. 2009. The early instrumental warm-bias: a solution for long central European temperature series 1760–2007. *Climatic Change* **101**: 41–67. DOI: 10.1007/s10584-009-9649-4.

Brandsma T, Van der Meulen JP. 2008. Thermometer screen intercomparison in De Bilt (the Netherlands) - Part II: Description and modeling of mean temperature differences and extremes. *International Journal of Climatology* **28**: 389–400. DOI: 10.1002/joc.1524.

Brázdil R, Dobrovolný P, Luterbacher J, Moberg A, Pfister C, Wheeler D, Zorita E. 2010. European climate of the past 500 years: New challenges for historical climatology. *Climatic Change* **101**(1): 7–40. DOI: 10.1007/s10584-009-9783-z.

Brohan P, Kennedy JJ, Harris I, Tett SFB, Jones PD. 2006. Uncertainty estimates in regional and global observed temperature changes: A new data set from 1850. *Journal of Geophysical Research* **111**(D12106). DOI: 10.1029/2005JD006548.

Brunet M, Asin J, Sigro J, Bañón M, García F, Aguilar E, Palenzuela JE, Peterson TC, Jones PD. 2011. The minimisation of the “screen bias” from ancient Western Mediterranean air temperature records: an exploratory statistical analysis. *International Journal of Climatology* **31**: 1879–1895. DOI: 10.1002/joc.2192.

- Brunet M, Saladie O, Jones PD, Sigro J, Aguilar E, Moberg A, Lister D, Walther A, Lopez D, Almarza C. 2006. The development of a new dataset of Spanish Daily Adjusted Temperature Series (SDATS) (1850-2003). *International Journal of Climatology* **26**: 1777–1802. DOI: 10.1002/joc.1338.
- Brunetti M, Maugeri M, Monti F, Nannia T. 2006. Temperature and precipitation variability in Italy in the last two centuries from homogenised instrumental time series. *International Journal of Climatology*. **26**(3): 345–381.
- Buisan S, Azorin-Molina C, Jimenez Y. 2015. Impact of two different sized Stevenson screens on air temperature measurements. *International Journal of Climatology* **4416**(February): 4408–4416. DOI: 10.1002/joc.4287.
- Camuffo D. 2002. History of the long series of daily air temperature in Padova (1725-1998). *Climatic Change* **53**(1-3): 7–75. DOI: 10.1023/A:1014958506923.
- Camuffo D, Bertolin C, Barriendos M, Dominguez-Castro F, Cocheo C, Enzi S, Sghedoni M, della Valle A, Garnier E, Alcoforado MJ, Xoplaki E, Luterbacher J, Diodato N, Maugeri M, Nunes MF, Rodriguez R. 2010. 500-Year temperature reconstruction in the Mediterranean Basin by means of documentary data and instrumental observations. *Climatic Change* **101**(1): 169–199. DOI: 10.1007/s10584-010-9815-8.
- Caussinus H, Mestre O. 2004. Detection and correction of artificial shifts in climate series. *Journal of the Royal Statistical Society: Series C (Applied Statistics)* **53**: 405–425. DOI: 10.1111/j.1467-9876.2004.05155.x.
- Conrad V, Pollak C. 1950. Methods in climatology. *Harvard University Press* 459.
- Della-Marta PM, Wanner H. 2006. A Method of Homogenizing the Extremes and Mean of Daily Temperature Measurements. *Journal of Climate* **19**(17): 4179–4197. DOI: 10.1175/JCLI3855.1.
- Di Napoli G, Mercalli L. 2008. *Il clima di Torino*. Società Meteorologica Subalpina: Torino, Italy
- Domonkos P. 2011. Adapted Caussinus-Mestre Algorithm for Networks of Temperature series (ACMANT). *International Journal of Geosciences*. **2**: 293–309. doi:10.4236/ijg.2011.23032

Fiebrich CA, Crawford KC. 2009. Automation: A Step toward Improving the Quality of Daily Temperature Data Produced by Climate Observing Networks. *Journal of Atmospheric and Oceanic Technology* **26**: 12461259.

Freitas L, Gonzalez M, Caramelo L, Mendes M, Nunes LF. 2013. Homogeneity of monthly air temperature in Portugal with HOMER and MASH. *Idojaras*, **117**: 69-90.

GCOS-171. 2013. The GCOS Reference Upper-Air Network (GRUAN) GUIDE. *WIGOS Technical Report No. 2013-03*.

Guttman NB, Baker BC. 1996. Exploratory Analysis of the Difference between Temperature Observations Recorded by ASOS and Conventional Methods. *Bulletin of the American Meteorological Society* **77**(12): 2865–2873. DOI: 10.1175/1520-0477(1996)077<2865:EAOTDB>2.0.CO;2.

Holder C, Boyles R, Syed A, Niyogi D, Raman S. 2006. Comparison of Collocated Automated (NCECNet) and Manual (COOP) Climate Observations in North Carolina. *Journal of Atmospheric and Oceanic Technology* **23**(5): 671–682. DOI: 10.1175/JTECH1873.1.

Hubbard KG, Lin X, Baker CB, Sun B. 2004. Air Temperature Comparison between the MMTS and the USCRN Temperature Systems. *Journal of Atmospheric and Oceanic Technology* **21**(10): 1590–1597. DOI: 10.1175/1520-0426(2004)021<1590:ATCBTM>2.0.CO;2.

Hubbard KG, Lin X. 2005. On the USCRN Temperature System. *Journal of Atmospheric and Oceanic Technology* **22**: 1095–1101.

Hubbard KG, Lin X, Walter-Shea EA. 2001. The Effectiveness of the ASOS, MMTS, Gill and CRS Air Temperature Radiation Shields. *Journal of Atmospheric and Oceanic Technology* **18**: 851–864. DOI: 10.1175/1520-0426(2001)018<0851:TEOTAM>2.0.CO;2.

Huwald H, Higgins CW, Boldi MO, Bou-Zeid E, Lehning M, Parlange MB. 2009. Albedo effect on radiative errors in air temperature measurements. *Water Resources Research* **45**(8). DOI: 10.1029/2008WR007600.

Joint Committee for Guides in Metrology (JCGM). 2012. International vocabulary of metrology - Basic and general concepts and associated terms (VIM). *International*

*Organization for Standardization Geneva ISBN 104*. DOI: 10.1016/0263-2241(85)90006-5.

Joint Committee for Guides in Metrology (JCGM). 2008. Evaluation of measurement data: Guide to the expression of uncertainty in measurement. (September). DOI: 10.1373/clinchem.2003.030528.

Jones PD, Osborn TJ, Briffa KR. 1997. Estimating sampling errors in Large-Scale Temperature Averages. *Journal of Climate*. **10**: 2548–2568. doi:10.1175/1520-0442(1997)0102.0.CO;2

Jones PD, Lister DH. 2002. The Daily Temperature Record for St. Petersburg (1743--1996). *Climatic Change* **53**(1): 253–267. DOI: 10.1023/A:1014918808741.

Joyce A, Adamson J, Huntley B, Parr T, Baxter R. 2001. Standardisation of temperature observed by automatic weather stations. *Environmental Monitoring and Assessment*. **68**: 127-136. doi: 10.1023/A:1010795108641

Knazovicka L, Strnad R. 2013. *Uncertainty budget of measured data collected in task 4.1 from different sources with respect of locality and data*. Deliverable task 4.1 MeteoMet project

Lin X, Hubbard KG. 2008. What are daily maximum and minimum temperatures in observed climatology? *International Journal of Climatology* **28**(3): 283–294. DOI: 10.1002/joc.1536.

Lin X, Hubbard KG. 2004. Sensor and Electronic Biases/Errors in Air Temperature Measurements in Common Weather Station Networks. *Journal of Atmospheric and Oceanic Technology* **21**: 1025–1032. DOI: 10.1175/1520-0426(2004)021<1025:SAEEIA>2.0.CO;2.

Linden J, Grimmond CSB, Esper J. 2015. Urban warming in villages. *Adv. Sci. Res.* **12**: 157-162. DOI: 10.5194/asr-12-157-2015

Lopardo G, Bertiglia F, Curci S, Roggero G, Merlone a. 2014. Comparative analysis of the influence of solar radiation screen ageing on temperature measurements by means of weather stations. *International Journal of Climatology* **34**(4): 1297–1310. DOI: 10.1002/joc.3765.

Lopardo G, Marengo D, Meda a., Merlone a., Moro F, Pennechi FR, Sardi M. 2012. Traceability and online publication of weather station measurements of temperature, pressure, and humidity. *International Journal of Thermophysics* **33**(8-9): 1633–1641. DOI: 10.1007/s10765-012-1175-3.

Manley G. 1974. Central England temperatures: Monthly means 1659 to 1973. *Quarterly Journal of the Royal Meteorological Society*. **100**(425): 389–405. DOI: 10.1002/qj.49710042511.

Maugeri M, Buffoni L, Chlistovsky F. 2002. ( 1763 – 1998 ): History of the Observations and Data and Metadata Recovery. *Climatic Change* **53**: 101–117.

Mestre O et al. 2013. HOMER : HOMogenisation softwarE in R- methods and applications. *Időjárás* **117**: 47–67.

Milewska E, Hogg WD. 2002. Continuity of Climatological Observations with Automation-Temperature and Precipitation Amounts from AWOS (Automated Weather Observing System). *Atmosphere-Ocean* **40**(3): 333–359. DOI: 10.3137/ao.400304.

Moberg A. 2002. Daily Air Temperature and Pressure Series. *Climatic Change* **53**: 213–252.

Nordli PO, Alexandersson H, Frich P, Forland EJ, Heino R, Jonsson T, Tuomenvirta H, Tveito OE. 1997. The effect of radiation screens on Nordic time series of mean temperature. *International Journal of Climatology* **17**(15): 1667–1681. DOI: 10.1002/(SICI)1097-0088(199712)17:15<1667::AID-JOC221>3.0.CO;2-D.

Parker DE, Legg TP, Folland CK. 1992. A new daily Central England Temperature series, 1772–1991. *International Journal of Climatology*, 317–342. DOI: 10.1002/joc.3370120402.

Parker D, Horton B. 2005. Uncertainties in central England temperatures 1878-2003 and some improvements to the maximum and minimum series. *International Journal of Climatology* **25**: 1173–1188. DOI: 10.1002/joc:1190.

Pavlašek P, Merlone A, Musacchio C, Olsen ÅAF, Bergerud RA, Knazoviccka L. 2015. Effect of changes in temperature scales on historical temperature data. *International Journal of Climatology*. DOI: 10.1002/joc.4404

- Perry MC, Prior MJ, Parker DE. 2007. An assessment of the suitability of a plastic thermometer screen for climatic data collection. *International Journal of Climatology* **27**: 267–276. DOI: 10.1002/joc.
- Peterson T et al. 1998. Homogeneity adjustments of in situ atmospheric climate data: a review. *International Journal of Climatology* **18**(13): 1493–1917.
- Picard F, Lebarbier E, Hoebeke M, Rigaiil G, Thiam B, Robin S. 2011. Joint segmentation, calling, and normalization of multiple CGH profiles. *Biostatistics* **12**(3): 413–428. DOI: 10.1093/biostatistics/kxq076.
- Preston-Thomas H. 1990. The International Temperature Scale of 1990(ITS-90). *Metrologia*, 3–10. DOI: 10.1088/0026-1394/27/1/002.
- Quayle RG, Easterling DR, Karl TR, Hughes PY. 1991. Effects of Recent Thermometer Changes in the Cooperative Station Network. *Bulletin of the American Meteorological Society* **72**(11): 1718–1723. DOI: 10.1175/1520-0477(1991)072<1718:EORTCI>2.0.CO;2.
- Romano F, Mercalli L. 1994. L'Osservatorio Meteorologico di Cuneo: dal 1877 “sentinella” della Granda. *Nimbus*. **3**: 8-15
- Slonosky V. 2015. The Meteorological Observations of Jean-Francois Gaultier , Quebec, Canada : 1742 – 56. *Journal of Climate* 2232–2247.
- Sun B, Baker CB, Karl TR, Gifford MD. 2005. A Comparative Study of ASOS and USCRN Temperature Measurements. *Journal of Atmospheric and Oceanic Technology* **22**: 679–686. DOI: 10.1175/JTECH1752.1.
- Taylor JR. 1997. *An introduction to Error Analysis. The study of uncertainties in physical measurements*. University Science Books: Sausalito, United States of America
- Trewin B. 2010. Exposure, instrumentation, and observing practice effects on land temperature measurements. *WIREs Climate Change* **1**: 490–506. DOI: 10.1002/wcc.46.
- Trewin B. 2012. A daily homogenized temperature data set for Australia. *International Journal of Climatology* **33**(6): 1510–1529. DOI: 10.1002/joc.3530.



Van der Meulen JP, Brandsma T. 2008. Thermometer screen intercomparison in De Bilt (The Netherlands), Part I: Understanding the weather-dependent temperature differences). *International Journal of Climatology* **28**: 371–387. DOI: 10.1002/joc.1531.

Venema VKC et al. 2012. Benchmarking homogenization algorithms for monthly data. *Clim. Past* **8**: 89–115. DOI: 10.5194/cp-8-89-2012. Wendland WM,

Wendland WM, Armstrong W. 1993. Comparison of Maximum-Minimum Resistance and Liquid-in-Glass Thermometer Records. *Journal of Atmospheric and Oceanic Technology*. 10: 233–237. doi:10.1175/1520-0426(1993)010<0233:COMRAL>2.0.CO;2

Wilks D. 2011. Statistical methods in atmospheric sciences (3<sup>rd</sup> edition). *Academic Press*. 704 p.

Willett KM, Dunn RJH, Thorne PW, Bell S, de Podesta M, Parker DE, Jones PD, Williams Jr. CN. 2014. HadISDH land surface multi-variable humidity and temperature record for climate monitoring. *Climate of the Past* **10**(6): 1983–2006. DOI: 10.5194/cp-10-1983-2014.

Willett KM, Williams CN, Dunn RJH, Thorne PW, Bell S, De Podesta M, Jones PD, Parker DE. 2013. HadISDH: An updateable land surface specific humidity product for climate monitoring. *Climate of the Past* **9**(2): 657–677. DOI: 10.5194/cp-9-657-2013.

Wood LE. 1946. Automatic weather stations. *Journal of Meteorology* **3**: 115–121. DOI: 10.1175/1520-0469(1946)003<0115:AWS>2.0.CO;2.

World Meteorological Organization. 2010. Guide to meteorological instruments and methods of observation. *WMO* **8**.

World Meteorological Organization. 1992. International Meteorological Vocabulary. Second edition. *WMO* **182**.

Wu H, Hubbard KG, You J. 2005. Some Concerns when Using Data from the Cooperative Weather Station Networks: A Nebraska Case Study. *Journal of Atmospheric and Oceanic Technology* **22**: 592–602. DOI: 10.1175/JTECH1733.1.

Ying W, Xiaoning L, Xiaohui J. 2004. Differences between Automatic and Manual Meteorological Observation. *Journal of Applied Meteorological Science* **15**(6): 719–726.

Ying W, Xiaoning L, Zhihua R. 2006. Initial analysis of AWS-Observed Temperature. *TECO-2006 - WMO Technical Conference on Meteorological and Environmental Instruments and Methods of Observation*. Geneva, Switzerland.

Zhang X, Zwiers FW, Hegerl G. 2008. The influences of data precision on the calculation of temperature percentile indices. *International Journal of Climatology* **29**(3): 321–327. DOI: 10.1002/joc.



## Annexes

### A.1 – Ebro Observatory temperature measurement systems installed

In sub-section 2.2.3 – What is an Automatic Weather Station (page 58) is shown that the AWS are composed by different parts.

In Ebro Observatory, under the project MeteoMet/REG-5 are installed two temperature measurement systems (page 73). The first one was installed in 2013 to try to do a correct comparison AWSc-MAN, the temperature measurement system before to be installed was calibrated. The second one was installed in April 2016 to try to analyse the differences between the Stevenson Screen and the Young screen. For this, the temperature measurement system is a clone of the first one (all the parts of the system are equal).

For both temperature measurement systems the sensor is a Pt100 (1/3 DIN four wires) and the CPU is composed by different modules.

As is explained to measure the temperature, the resistance works due to the voltage variation, this means that is necessary to creat a circuit where has been measured the output voltage when a determinate power supply is applied. The both Pt100 installed in Ebro Observatory are a Pt100 1/3 DIN 4 wires (Figure A1.1), this means that the sensor power supply and the measurement are independent, there is a cable for the power supply and another for the measurement. The datalogger is in charge to provide the required voltage to obtain the data.



*Figure A1.1: Image of the 4 wires Pt100 connected to the harness. Image source: A. Gilabert*

The CPU is composed by:

- The computation unit (Figure A1.2) installed in Ebro Observatory is composed by three main parts:

**The A/D converter:** the sensor output is directly connected to an A/D converter (analogic – digital). Generally, the output signal of the sensors is analogical, for the temperature sensors, generally the output signal comes from 0 to 5 V for a temperature range of -40 to 85 °C. The problem is that the microprocessor needs to transmit information as a binary data. So the A/D converter converts the analog signal (in this case voltage) to digital data composed by 0 and 1. The resolution of the A/D installed in Ebro Observatory is 16 bits, which means 65536 counts; from 0 to 5 V, thus the resolution is 0.002 °C. This system offers a resolution lower than the output measurement (0.01 °C). This means that the system does not introduce additional errors or loss of information on the sensor output. So the integrity of the data is guaranteed.

**The microcontroller:** is the part in charge to obtain the information from the A/D and provide this information to the RS485 module.

**The RS485 module:** is the component that converts the digital information provided by the microcontroller to the RS485 data transmission protocol (D+ and D-) that will be send through the antenna.

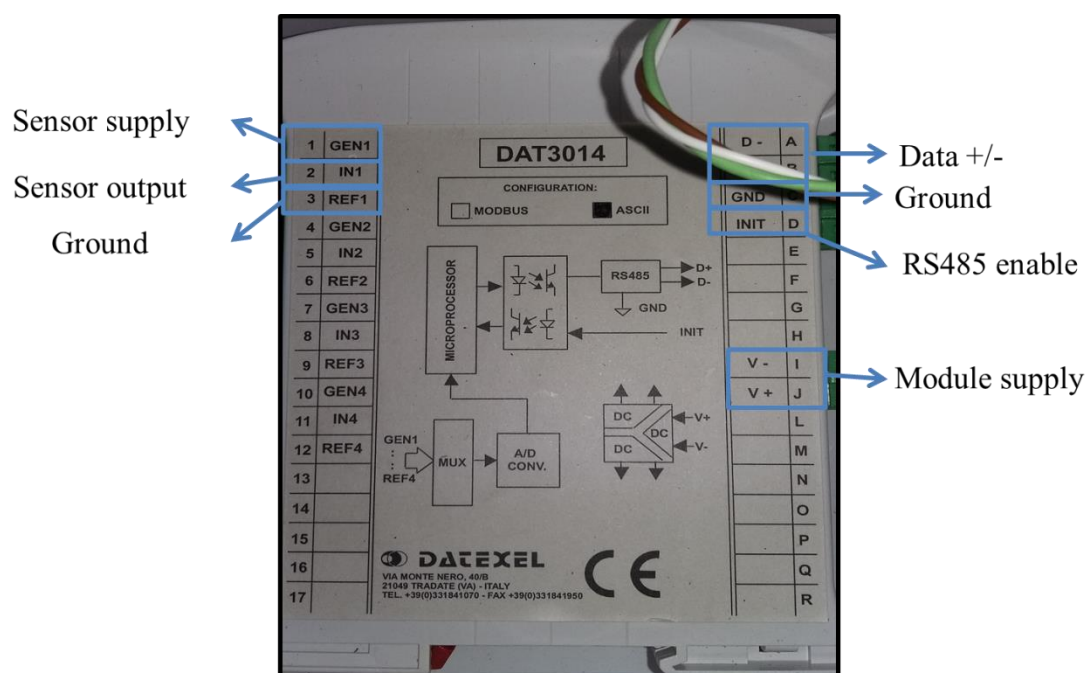


Figure A1.2: Image of the computation unit installed in Ebro Observatory field trial.  
 Image source: A. Gilabert

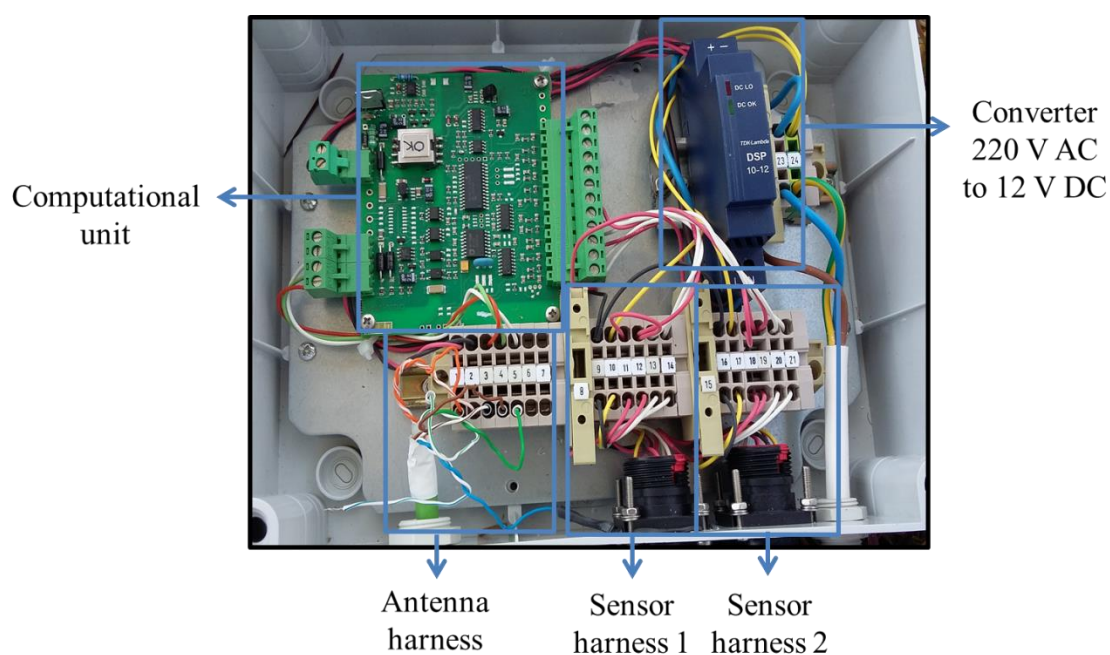


Figure A1.3: Image of the measuring and transmitting module installed in Ebro Observatory field trial. Image source: A. Gilabert

- The radio transceiver (Figure A1.4): to connect the measuring and transmitting module and the receiving module. Composed by two antennas.



Figure A1.4: Image of the two antennas, (a) connected to the measuring and transmitting module and (b) connected to the receiving module. Image source: A. Gilabert

- The receiving module (Figure A1.5): is composed by RS485 to RS232 converter and its associated power supply. The output of the receiving module is connected to a datalogger through RS232 communication protocol

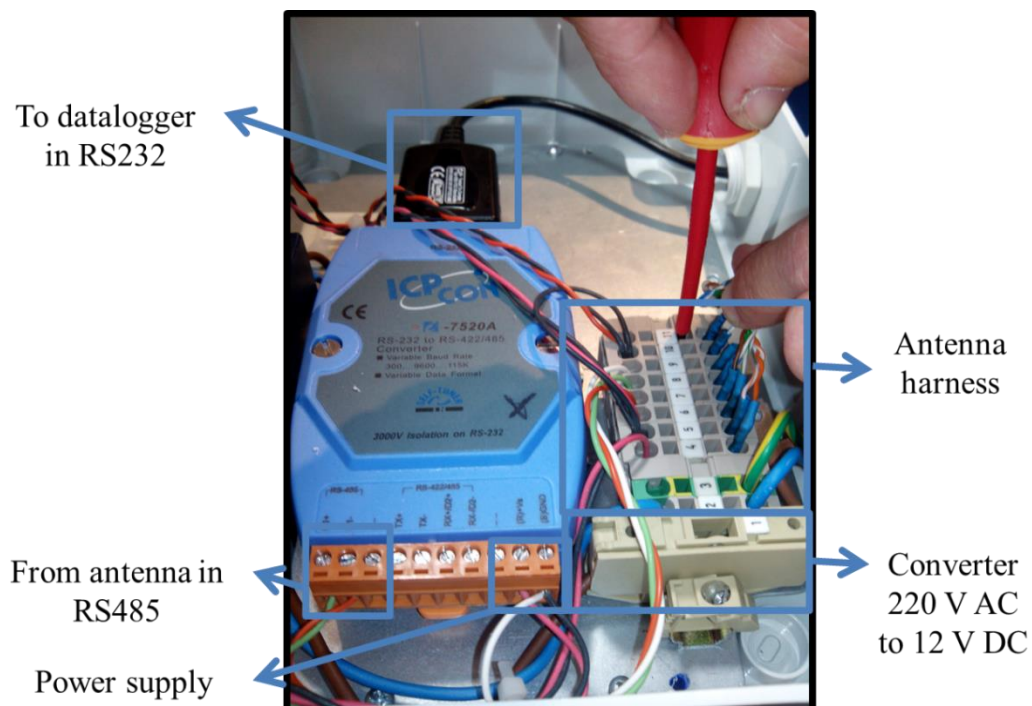


Figure A1.5: Image of the receiving module installed in Ebro Observatory field trial. Image source: A. Gilabert

- The datalogger: is composed by the computer and the program that transforms the data



*Figure A1.6: The computer that stores the data and in which is installed the program which manages the temperature measurement system and transforms the data. Image source: A. Gilabert*



*Figure A1.7: Image inside the Stevenson Screen (in which there is installed the AWSc 1) and image of the Stevenson Screen and at rear the Young Screen (in which there is installed the AWSc 2). Image source: A. Gilabert*



## A.2 – Other results

Table A2.1: The percentage of the daily maximum and minimum temperature differences AWSu – MAN of Ebro Observatory ( $\Delta T_{max}$  and  $\Delta T_{min}$ ) for the 8 HSPs detected for the differences lower than  $-1.5$  °C, between  $-1.5$  and  $-1$  °C, between  $-1$  and  $-0.5$  °C, between  $-0.5$  and  $0.0$  °C, between  $0$  and  $0.5$  °C, between  $0.5$  and  $1$  °C, between  $1$  and  $1.5$  °C and greater than  $1.5$  °C.

		< -1.5 °C	-1.5, -1 °C	-1, -0.5 °C	-0.5, 0 °C	0, 0.5 °C	0.5, 1 °C	1, 1.5 °C	> 1.5 °C
SEAC2	$\Delta T_{max}$ [%]	16.8	<b>54.2</b>	26.0	2.9	0.1	0.0	0.0	0.0
	$\Delta T_{min}$ [%]	1.3	48.3	<b>48.7</b>	1.2	0.3	0.1	0.0	0.1
SEAC1	$\Delta T_{max}$ [%]	1.4	20.3	<b>54.1</b>	20.3	3.8	0.1	0.0	0.0
	$\Delta T_{min}$ [%]	1.3	21.8	<b>75.1</b>	1.5	0.1	0.1	0.1	0.0
SOSS3	$\Delta T_{max}$ [%]	0.0	0.2	0.2	20.9	<b>72.5</b>	6.2	0.0	0.0
	$\Delta T_{min}$ [%]	0.0	0.0	0.0	20.8	<b>77.7</b>	1.3	0.2	0.0
SOSS2	$\Delta T_{max}$ [%]	0.0	0.0	1.9	22.2	<b>53.4</b>	21.5	1.0	0.0
	$\Delta T_{min}$ [%]	0.1	0.0	0.0	1.3	<b>60.1</b>	36.4	1.8	0.2
SOSS1	$\Delta T_{max}$ [%]	0.1	0.0	0.5	11.6	<b>70.6</b>	17.2	0.2	0.0
	$\Delta T_{min}$ [%]	0.0	0.0	0.2	5.8	<b>87.6</b>	5.5	0.6	0.2
ESOS3	$\Delta T_{max}$ [%]	0.0	0.3	11.1	<b>79.9</b>	8.3	0.4	0.0	0.0
	$\Delta T_{min}$ [%]	0.0	0.4	19.0	<b>73.7</b>	5.6	1.0	0.1	0.0
ESOS2	$\Delta T_{max}$ [%]	0.0	0.0	0.7	<b>58.5</b>	40.8	0.0	0.0	0.0
	$\Delta T_{min}$ [%]	0.0	0.0	0.0	<b>66.2</b>	33.8	0.0	0.0	0.0
ESOS1	$\Delta T_{max}$ [%]	0.0	0.0	2.0	<b>87.9</b>	10.1	0.0	0.0	0.0
	$\Delta T_{min}$ [%]	0.3	0.7	1.3	<b>82.7</b>	13.4	1.0	0.3	0.3

Table A2.2: Basic statistics estimated for each homogeneous sub-period (HSP) mean differences and root-mean square deviation (RMSD) for maximum temperature differences ( $\Delta T_{max}$ ) and minimum temperature differences ( $\Delta T_{min}$ ) for the difference seasons of Ebro Observatory.

		Mean				RMSD			
		DJF	MAM	JJA	SON	DJF	MAM	JJA	SON
SEAC2	$\Delta T_{max}$ [%]	-1.0	-1.2	-1.3	-1.0	1.0	1.2	1.4	1.1
	$\Delta T_{min}$ [%]	-0.9	-0.9	-1.0	-0.9	0.9	0.9	1.0	1.0
SEAC1	$\Delta T_{max}$ [%]	-0.5	-0.8	-0.9	-0.5	0.7	0.9	0.9	0.6
	$\Delta T_{min}$ [%]	-0.9	-0.9	-0.8	-0.8	1.0	0.9	0.8	0.8
SOSS3	$\Delta T_{max}$ [%]	0.3	0.2	0.1	0.3	0.4	0.3	0.2	0.3
	$\Delta T_{min}$ [%]	0.2	0.1	0.1	0.2	0.2	0.2	0.1	0.3
SOSS2	$\Delta T_{max}$ [%]	0.5	0.2	0.0	0.4	0.6	0.4	0.3	0.5
	$\Delta T_{min}$ [%]	0.5	0.6	0.4	0.5	0.5	0.6	0.5	0.6
SOSS1	$\Delta T_{max}$ [%]	0.4	0.3	0.2	0.4	0.5	0.4	0.3	0.5
	$\Delta T_{min}$ [%]	0.3	0.3	0.3	0.3	0.4	0.3	0.3	0.4
ESOS3	$\Delta T_{max}$ [%]	-0.1	-0.2	-0.3	-0.3	0.3	0.3	0.4	0.3
	$\Delta T_{min}$ [%]	-0.2	-0.3	-0.4	-0.3	0.3	0.4	0.4	0.4
ESOS1	$\Delta T_{max}$ [%]	-0.2	-0.2	-0.1	-0.1	0.2	0.2	0.2	0.2
	$\Delta T_{min}$ [%]	-0.1	-0.1	0.0	-0.1	0.5	0.2	0.4	0.3

Table A2.3: The mean for maximum and minimum temperature difference series AWSu-MAN of Ebro Observatory of SEAC2, SOSS2 and ESOS2 according the stratification of the days depending the wind speed and the sunshine hours. W-O windy and overcast days, W-C (windy and clear days), C-O (calm and overcast days) and C-C (calm and clear days). On methodology (Page 93) to see the wind speed and sunshine hours thresholds.

	SEAC2		SOSS2		ESOS3	
	$\Delta T_{max}[^{\circ}C]$	$\Delta T_{min}[^{\circ}C]$	$\Delta T_{max}[^{\circ}C]$	$\Delta T_{min}[^{\circ}C]$	$\Delta T_{max}[^{\circ}C]$	$\Delta T_{min}[^{\circ}C]$
W-O	-1.2	-1.0	0.3	0.5	-0.4	-0.3
W-C	-1.2	-1.0	0.2	0.5	-0.3	-0.3
C-O	-1.0	-0.9	0.4	0.5	-0.3	-0.3
C-C	-1.3	-0.9	0.2	0.5	0.0	-0.3
Winter						
W-O	-1.1	-1.1	0.3	0.5	-0.3	-0.3
W-C	-1.1	-1.0	0.3	0.5	-0.2	-0.3
C-O	-1.0	-0.9	0.4	0.5	-0.3	-0.4
C-C	-0.7	-0.9	0.8	0.5	0.1	-0.2
Summer						
W-O	-1.3	-1.0	0.2	0.6	-0.4	-0.4
W-C	-1.3	-1.0	0.0	0.5	-0.4	-0.3
C-O	-1.3	-1.0	0.1	0.4	-0.3	-0.3
C-C	-1.4	-1.0	0.0	0.4	-0.3	-0.3

*Table A2.4: The percentage of the daily maximum and minimum temperature differences AWSu – MAN of Fabra Observatory ( $\Delta T_{max}$  and  $\Delta T_{min}$ ) for the 6 HSPs detected for the differences lower than  $-1.5$  °C, between  $-1.5$  and  $-1$  °C, between  $-1$  and  $-0.5$  °C, between  $-0.5$  and  $0.0$  °C, between  $0$  and  $0.5$  °C, between  $0.5$  and  $1$  °C, between  $1$  and  $1.5$  °C and greater than  $1.5$  °C.*

		< -1.5 °C	-1.5, -1 °C	-1, -0.5 °C	-0.5, 0 °C	0, 0.5 °C	0.5, 1 °C	1, 1.5 °C	> 1.5 °C
MCV1.2	$\Delta T_{max}$ [%]	0.0	0.3	0.2	2.1	2.4	1.5	1.8	<b>91.7</b>
	$\Delta T_{min}$ [%]	5.2	14.1	<b>39.2</b>	34.4	5.2	0.6	0.3	1.0
MCV1.1	$\Delta T_{max}$ [%]	1.1	1.7	4.9	9.8	12.3	20.8	18.4	<b>30.9</b>
	$\Delta T_{min}$ [%]	3.3	9.8	15.4	<b>41.7</b>	21.9	7.2	0.2	0.5
MCV2.3	$\Delta T_{max}$ [%]	4.7	5.3	12.2	12.4	15.0	<b>19.9</b>	15.0	15.6
	$\Delta T_{min}$ [%]	3.6	22.2	<b>55.6</b>	17.2	0.8	0.4	0.0	0.2
MCV2.2	$\Delta T_{max}$ [%]	0.0	0.0	0.6	1.8	7.8	12.7	21.1	<b>55.9</b>
	$\Delta T_{min}$ [%]	0.8	1.2	8.3	<b>44.7</b>	39.6	5.0	0.4	0.0
MCV2.1	$\Delta T_{max}$ [%]	0.0	0.4	1.1	6.4	11.6	18.4	21.1	<b>41.0</b>
	$\Delta T_{min}$ [%]	0.2	5.5	39.2	<b>50.1</b>	4.8	0.0	0.0	0.2
Vaisala	$\Delta T_{max}$ [%]	0.0	0.0	6.6	<b>65.0</b>	27.5	0.8	0.1	0.0
	$\Delta T_{min}$ [%]	0.0	0.2	8.7	<b>84.8</b>	6.4	0.0	0.0	0.0

Table A2.5: The mean for maximum and minimum temperature difference series AWSu-MAN of Fabra Observatory of MCV1.2, MCV2.2 and Vaisala according the stratification of the days depending the wind speed and the sunshine hours. W-O windy and overcast days, W-C (windy and clear days), C-O (calm and overcast days) and C-C (calm and clear days). On methodology (Page 93) to see the wind speed and sunshine hours thresholds.

	MCV1.2		MCV2.2		Vaisala	
	$\Delta T_{max}[^{\circ}C]$	$\Delta T_{min}[^{\circ}C]$	$\Delta T_{max}[^{\circ}C]$	$\Delta T_{min}[^{\circ}C]$	$\Delta T_{max}[^{\circ}C]$	$\Delta T_{min}[^{\circ}C]$
W-O	1.9	-0.5	0.9	0.1	-0.2	-0.3
W-C	4.2	-0.6	2.6	-0.1	-0.1	-0.2
C-O	2.8	-0.5	1.1	0.0	-0.1	-0.2
C-C	4.0	-0.7	2.1	-0.2	0.1	-0.1
Winter						
W-O	0.2	-0.5	0.6	0.2	-0.3	-0.4
W-C	2.8	-0.5	1.4	-0.1	-0.3	-0.3
C-O	2.1	-0.6	0.9	0.0	-0.2	-0.2
C-C	4.5	-1.3	1.8	0.0	-0.3	-0.2
Summer						
W-O	3.5	-0.7	2.4	0.0	-0.1	-0.2
W-C	4.3	-0.5	3.5	0.0	0.1	-0.1
C-O	3.0	-0.5	0.8	-0.2	0.1	-0.1
C-C	4.0	-0.4	2.1	-0.5	0.1	-0.1

*Table A2.6: The percentage of the daily maximum and minimum temperature differences AWSu – MAN of Murcia Observatory ( $\Delta T_{max}$  and  $\Delta T_{min}$ ) for the 4 HSPs detected for the differences lower than  $-1.5$  °C, between  $-1.5$  and  $-1$  °C, between  $-1$  and  $-0.5$  °C, between  $-0.5$  and  $0.0$  °C, between  $0$  and  $0.5$  °C, between  $0.5$  and  $1$  °C, between  $1$  and  $1.5$  °C and greater than  $1.5$  °C.*

		< -1.5 °C	-1.5, -1 °C	-1, -0.5 °C	-0.5, 0 °C	0, 0.5 °C	0.5, 1 °C	1, 1.5 °C	> 1.5 °C
SEAC4	$\Delta T_{max}$ [%]	0.0	0.4	6.5	40.3	<b>46.3</b>	5.8	0.5	0.4
	$\Delta T_{min}$ [%]	0.0	0.0	0.2	5.2	<b>46.0</b>	44.9	3.1	0.6
SEAC3	$\Delta T_{max}$ [%]	2.7	12.7	33.1	<b>33.3</b>	16.2	2.0	0.0	0.0
	$\Delta T_{min}$ [%]	0.0	0.0	0.3	3.0	16.3	<b>47.1</b>	27.2	6.0
SEAC2	$\Delta T_{max}$ [%]	0.0	0.2	1.2	10.5	<b>56.0</b>	30.2	1.9	0.0
	$\Delta T_{min}$ [%]	0.0	0.2	1.2	17.2	<b>56.4</b>	23.2	1.6	0.2
SEAC1	$\Delta T_{max}$ [%]	0.3	1.5	5.0	<b>43.6</b>	42.7	6.2	0.5	0.2
	$\Delta T_{min}$ [%]	0.0	0.5	2.7	24.1	<b>60.0</b>	11.8	0.8	0.2

Table A2.7: The mean for maximum and minimum temperature difference series AWSu-MAN of Murcia Observatory of SEAC4, SEAC3, SEAC2 and SEAC1 according the stratification of the days depending the wind speed and the sunshine hours. W-O windy and overcast days, W-C (windy and clear days), C-O (calm and overcast days) and C-C (calm and clear days). On methodology (Page 93) to see the wind speed and sunshine hours thresholds.

	SEAC4		SEAC3		SEAC2		SEAC1	
	$\Delta T_{max}$ [°C]	$\Delta T_{min}$ [°C]	$\Delta T_{max}$ [°C]	$\Delta T_{min}$ [°C]	$\Delta T_{max}$ [°C]	$\Delta T_{min}$ [°C]	$\Delta T_{max}$ [°C]	$\Delta T_{min}$ [°C]
W-O	0.0	0.6	-0.3	0.8	0.2	0.2	-0.2	0.2
W-C	0.1	0.6	-0.7	0.8	0.5	0.3	0.0	0.1
C-O	0.1	0.4	0.0	0.9	0.3	0.2	0.0	0.3
C-C	-0.1	0.4	-0.6	0.8	0.6	0.5	0.3	0.2
Winter								
W-O	0.1	0.5	0.1	1.1	0.2	0.2	-0.2	0.2
W-C	-0.1	0.4	-0.5	0.5	0.5	0.3	0.0	0.1
C-O	0.2	0.4	0.2	1.0	0.3	0.2	0.0	0.3
C-C	-0.1	0.5	-0.3	1.1	0.6	0.5	0.3	0.2
Summer								
W-O	0.1	0.5	-0.4	0.6	0.5	0.6	0.3	0.2
W-C	0.1	0.7	-0.8	0.7	0.8	0.8	-0.2	0.1
C-O	0.1	0.3	-0.7	0.5	0.7	0.5	0.1	0.2
C-C	0.1	0.7	-0.7	0.3	0.5	0.5	0.0	0.2

### A.3 – List of equations

<i>Eq. 2.1 – Equation to determine temperature triple point of water</i> .....	54
<i>Eq. 2.2 – Interpolation temperature function -200 to 0 °C</i> .....	54
<i>Eq. 2.3 – Interpolation temperature function 0 to 850 °C</i> .....	54
<i>Eq. 3.1 – Calibration function</i> .....	76
<i>Eq. 3.2 – RMSD</i> .....	93
<i>Eq. 3.3 – Combined calibration uncertainty</i> .....	95
<i>Eq. 3.4 – Heidke Skill Score Standard</i> .....	98
<i>Eq. 3.5 – Uncertainties related to the homogenisation procedure</i> .....	99
<i>Eq. 3.6 – Calibration uncertainty of the reference stations</i> .....	99
<i>Eq. 3.7 – Instrumental uncertainty of the candidate station</i> .....	99
<i>Eq. 3.8 – Joint-estimation of the instrumental plus homogenisation uncertainty budget</i> .....	99
<i>Eq. 3.9 – Ordinary Least Squares</i> .....	100
<i>Eq. 3.10 – Weighted Least Squares</i> .....	100



